Max-Planck Institute for
Brain Research

Technische Universität
Darmstadt

Reversible Visual Hemineglect: the Role of Neural Oscillations in Primary Visual Cortex

Technische Universität Darmstadt
Fachbereich Biologie

zur Erlangung des Grades
Doktor rerum naturalium (Dr. rer. nat.)

genehmigte Dissertation
von William Halley Barnes M.S.
aus Dallas, USA

1. Prüfer: Dr Prof Ralf A.W. Galuske
2. Prüfer: PD Dr. Matthias H.J. Munk

Tag der Einreichung: October 22, 2014
Tag der mündlichen Prüfung: December 16, 2014
Darmstadt 2016
D17

to Andre

Table of Contents

Summary

Visual hemineglect is a pathology where damage to any of a number of areas in the brain can result in visual stimuli contralateral to neural damage not entering perceptual awareness. In the cat, the superior colliculus (SC) and cortical areas on the medial bank of posterior middle suprasylvian sulcus (pMS) are regions that when unilaterally damaged result in contralateral visual hemineglect. In this dissertation, electrophysiological recordings of population activity in cat primary visual cortex were made while either the SC or pMS were deactivated. The goal of this experimental set-up was to ascertain the effects of SC or pMS deactivation on the electrophysiological population signal as a visual stimulus enters the cortical processing network at its main entry point, primary visual cortex. Four projects were executed for this thesis involving: 1) anesthetized SC-deactivation, 2) anesthetized pMS-deactivation, 3) awake pMS deactivation, and 4) pMS-deactivation in the awake-behaving cat. Advanced recording techniques to monitor neural activity in the awake-behaving cat (project 4) while cortex was both active and deactivated were developed for this thesis to compliment thesis projects 1-3 involving classical recording techniques in animals passively viewing a square-wave visual stimulus.

The results are as follows: in the awake cat performing a visual perimetry task (project 4), neural activity when 1) unilateral pMS was deactivated and contralateral stimuli neglected versus when 2) pMS was active and stimuli were attended, reveals a significant drop in high-frequency gamma (52-90 Hz) oscillations and low-frequency theta (4-8 Hz) oscillations bilaterally in primary visual cortex.

The drop in gamma and theta power was mirrored in anesthetized recordings during pMS deactivation (project 2). In this experimental set-up the cat was anesthetized and square-wave gratings were used as a visual stimulation. Gamma and theta power decreased during pMS deactivation relative to the condition where pMS

was active. A similar trend, though statistically insignificant, were made when performing the same experiment as project 2, but in awake cats (project 3). The lack of statistical significance is presumably due to increased ongoing, internally generated, activity in the awake preparation.

The findings in projects 2 & 3 confirm the visual perimetry finding in project 4 with the caveat that the passive viewing projects 2 & 3 yield a cooling-induced interhemispheric imbalance in theta and gamma power, whereas power changes for the awake-behaving cat in project 4 were bilateral with no interhemispheric imbalance. The strong unilateral effect in project 2 is presumably due to anesthesia inhibiting interareal interaction, or could as-well reflect reduced processing demands relative to the perimetry task. The perimerty task is a behavioral task and may necessitate the recruiting of a larger network involving both hemispheres in order to orient attention to a low-salience LED located in the visual periphery.

The anesthetized project was repeated, but with SC rather than pMS deactivation (thesis project 1). The SC deactivation led to an ipso deactivation loss of gamma, but not theta power.

Taken together, the meaning of the results in projects 1-4 is as follows: unilateral deactivation of the pMS or SC results in a visual hemineglect in the awake behaving animal. Unilateral deactivation of either structure also leads to a loss of gamma power. This loss in gamma power during pMS or SC deactivation lends support to the binding by synchrony hypothesis (Gray et al 1989) whereby high-frequency oscillations act as a carrier frequency through which a larger cortical network can represent a stimulus via synchronous activity in the disparate neural processing nodes. Along this line, loss of gamma power would indicate a break-down in network communication that leads to a neglect of contralateral visual stimuli. A cooling induced interhemispheric imbalance in gamma power, as found in passive-viewing projects 1-3, could explain visual hemineglect because the primary visual cortex

respresenting the neglected hemifield has less gamma power than the hemisphere responsible for the intact visual hemispace. However, interhemispheric gamma power imbalance does not occur in the behaving cat. In light of a *bilateral* loss of gamma power for neglect trials following pMS inactivation in project 4, an explanation beyond interhemispheric gamma power imbalance must be formed to explain behavioral hemineglect, at least with regards to pMS inactivation

The loss of theta power for pMS but not SC deactivation lends support to the attention to memory hypothesis (Cabeza et al 2008). This hypothesis views the posterior parietal cortex (PPC), of which pMS is a part, as an area involved in directing attention to internal memories and goals. Anatomical links between the PPC and the hippocampus, where a theta rhythm is generated, may implicate the pMS in more than just reflexive orienting behavior. Moreover, posterior parietal cortex, of which pMS is a key part, is known from anatomical studies (Markov et al 2014) to be one of the network hubs in the brain The loss of theta power following pMS deactivation may indicate a global loss network connectivity with one result being a loss in the ability to create an egocentric coordinate system in the hemispace contralateral to pMS deactivation. Deactivation of the pMS could also lead to a context dependent loss in the ability to retain awareness that behaviorally relevant stimuli have occurred in the hemispace contralateral to pMS deactivation. Both spatial coordinates and memories are functions inextricably intertwined with the hippocampus. Moreover, cross-frequency coupling between theta and gamma is well established. This frequency coupling, with small amplitude gamma oscillation riding on top of large-amplitude theta oscillations, would allow the membrane potentials in participating distributed brain regions to depolarize and simultaneously spike thereby generating a distributed neural signature that could underly perceptual awareness. This binding mechanism appears to be compromised in visual hemineglect.

Zusammenfassung

Visueller Hemineglect ist eine pathologische Störung, bei der Schäden an bestimmten Arealen des Gehirns eine bewusste Wahrnehmung von visuellen Reizen im Gesichtsfeld kontralateral zur Schädigung unterbinden. Bei Katzen verursacht eine unilaterale Läsion der Colliculli Superiores (SC) oder von Kortexregionen im medialen posterioren suprasylvischen Sulcus (pMS) diesen kontralateralen visuellen Hemineglect. Für vorliegende Dissertation wurden elektrophysiologische Messungen an Neuronenpopulationen im primären visuellen Kortex von Katzen durchgeführt, wobei entweder SC oder pMS deaktiviert wurden. Ziel dieser Experimente war es, den Effekt von SC oder pMS Deaktivierung auf das elektrophysiologische Populationssignal zu untersuchen, wenn eine visuelle Reizung des primären visuellen Kortex sowie des gesamten visuellen Informationsverarbeitungsnetzwerk erfolgte. Für diese Arbeit wurden vier verschiedenen Projekte durchgeführt: 1) Deaktivierung von SC unter Anästhesie; 2) Deaktivierung von pMS unter Anästhesie; 3) Deaktivierung von pMS bei wachen Katzen; 4) Deaktivierung von pMS bei wachen Katzen während Verhaltenstests. Um die neuronale Aktivität in den Verhaltensexperimenten am wachen Tier erfassen zu können, wurden spezielle Messtechniken entwickelt. Diese ergänzen die klassischen Messtechniken, die für Projektteile 1-3 verwendet wurden.

Die Ergebnisse sind wie folgt: Während der Durchführung einer visuellen Perimetrie-Aufgabe im Verhaltenstest (Projekt 4) zeigte sich in der neuronalen Aktivität A) bei unilateraler pMS Deaktivierung mit kontralateralem Stimulusneglect im Vergleich zu B) bei aktivem pMS und Aufmerksamkeitsausrichtung auf den Stimulus ein signifikant verringerter Anteil an hochfrequenten Gammaband Oszillationen (25-90Hz) sowie an niedrigfrequenten Thetaband Oszillationen (4-8Hz) bilateral im primären visuellen Kortex.

Die verminderte Gamma- und Thetaband Aktivität konnte auch bei anästhesierten Tieren während der pMS Deaktivierung festgestellt werden (Projekt 2). In diesem Teil der Studie wurden anästhesierte Katzen mit bewegten Balkengittern (square waved moving gratings) stimuliert. Während der pMS Deaktivierungsphase zeigte sich, dass die Deaktivierung von pMS zu einer Verminderung von Gamma- und Thetabandaktivitäten führte. Ein ähnlicher Trend, jedoch ohne statistische Signifikanz, konnte bei wachen Katzen während der Durchführung der

für Projekt 2 beschriebenen Aufgabe (Projekt 3) beobachtet werden. Die fehlende statistische Signifikanz kann vermutlich durch ein erhöhtes Maß an intern generierter Aktivität im Wachzustand erklärt werden.

Die Ergebnisse aus Projekt 2 und 3 bestätigen die Ergebnisse der Verhaltenstests, die in Projekt 4 gewonnen wurden. Allerdings wurden während der passiven Projekte 2 und 3 durch Kühlung bedingte, interhemisphärische Unterschiede im Gamma- und Thetaband beobachtet, wohingegen Änderungen in der Aktivität in Projekt 4 bei wachen Katzen bilateral, d.h. ohne interhemisphärische Unterschiede, auftreten. Der stark unilaterale Effekt in Projekt 2 ist vermutlich durch eine anästhesiebedingte Hemmung interarealer Kommunikation erklärbar, könnte aber auch verringerte Informationsverarbeitungsanforderungen im Vergleich zwischen passiver und aktiver Aufgabe widerspiegeln. Die Perimetrie-Aufgbe ist eine Verhaltensaufgabe, bei der möglicherweise die Rekrutierung größerer Netzwerke und die Involvierung beider Hemisphären erforderlich ist, um die Aufmerksamkeit auf einen LED Reiz niedriger Salienz in der visuellen Peripherie richten zu können.

Auch in den Experimenten mit anästhesierten Tieren gibt es interessante Unterschiede. Dabei zeigte sich, dass die Deaktivierung von pMS und die Deaktivierung des SC unterschiedliche Konsequenzen hatten: während die pMS Deaktivierung zu einem breiten Zusammenbruch im Oszillationsspektrum führte, beobachteten wir bei SC Deaktivierung nur einen Verlust von Gamma-, nicht jedoch von Thetabandaktivität.

Zusammengenommen bedeuten die Ergebnisse der Projekte 1-4 nun Folgendes: Unilaterale Deaktivierung von pMS oder SC führt im Verhaltensexperiment an wachen Katzen zum Hemineglect und außerdem zu einem Verlust von Gammabandaktivität. Dieser Verlust von Gammabandaktivität während der pMS oder SC Deaktivierung stützt die ‚binding by synchrony' Hypothese (Gray et al 1989), nach der hochfrequente Oszillationen als Trägerfrequenzen dienen, durch die Stimuli in größeren kortikalen Netzwerken durch Synchronizität zwischen Netzwerkpunkten repräsentiert werden. Nach dieser Logik wäre ein Verlust an Gammabandaktivität ein Zeichen für das Zusammenbrechen der Netzwerkkommunikation, was dann zum Neglect von kontralateralen visuellen Stimuli führt. Die durch die Kühlung induzierten interhemisphärischen Unterschiede in der Gammabandaktivität, die wir in den passiven Projekten

1-3 fanden, könnten eine Erklärung für den visuellen Hemineglect sein, da der primäre visuelle Kortexanteil, der für das vom Neglect betroffene Hemifield verantwortlich ist, weniger Gammabandaktivität zeigt als der für das intakte Gesichtsfeld verantwortliche. Diese interhemisphärischen Unterschiede zeigen sich nicht nur während der Verhaltensexperimente. Unter Bezugnahme auf einen bilateralen Verlust von Gammabandaktivität bei Neglect Durchgängen, der einer pMS Inaktivität in Projekt 4 folgt, sind zusätzlich zum interhemisphärischen Gammaband-Ungleichgewicht weitere Erklärungen erforderlich, um die Verhaltenseffekte beim Hemineglect zu erklären, zumindest in Bezug auf eine pMS Inaktivierung.

Der Verlust von Thetaband Aktivität bei pMS Deaktivierung, nicht aber bei SC Deaktivierung, kann im Sinne der 'attention to memory' Hypothese (Cabeza et al 2008) erklärt werden. Dieser Hypothese zufolge ist der posteriore parietale Kortex (PPC), zu dem auch der pMS gehört, in die Ausrichtung von Aufmerksamkeit auf interne Erinnerungen und Ziele involviert. Anatomische Verbindungen zwischen PCC und Hippocampus, der für die Generierung von Thetabandaktivität verantwortlich ist, lassen vermuten, dass der pMS wahrscheinlich für mehr als nur ein reflexbedingtes Orientierungsverhalten eine Rolle spielt. Des Weiteren haben viele Studien gezeigt, dass der PPC eine Schlüsselstellung in einem aufmerksamkeitsgesteuerten visuellen, aber auch multimodalen, Netzwerk spielt. Daher ist der Verlust von Theta Oszillationen durch pMS Deakivierung vermutlich ein Indikator für den Verlust der globalen Netzwerkkonnektivität auf funktioneller Ebene. Das Resultat wäre dann der Verlust der Fähigkeit, ein egozentrisches Koordinatensystem aufzubauen, was dem klinischen Bild sehr nahe kommt.

Sowohl räumliche Koordination als auch Gedächtnis sind Funktionen, bei denen der Hippocampus eine wichtige Rolle spielt. Die Kopplung zwischen Gammaband und Thetaband Oszillationen ist gut belegt und bekannt. Diese Kopplung zwischen niederfrequentem und niederamplitudigem Gammaband mit geringerfrequenten aber höheramplitudigen Oszillationen würde in beteiligten Hirnregionen zur Depolarisierung von Neuronen führen bei gleichzeitiger Generierung von Spikes. Dabei könnte eine neuronale Signatur generiert werden, die dem perzeptuellen Bewusstsein zugrunde liegt. Dieser Bindungsprozess scheint eben der zu sein, der bei visuellem Hemineglect beeinträchtigt ist. Aber auch die Rolle von GammaOszillationen muss weiter beobachtet werden, da sie sehr wichtige seitenspezifische Resultate gezeigt hat.

Introduction

1.1 - The neglect pathology

Visual hemineglect is a pathology involving a disruption in any of a number of modules or connections between modules in the attentional network. This network disruption results in a situation in which attention to contralateral stimuli can no longer be allocated.

In humans, neglect results largely from right hemisphere lesions causing a neglect of left visual hemispace. Neglect differs from a scotoma in that a patient with a scotoma will try to compensate for the missing portion of the visual field by moving the retina so that the missing stimulus is brought into view. Neglect patients, in contrast, make no attempt to access the neglected hemifield and thus, in essence, neglect their own neglect. Moreover, as detailed through various experimental paradigms, there is still some level of subconscious processing of neglected stimuli, which is not the case with stimuli obscured by a scotoma. It could therefore be said that a scotoma results from a failure in lower-level visual processing, while neglect is the failure to produce a higher-order stimulus representation involving the attention system.

Human behavioral manifestations of neglect are manifold. A simple line-bisection task reveals the complex nature of the syndrome. In this task, patients are asked to mark the center of a horizontal line. Where controls place the mark at the approximate middle of the line, neglect patients who neglect the left hemifield, place

the mark far to the right, indicating that the left end of the line has been neglected. If the line is lengthened, neglect patients indicate the position of the midline, relative to the true endpoints the line, as being similarly far to the right in relative terms. Thus, if the midpoint was placed at 9cm on a 10cm line, it will be placed at 18cm on a 20cm line (Harvey 1995, Mozer 1997, Monaghan & Schillcock 1998). This shows that neglect is a "post-sensory phenomenon directed to an internal representations" (Mesulam 1999) because moving the location of the bisection mark requires the awareness, at some level, that the line has been extended leftward.

A clear example of how neglect can distort internal representations is an experiment performed by Bisiach et al 1981. Neglect patients were told to imagine that they were at Piazza del Duomo in Milan facing the cathedral. When asked to recall the square, they were better at recalling details to the right of their vantage point. Upon being instructed to recall the square facing *away* from the cathedral, they again recalled details to the right of their vantage point, but this time they recalled aspects from the opposite side of the square, thus bringing information that they had previously neglected into awareness, and neglecting the information they had previously recalled. This experiment shows a failure to create and accurate *internal* representation of the square

Neglected content can still be used for behavioral decisions. In one case study, a woman with neglect was asked if pictures of two houses were different. The houses were identical except that the left side of one house was on fire. The woman identified the houses as being identical to each other, commiserate with her contralateral visual neglect. When asked however which house she would rather live

in, she repeatedly choose the house that was not on fire, thus showing that she had indeed at some level recognized the flames (Marshall & Halligan 1988).

The neglect phenomenon also affects modalities outside of vision. In one experiment, neglect patients had a 90^0 mirror placed in front of them so that stimuli in the neglected *hemispace* appeared in the non-neglected *hemifield*. The behavioral task involved reaching for visual stimuli in the neglected hemispace. As the mirror brought the neglected stimulus into the non-neglected hemifield, a disassociation was created between where the neglect patient had to reach, the neglected hemispace, and where the patient had to look, the non-neglected hemifield. The experimental finding revealed that some patients who neglected to reach for stimuli without the mirror would reach for them after the mirror was introduced, while other patients continued to neglect reaching for the stimuli (Tegnér & Levander 1991). This reveals that neglect is not only a failure to look left, but in some cases, also a failure to reach left.

Since it can be shown that low-level basic encoding of stimuli remains largely intact for neglect patients, the above experimental findings seem to suggest that an attentional map of the object/scene that the patient is currently interacting with, has been distorted. Within an individual, multiple frames of reference interact to create a map of the stimulus (Mesulam 1991, Driver & Vuilleumier 2001). Possible coordinate systems include retinotopic, cephalocentric, gravitational, somatocentric, and object-centered, among others (Mesulam 1991). Twisting the body of a neglect patient toward a neglected stimulus while the eyes and head remain static can, in some cases,

bring a stimulus into awareness (Karnath et al. 1991). Similarly, varying the position of the eye within the orbit (Kooistra & Heilman 1989, Vuilleumier et al 1999) or relative to the head and neck (Karnath et al 1991, Vuilleumier et al. 1999), can also bring a neglected stimulus into awareness (Driver & Vuilleumier 2001).

Though human parietal cortex at the temporal-parietal junction (TPJ) is the focal point for injury in neglect patients (Vallar 2001, Morte 2003), other areas have also been indicated to be involved, namely the thalamus, basal ganglia, and dorsolateral prefrontal cortex, among others (Vallar 2001, Karnath et al. 2002). The neurotransmitter Acetylcholine is believed to be the main neurotransmitter for this orienting system (Peterson & Posner 2012), and a neurotransmitter centrally involved in the generation of neuronal oscillations (Munk et al. 1996, Herculano-Houzel et al. 1999). Thus it has been suggested that the neglect syndrome arises from a dysfunction in the interaction of a larger brain network involving any of a number of network nodes (Mesulam 1981, Heilman et al. 1993) or a disconnection between the nodes (Bartolomeo 2007).

Critical to interpreting the results of the neglect pathology is recognizing the heterogeneity of the underlying lesions in human neglect cases. The lesions were not performed with surgical precision, but were rather the result of unplanned brain damage. The resulting pathological behavioral alterations often include areas that are not known to be involved in the neglect syndrome. Thus, to further inform our view of hemispatial neglect, the role that putative brain regions associated with neglect play outside of the neglect syndrome, in the normal functioning brain, is useful.

1.2 - The Attention to Memory hypothesis

A compelling theory explaining the role of human posterior parietal cortex (PPC), a hub of the neglect syndrome, is the *attention to memory* (AtoM) hypothesis (Cabeza et al. 2008; Ciaramelli et al. 2008; Olson and Berryhill 2009, Ciaramelli et al. 2010). This hypothesis divides the PPC into a dorsal and a ventral area. The dorsal area is involved in directing attention internally to memories and goals while the ventral PPC promotes a reorientation of the locus of attention to external stimuli. The AtoM hypothesis thereby extends the role of PPC, an area seen as a hub of the neglect syndrome, from an area dealing with behaviorally relevant external events, to an area also involved in internally generated content and goals (Hutchinson et al. 2009). Thus, the neglect syndrome could involve, as shown in the above example involving the Piazza del Duomo in Milan (Bisiach et al 1981), a failure of internal memory search as much as a failure in external stimulus search.

The neural computations that allow this search to be projected onto an attentional map of the external world (or the internal map of the external world) are by no means clear. There appears to be at least five retinotopically organized attentional maps in the intraparietal sulcus of the PPC (Swischer et al 2007, Hutchinson et al 2009), moreover, the specificity of PPC in sensory verses motor processing is not fully clear (Peterson & Posner 2012).

1.3 - Animal models of neglect

Visual hemineglect can be induced in a broad range of laboratory animals including rodents, cats, and monkeys (Payne & Rushmore 2003). As with human

neglect, the animal models include four main components. 1) There is a network hub at the temporal-occipital-parietal junction (PPC in humans) which, when damaged, leads to an inability to transform external signals into an internal coordinate system (Payne & Rushmore 2003). 2) A frontal component, involved in a covert or overt motor response to stimuli. 3) A limbic node, involved in an emotional or motivational component of neglect. 4) A collicular node, with a sensory and motor component (Payne & Rushmore 2003). Unlike humans, with their primarily left-lateralized language centers and right lateralized 'neglect network', animals show no right-lateralization of the neglect network. Damage to both the left or right hemisphere can induce contralateral neglect in animals (Payne & Rushmore 2003).

In monkey models of neglect, a lesion of the inferior parietal lobule (Watson et al 1994), at the temporal-occipital-parietal junction, or reversible deactivation of unilateral lateral intraparietal area (LIP) (Wilke et al 2012), has been shown to induce visual extinction, a form of neglect. For Monkeys with an inferior parietal lobule lesion, addition of a contralateral homeotopic lesion has been shown to lead to a cancellation of the visual extinction (Watson et al 1994).

1.3.2 - Neglect in cats

The study of visual neglect has a long history in cats, starting with the publication of what later became known as the Sprague effect (Sprague 1966). In this seminal work, Sprague showed that contralateral visual neglect induced by a complete lesion of the occipito-temporal neocortex could be reversed by a lesion of the superior colliculus (SC) contralateral to the neocortex lesion. Visual neglect in the cat has

been more recently induced by reversible thermal deactivation of the SC or the posterior middle suprasylvian sulcus (pMS) (Payne BR et al 1996). Thus, in the parietal cortex of the cat, the pMS, at the temporo-occipital-parietal junction, appears to be the focus of the neglect syndrome. Neglect caused by unilateral cooling of either SC or pMS can be reversed by deactivation of the homeotopic or heterotopic contralateral SC or pMS (Lomber & Payne, 1996). Thus, no single structure, unilateral or bilateral, is the 'neglect area', but rather a larger network dynamic underlies the neglect syndrome.

The neural substrate of cat visual hemineglect and its reversal have been the focus of much research (Sprague 1966, Wallace et al. 1989, Wallace et al. 1990, Lomber & Payne 1996, Payne et al. 1996, Hardy & Stein 1988, Durmer & Rosenquist 2001, Jiang et al. 2003, Rushmore 2006, Jiang et al. 2011). Already in 1966 Sprague suggested that there was mutual inhibition between the two SC's. He showed that an intertectal commissure transection was enough to restore visual orienting after unilateral lesion of visual cortex. In the model proposed by Sprague a winner-takes-all phenomenon occurs, where one SC becomes disinhibited by a lack of inhibition coming from the damaged contralateral primary visual cortex. The inhibition is removed either by intertectal commissure transection, or by removal of excitation from the intact visual cortex (including pMS cortex) to the SC ipsilateral to visual cortical lesion and contralateral to the disinhibited SC.

Rushmore et al in 2006 confirmed this cortical imbalance hypothesis using a 2-deoxyglucose (2-DG) technique. This technique involves radio labeled glucose. As

cells metabolize the 2-DG, radioactivity accumulates in the cell and this acts as a marker for metabolism and neuronal activity. Rushmore et al. 2006 show that unilateral cooling of pMS cortex, or to a greater extent unilateral lesion of all contiguous visual cortical areas, leads to a decrease in activity in the superficial

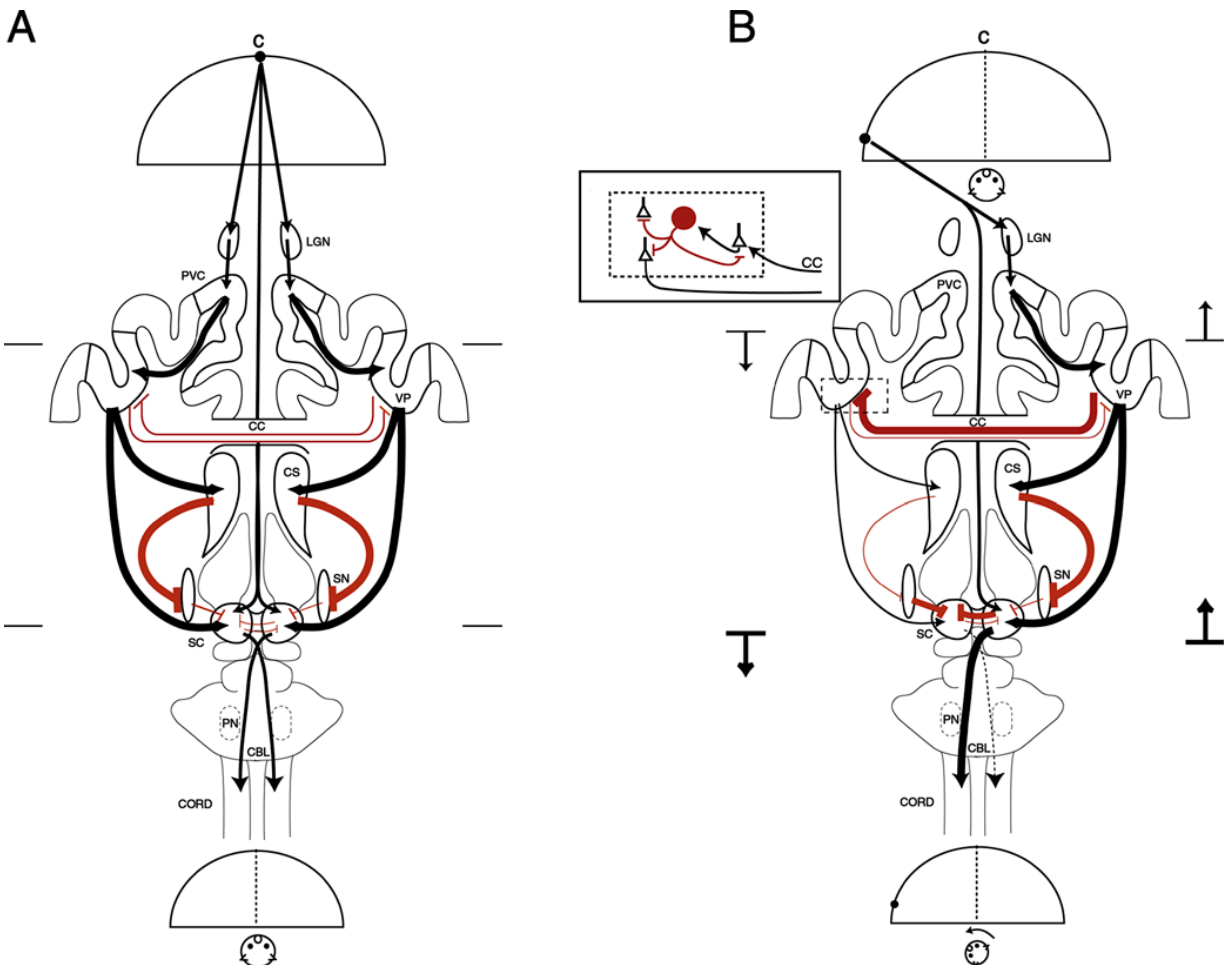

Fig 1.1 – visual orienting network of the cat. The left side, A, is the orienting network when the cat fixates in the middle of a visual perimetry. The right side, B, is the network when the cat reorients to the left. The top semicircle in both A and B is the location of the visual stimulus. Black network connections are excitatory, red are inhibitory. The inset shows corpus callosum (CC) neurons synapsing on inhibitory satellite cells. The vertical arrows in B indicate changes in activity in VP cortex (top) and the SC (bottom) for areas contralateral to stimulation (right arrows) and ipsilateral (left arrows). Abbrevations: PVC-primary visual cortex, VP-visuoparietal cortex, CBL-cerebellum, CS-corpus striatum, CBL-cerabellum, PN-pontine nuclei, SN-substantia niagra. (figure reproduced with permission from Payne & Rushmore 2004)

(primarily visual [Weasel & Illing 1980, Leventhal et al. 1985]) layers of the ipsilateral SC. The SC contralateral to deactivation or lesion revealed an increase in 2-DG uptake in the intermediate (multimodal [Meredith and Stein 1986]) and deep (saccade-related [Stein and Meredith 1991]) layers. Reversal of cortical lesion-induced neglect by contralateral pMS or SC cooling, while still resulting in a slight reduction in SC activity relative to baseline, largely brought 2-DG uptake levels in equivalent layers of both SC's back into balance. A change in 2-DG uptake in the contralateral pMS was not present. Thus, it seems that the SC plays a critical role in neglect and its reversal.

The anatomical connections involved in neglect and its reversal are manifold (fig 2.1). Globally, it appears that mutual inhibition exists between the pMS corticies and between the Superior Colliculi, which can lead to a pathological disinhibition contralateral to unilateral deactivation. A detailed review of this circuit can be found in Payne and Rushmore (2004). In brief, connections between the two pMS corticies run via the corpus callosum and appear to largely be connected via excitatory connections that terminate on local inhibitory cells. These inhibitory cells, in turn, innervate the contralateral pMS thus inhibiting it (Fairen & Valverde 1980, Peters 1984). Direct transcallosal inhibitory connections have also been found between cat primary visual cortex (Peters et al 1990, Buhl & Singer 1989). Connections between visual cortex and the ipsilateral SC, both direct and multisynaptic via the caudate, putamen and substantia nigra, are excitatory (McIlwain 1977, Berson & McIlwain 1983, Royce & Laine 1984, Behan et al. 1987, Berson 1988, Harting 1988, Updyke et al. 1993, McHaffie et al. 1993, Smith et al. 1998, Jiang et al. 2011). Substantial inhibitory

interactions dominate the connections between the superior colliculi (Hoffman & Straschill 1971, Buchtel et al 1979, Waleszczyk et al 1993).

Recently, using orthodromic stimulation in the lateral pMS and antidromic stimulation in bilateral SC while recording from the substantia nigra, Jiang et al 2011 describes a pathway from the lateral pMS cortex, via the striatum and substantia nigra, that provides excitation to the ipsilateral SC and inhibition to the contralateral SC as a result of lateral pMS stimulation. This pathway provides a clear example of how unilateral inactivation of pMS could result in an imbalance in SC activity. Other pathways, as noted above, are doubtless also involved in the cat neglect syndrome.

1.3.3 – Task specific effects of SC and pMS inactivation in the cat

Cats were tested on three behavioral tasks during unilateral and bilateral SC (Lomber et al 2001) and pMS (Lomber & Payne 2001) deactivation with differing results. Task one was a visual perimetry task where the stimuli were inserted through the floor of a visual perimetry apparatus (fig 1.2, A). The second task was the visual perimetry also, but instead of a moving stimulus, a stationary LED was used to indicate where the food reward was located (fig 1.2, B). The third task was a landmark task where the cat had to judge if a small box was closer to the right or the left of a large rectangular testing apparatus (fig 1.2, C). In this landmark task, the cat showed weather it judged the landmark to be on the left or right half of the testing apparatus by approaching the food reward that was hidden on the same side of the testing apparatus as the landmark.

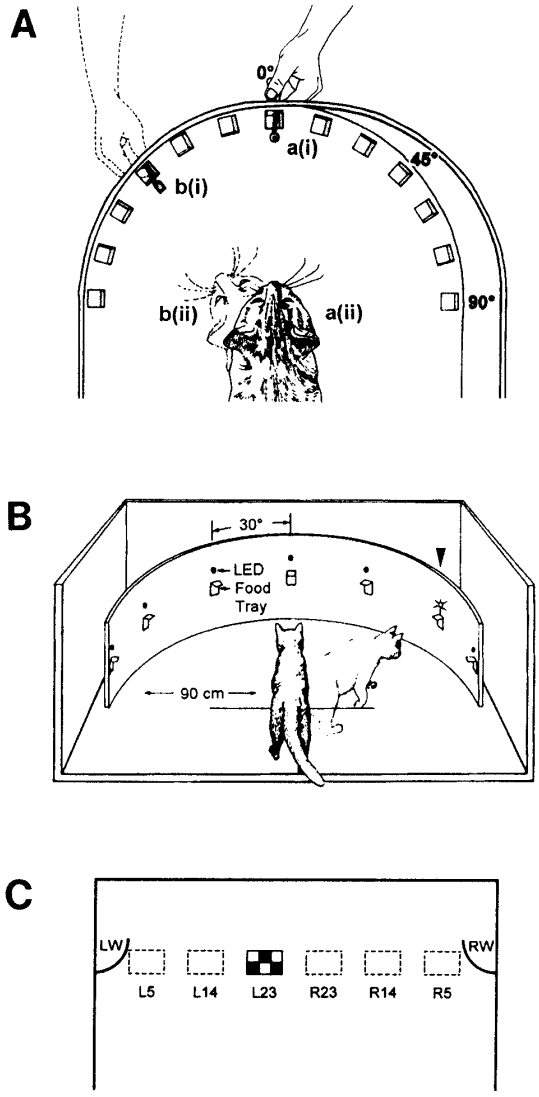

Fig 2.2 – **A**: visual perimetry task with moving stimuli. A love incentive stimuli was introduced in the middle of the arena, a(i), to which the cat attended, a(ii). A second, high incentive stimulus was moved into the visual field, b(ii), to which the cat reoriented its attention, b(ii). **B**: visual perimetry task with static stimuli. This task is the same as in A, except that LED's rather than moving stimuli were used. **C**: the landmark task. A visual landmark was placed 5, 14, or 23cm from the left, L, or right, R, wall of a testing apparatus. The cat indicated weather it perceived the landmark as being more to the left or right by approaching wither the left reward well, LW, or right reward well, RW. (figure reproduced from Lomber et al 2001)

Unilateral SC or pMS deactivation led to a contralateral neglect in all three tasks. Bilateral SC or pMS cooling caused a restoration of performance in the visual perimetry task with the moving stimuli, but a complete loss of bilateral performance in the perimetry task using the stationary LED stimulus. The difference in bilateral cooling between moving and static stimuli is presumably due to the greater salience of the moving stimulus as compared to the LED stimulus. Of note is the similarity in behavioral outcomes for unilateral and bilateral deactivations of the SC and pMS for

both visual perimetry tasks. The deactivation effects were the same for both the SC and the pMS.

The landmark task showed a different outcome between bilateral SC and bilateral pMS deactivations (Lomber et al 2001). Bilateral SC deactivation led to a restoration of performance for the landmark task. In contrast, bilateral pMS deactivation removed the contralateral neglect induced by unilateral deactivation, but reduced behavioral performance to chance. This means that during bilateral pMS deactivation the cat approached the left and right food reward well with equal likelihood regardless of whether the landmark was on the left or right half of the testing apparatus. It can therefore be concluded that though the pMS and SC perform overlapping contributions to visual orienting, they diverge when it comes to the landmark task thereby indicating a more nuanced involvement of the pMS in the analysis of space (Lomber et al 2001).

The results of the landmark task for bilateral pMS deactivation indicate the more complex role cat parietal cortex plays relative to the SC in spatial awareness. This complex role is commensurate with the role parietal lesions play in human neglect. The examples of human neglect described above show that neglect is not just an orienting deficit, but also a general problem with internal spatial coordinates. More abstract theories of parietal cortex in humans formed outside of the realm of neglect research, like the attention to memory hypothesis, may point to an interplay between 1) spatial mapping of environments and 2) episodic and semantic memory. This interplay is not a novel concept. Hippocampal place cells and entorhinal grid

cells map allocentric space, but are also likely involved in episodic and semantic memories (Buzsaki, 2006). Further discussion of the interplay between spatial mapping and memory will be made in the discussion section of this thesis.

1.4 - General build of the cat visual system

Now that the human pathology of neglect and the general mechanisms of neglect in the cat have been introduced, a brief summary of cat visual cortex will be made. With the exception of the pMS and the lateral posterior(LP)/pulvinar complex, Payne & Peters chapter: 'The Concept of Cat Primary Visual Cortex' 2002, contains a good review of the cat visual system leading-up to primary visual cortex. The goal of this review should be to engender a sense of 1) the general build of the retino-genigulate pathway, and 2) show the complexities of intracortical interactions within the visual system, interactions that are complex and poorly understood when compared to retino-geniculate input to the system.

1.4.2 - Retinal ganglion cells

In brief, the visual system starts in the retina with retinal ganglion cells. The major subtypes are: beta - composing 55% of retinal ganglion cells, alpha - composing 5%, and gamma - composing 40% of ganglion cells (Boycott & Wässle, 1974). The gamma subtype can be further broken-down into eta, delta, zeta, and epsilon subtypes (Fig 1.3). As the retinal ganglion cells are placed right after the transduction of photons to biological signals, the structure and physiology of the ganglion cells determine the initial constraints on the visual signal as it enters the visual processing network (Stone 1983, Shapley & Perry 1986, Wässle & Boycott 1991). The beta

morphological cell type, with their dense and circumscribed dendritic arborizations, correspond to the X-physiological cell type. These cells respond with sustained and vigorous firing to high-contrast high-spatial frequency visual stimuli, are densely packed in the central retina, and compose our high-acuity vision (Enroth-Cugell & Robson 1966, Cleland et al. 1979, Peichl & Wässle 1979, Stone 1983). The alpha morphological cell type, with their broad and sparser dendritic arborization relative to X-cells, correspond to the Y-physiological cell type. These cells have transient firing to low-contrast low spatial-frequency visual stimuli (Enroth-Cugell & Robson 1966, Shapley & Perry 1986, Stone 1983, Troy 1987). Y-cells detect stimulus onset well and are involved in coarser, more global aspects of vision. The gamma morphological class of cells corresponds to the W-cell physiological class. This class of cells is

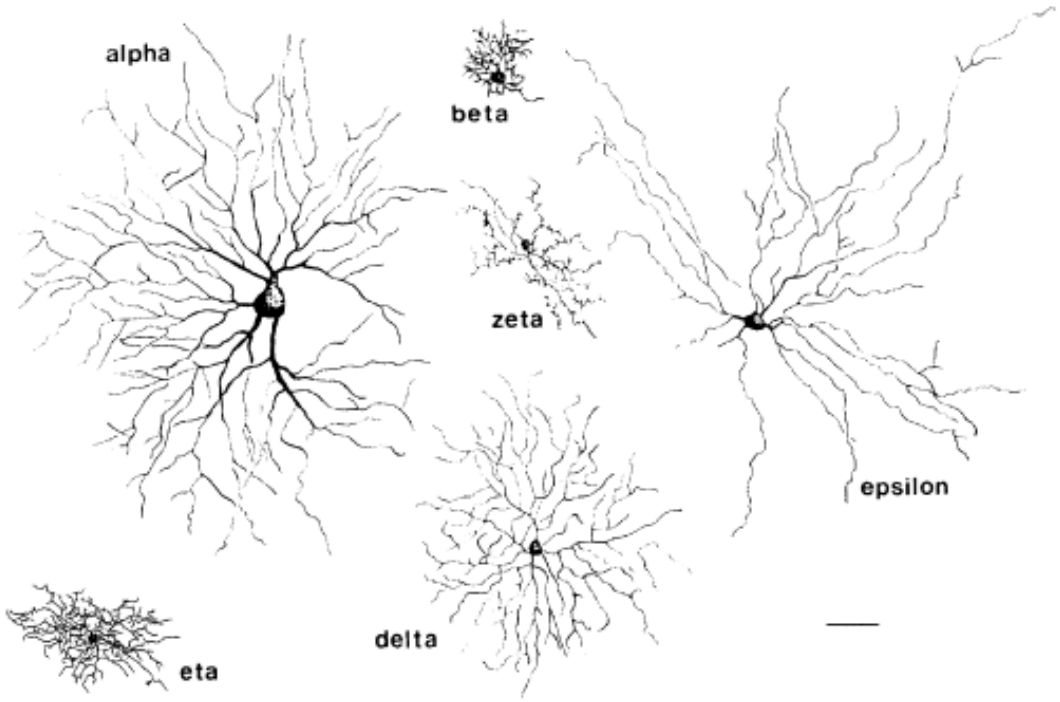

Fig 1.3 – dendritic trees of the various retinal cell types. Cell types delta, eta, zeta, and epsilon are grouped into the gamma class of retinal ganglion cells. (figure reproduced from Berson et al. 1999)

heterogeneous with sluggish responses to visual stimuli and, as a class of cells, are poorly understood (Rowe & Palmer 1995, Berson et al. 1998, Berson et al. 1999, O'Brien et al. 1999, Isayama et al. 2000).

The retinal ganglion cells project primarily to the LGN, the SC, and the pretectum. The pretectum is a midbrain structure involved in the pupilary eye reflex, the optokinetic reflex, and changes to circadian rhythms. The role of the pretectum in profoundly reflexive parts of vision will exclude it from further discussion in this thesis.

1.4.3 - Dorsal Lateral Geniculate Nucleus (LGN)

The LGN is the primary recipient of the retinal ganglion cells. It receives input from the temporal retina of the ipsilateral eye and from the nasal retina of the contralateral eye. Thus, the visual hemifield contralateral to each LGN is represented. The LGN is a layered structure with contralateral X and Y ganglion input going to the top layer, layer A. The second layer, layer A1, receives input from the ipsilateral X and Y ganglion cells. The next more ventral layer is layer Cm. It receives contralateral Y input. The final layer is Cp which receives ipsilateral and contralateral input from W type ganglion cells. All layers contain a retinotopic map of visual space and the retinotopic maps are in register with each other thereby creating conceptual structures termed 'projection columns' (Bishop et al 1962, Sanderson 1971, Payne & Peters 2002). The medial interlaminar nucleus (MIN) is part of the LGN, also has a laminated structure, has retinotopic organization, and contains projections from Y and W retinal ganglion cells (Sanderson 1971). While X and W cells usually innervate a

single layer in the LGN, axons from the Y ganglion cells can contact several layers in the projection column (Bowling & Michael 1984, Sur et al. 1987, Tamamaki et al. 1995, Payne & Peters 2002). A final subsection of the LGN is the 'geniculate wing' (Guillery

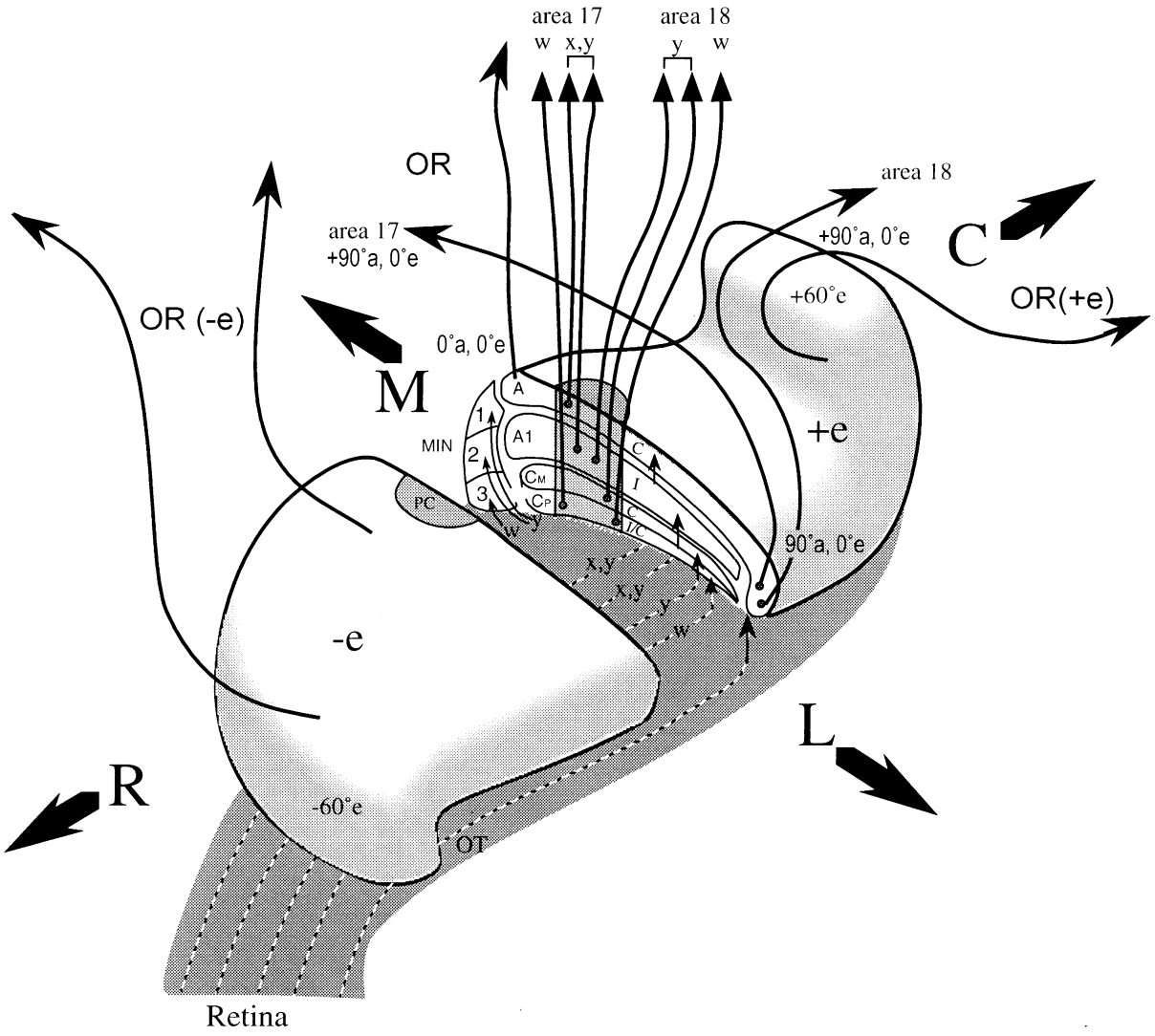

Fig 1.4 - anterolateral view of cat LGN. A cross section of the LGN is visible with the layers A, A1, Cm, and Cp visible. The letters C and I in the layers represent retinal input from the contralateral and ipsilateral eyes. The MIN (medial inter laminar nucleus) is also visible in the cross section. The optic tract (OT) leading from the Retina is under the LGN and the x,y, and w inputs to the LGN are labeled on the OT. The destination of the LGN cells is also labeled (area 17 or 18). The directions in the brain are also labeled (C) caudal, (R) rostral, (M) medial, and (L) lateral. (figure reproduced from Payne & Peters 2002)

et al., 1980) which receives primarily W-type ganglion cells from both eyes (Berman & Jones 1977, Guillery et al. 1980).

1.4.4 - Superior Colliculus

The SC is a layered structure at the roof of the midbrain. It contains retinotopic visual maps in its superficial layers, and auditory and somatosensory maps in the deeper layers (Meredith & Stein 1986). The maps in the various layers are in register allowing the SC to coordinate space in the different modalities. Outputs of the deep layers are involved in orienting behaviors. Projections from the retinal ganglion cells to the superficial layers of the SC include: 100% of Y-cells via collaterals that also go to the LGN, approximately 10% of X-cells via collaterals that also go to the LGN, and 100% of W-cells through either direct connections or via collaterals that also project to the LGN (Illing & Wässle 1981, Sawai et al. 1985, Sur et al. 1987, Hada & Hayashi 1990). The superficial layers of the SC send a large output to the medial portion of the lateral-posterior pulvinar, otherwise known at the tecto-recipient zone (Abramson & Chalupa, 1988).

1.4.5 - Area 17 and 18

Layers A, A1, C as-well-as the MIN of the LGN all send their primary projections to area 17 and 18, which can be grouped together under the label ‘cat primary visual cortex’ (Payne & Peters 2002). Area 17 receives projections from X, Y, and W cells, while area 18 receives input primarily from Y and W cells. Both areas contain retinotopic maps of the contralateral visual field with the common border between 17 and 18 creating a line across which the retinotopic maps in each area form a mirror

image of eachother. The border between 17 and 18 has a transition zone containing a central visual field representation which includes a condensed representation of the ipsilateral visual field (Payne & Siwek 1990). The first point where the signals from both eyes interact is not in the LGN, but rather in area 17 and area 18 (Garey & Powell 1967, Niimi & Sprague 1970, Doty 1971, Payne & Peterson 2002), thus forming ocular dominance columns in primary visual cortex, composed of interdigitating columns with inputs from the left or right eye.

The separation of X and Y input to areas 17 and 18 respectively, is a point of contention when comparing cat data to monkey or human data, where this divergence at the level of the primary visual cortex is not present. It is important, however, to note the diversity of projections to areas 17/18 and the flexibility of receptive field properties. First, a single projection neuron from LGN to primary visual cortex in the cat can send collaterals to both area 17 and 18 (Stone & Dreher 1973, Geisert 1980, Freund et al. 1985, Humphrey et al. 1985). Furthermore, LGN axons may terminate over a space of several millimeters, thus innervating a large part of the map in primary visual cortex (Gilbert & Wiesel 1979, Gilbert & Wiesel 1983, Martin & Whitteridge 1984, Freund et al. 1985, Humphrey et al. 1985). In the case of area 18, this could extend to over half of area 18 (Humphrey et al. 1985). It can thus be said that 'the concept of point-to-point representation in visual pathways is true only in a statistical sense' (Payne & Peters 2002). Moreover, as little as 5% of the synapse in layer 4 in cat primary visual cortex come from the LGN (Ahmed et al. 1994, Peters & Payne 1993). Further confounding the idea of area 17/18 as a point-to-point map of the external visual world are the projections of layer VI cells to the dLGN (Gilbert &

Kelly 1975, Ojima et al. 1996) which could perform stimulus filtering of visual signals at the level of the LGN in the awake behaving animal. Projections from other visual areas in cortex further modulate, perhaps substantially, receptive field properties in areas 17 and 18.

The concept of orientation columns in primary visual cortex has been long established. It describes orientation preferences to visual stimuli for cortical columns in cat primary visual cortex that is overlaid on primary visual cortex spatial maps. A recent study using optical imaging and electrophysiology in the cat further refined this concept (Sharon et al 2007). In this study full screen square-wave gratings as-well-as square-wave gratings occupying only 4 visual degrees were used. Using voltage sensitive dye imaging, It was found that a sub-spiking threshold component was largely correlated with the spatial location but not the orientation of the stimulus, while the supra threshold (spike) component correlated highly with the orientation of the grating. The orientation of the grating for the stimuli contending four visual degrees

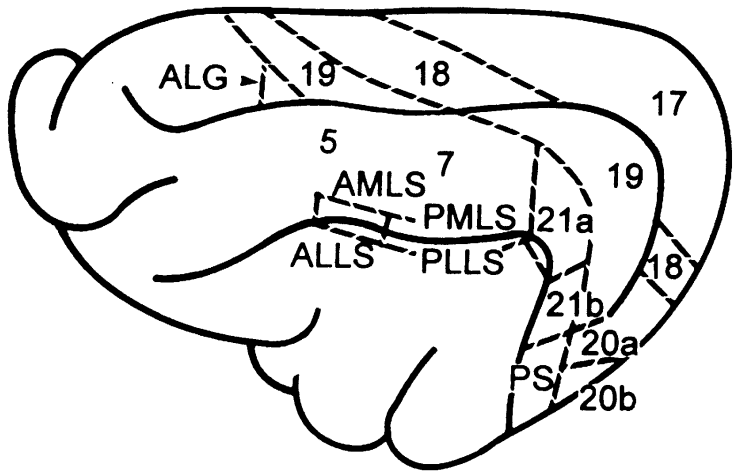

Fig 1.5 - lateral view of the cat brain with all visual areas labeled. Areas 17 and 18 are primary visual cortex. The posterior mediolateral suprasylyian (PMLS) sulcus is a hub for the neglect syndrome in the cat. (reproduced from MacNeil et al 1996)

compromised 4.8% of the total VSD signal for a cortical column, while whole-field gratings had an orientation-related response that was in the range of 20% (Sharon et al

2007), thus four times greater. This indicates the ability of stimuli located outside of a local primary visual cortex receptive field to affect the response of the receptive field presumably through lateral connections.

1.4.6 - MS cortex

The middle suprasylvian (MS) cortex, one of two areas (the other being the SC), deactivated in this thesis, is an area known to be involved in visual orienting, motion discrimination, and the discrimination of moving but not static patterns (Hardy 1988, Lomber et al. 1996). The monkey analogue to cat MS cortex is area MT. MS cortex receives input from areas 17 and 18 (Sherk 1986, Grant & Shipp 1991, MacNeil et al. 1996, Sherk 2010), the LGN (Tong 1982), and the pulvinar (Huges 1980). MS cortex is further subdivided into the posteromedial lateral suprasylvian sulcus (PMLS) and the posterolateral suprasylvian sulcus (PLLS) (Palmer et al 1978). Projections from PMLS to area 18 reveal two feedback streams to area 18: one broad and unspecific, the other more functionally specific (Jaehner et al. 2012). The pattern of connections between PMLS and area 18 is indicative of lateral connections between two areas that are located at the same processing hierarchy level rather than feedback from a higher-order area to a lower-order area (Jaehner 2013).

Both PMLS and PLLS send excitatory projections to the superficial and deep layers of the SC (Harting et al. 1992). Indeed, SC cells with binocular visual fields that are sensitive to visual motion are disproportionately silenced by cooling MS cortex (Stein 1984) showing that these response properties in the SC cells may actually be largely conferred by MS cortex. One anatomical link between MS cortex and the SC

has been shown to travel via the basal ganglia (Jiang et al 2011), an area involved in movement selection, among other things.

Furthermore, PMLS receives direct input from the MIN and C lamina of the LGN (Tong et al 1982). This pathway bypasses area 17/18 and has been implicated in blindsight in humans and monkeys.

1.4.7 - Pulvinar

The pulvinar is a large thalamic nucleus that has been implicated as a relay and coordinator between cortical areas. Among others, it has been shown to be involved in visual salience (Robinson & Peterson 1992). Deactivation of lateral pulvinar in prosimian primates prevents supragranular V1 neurons from responding to visual stimuli. After lesions of LGN neurons, focal excitation of the pulvinar neurons increases responses in V1 receptive fields fourfold. (Purushothaman 2012). There is a direct, electrophysiologically defined pathway from the superficial layers of the SC via the Pulvinar to monkey MT (Berman & Wurtz 2010) which bypasses primary visual cortex. A reciprocal connection, coming from the MT and terminating on the inferior pulvinar appears to confer receptive field properties to the pulvinar neurons (Berman & Wurtz 2011).

1.4.7.2 - Cat pulvinar

In the cat, the volume of the LGN is 39mm^3 (Lee 1999) while the volume of pulvinar is 124mm^3 (Chalfin et al 2007), making the pulvinar three times larger than the LGN. Cat pulvinar entertains strong reciprocal connections with areas 17, 18, and

PMLS (Hughes 1980, Huppe-Gourgues et al. 2006), with individual points in the cortical areas terminating in broad line-shaped termination fields in the pulvinar (Hughes 1980). The SC sends a strong projection to the Lateral Posterior nucleus (LP)-Pulvinar complex which, in turn, sends projections to PLLS (Hughes 1980). Histological examination of the termination patterns of collicular input to the LP, combined with physiological evidence, suggest that an integration of collicular and cortical inputs contributes to the response properties of LP neurons (Kelly 2003).

On a functional level, pulvinar cells respond to veridical (pattern) motion of plaid stimuli (Merabet 1998), and lesions of the pulvinar leads to attentional deficits in the cat (Fabre-Thorpe 1986). Deactivation of the pulvinar in the anesthetized cat causes a break-down in oscillatory activity in areas 17 & 18 (Molotchnikoff & Shumikhina 1996, Shumikhina & Molotchnikoff 1999).

1.5 - Concept of visual cortex

Historical views of neural function have been informed by the fields of machine vision and artificial intelligence (Churchland et al. 1993, Olshausen 2010) and further constrained by the experimental technology available at the time. A more classical view, in line with concepts embodied by researchers such as Hubel and Wiesel in the 1950's and 60's, where a retinal image, recorded in an anesthetized animal, travels up a hierarchy of visual processors through a chain of logical computations to a final image reconstruction, has come to be modified by the inclusion of internal neural states and motivation. Indeed, machine learning attempts to account for "inferential

computation in which data is combined with prior knowledge in order to estimate the underlying causes of a [visual] scene (Mumford 1994, Knill & Richards 1996, Rao et al. 2002, Kersten Mamassian et al. 2004). This is due to the fact that natural images are full of ambiguity. The causal properties of images - illumination, surface geometry, reflectance (material properties), and so forth - are entangled in complex relationships among pixel values. In order to tease these apart, aspects of scene structure must be estimated simultaneously" (Olshausen 2010). The ability of the brain to assess a multivariate visual scene likely requires multiple processing nodes acting in concert. Ouellette and Casanova showed in 2006 in the anesthetized cat, that when stimulus properties are optimized for the following visual areas: area 17, PMLS, LP-pulvinar, AMLS, and AEV, there is no statistical difference in latencies between the areas. The areas, when engaged with their 'preferred' stimulus properties, could function in concert. Recordings in the anesthetized cat have revealed concerted neural activity in the form of synchrony between the SC, pMS, and primary visual cortex (Brecht et al 1998). The simultaneous functioning of multiple cortical nodes combined with internal behavioral motivation of the awake cat, could turn the classily understood processing hierarchy on its head, with internal motivation and neural states driving neural activity and the external stimulus acting as a modifying influence.

1.6 - Oscillations

The nature of the interaction between the numerous neural nodes involved in visual hemineglect is key to understanding the pathology. Neural synchrony, as

evidenced by oscillatory activity in the beta/gamma range (20-80Hz) (Gray et al 1989), provides a likely neural substrate through which attended stimuli can be internally represented by simultaneous activity in multiple network nodes. The binding by synchrony (BBS) hypothesis states that synchronous firing of multiple neurons in the millisecond range can act as an internal neural representation that binds multiple stimulus features into a unified percept.

In the case of visual hemineglect, a failure of the visual network to generate high-frequency oscillations could suppress the ability to bring neglected stimuli into awareness. Visual networks, with their numerous processing nodes, have been trained through experience, with various network nodes sending and receiving input in a behaviorally relevant way. As effective communication within a distributed network relies on precise temporal relationships (Fries 2005, Fries et al. 2007, Fries et al. 2008), a timing disruption in the network responsible for the processing of visual information, though brain damage in the human or neural deactivation in the research animal, may prevent the network from achieving a state where stimuli can be attended, resulting in neglect. The thalamus, with its vast connections to cortex, is a likely network hub that could induce synchrony between distant neural nodes (Uhlhaas et al 2009). Such a V-shaped configuration, with for example the pulvinar connecting two outer network nodes, has been shown computationally to naturally induce synchronization between the outer nodes for any conduction delay between populations (Vicente et al, 2008).

As noted, neglect is a post sensory phenomenon. Though neglect patients are aware of neglected stimuli at some level, they are unable to behaviorally interact with the stimuli. A cat with visual hemineglect will circle in the direction contralateral to the neglected hemifield, thereby displaying an internal state where the cat fails to appreciate the behavioral relevance of the neglected hemifield. Neuenschwander et al (2008) showed in the monkey that gamma oscillations in primary visual cortex were modulated not by the visual stimulus, but rather by a central state likely associated with perceptual readiness. This neural state may not emerge in the visual network in neglect because there is no internal motivation to attend to the neglected hemifield.

1.7 - Dissertation goals

The goal of the current thesis is to investigate the role of oscillations in the neglect pathology. A more classical experimental set-up was initially used, involving the anesthetized cat stimulated with a square-wave grating whose stimulus properties were optimized for primary visual cortex. Deactivations of the SC (project 1) or pMS (project 2) were performed during visual stimulation and oscillatory signals derived from primary visual cortex were compared between the intact visual system and the visual system as it is during visual neglect. The same experimental set-up was then used in the awake cat with only the pMS deactivated (project 3). Finally, as neglect is a network-state involving perception, recordings were made in the awake-behaving cat while it performed a visual perimetry task (project 4). Signals were compared between the normal trials, with all stimuli attended, and the trials where pMS cortex

was deactivated unilaterally and all visual targets contralateral to deactivation were neglected.

Materials & Methods

2.1 - Research model

This doctoral work was performed with 11 cats. All cats were bred at the Max Planck Institute for Brain Research (MPIH) in Frankfurt, Germany. Experiments conformed to stringent German ethical guidelines for animal experimentation as-well-as the global guidelines for animal research set by the Society for Neuroscience.

2.2 - Overview of projects

As each of the four projects in this thesis was an outgrowth of the previous project, this work is organized in the order in which the projects were executed. All four projects involved recording from primary visual cortex. The first three projects were performed with a square-wave grating as a stimulus, while the fourth project was a visual perimetry task. In sum, the four projects were: 1) anesthetized recordings during reversible deactivation of the SC with square-wave gratings as a stimulus, 2) anesthetized recordings during reversible deactivation of the pMS with square-wave gratings as a stimulus, 3) awake recordings during reversible deactivation of the pMS with square-wave gratings as a stimulus, 4) awake recordings while the cat performed a visual perimetry task.

2.2.1.1 - Passive viewing

The passive viewing stimulus used in projects 1-3 had the following properties. It consisted of three phases: a two second gray screen, a two second stationary

square-wave grating, and a four second moving grating (see figure 2.1). The grating was a high-contrast black and white square-wave grating with a spatial frequency of 15 cycles per degree of visual angle. The grating contained four different orientations (0°, 45°, 90°, and 135°) and moved in 8 directions (two orthogonal directions for each of the four orientations).

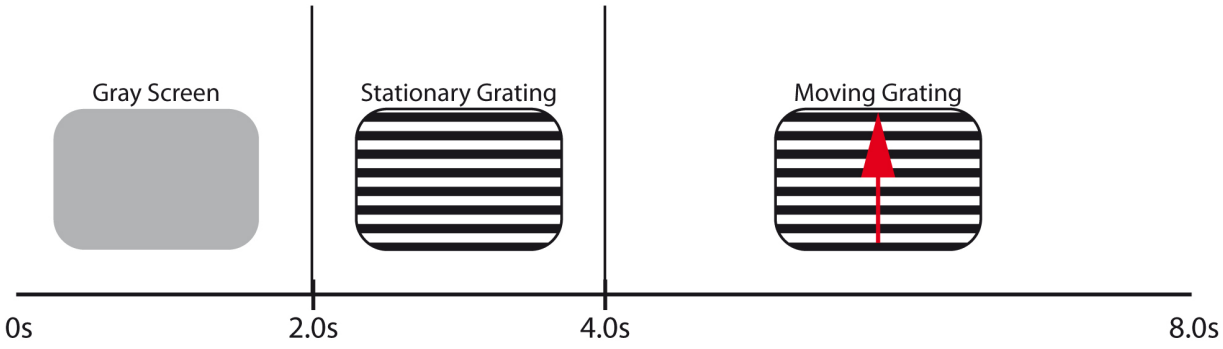

fig 2.1 – the Passive Viewing stimulus. Time in seconds is represented at the bottom. The stimulus period Gray Screen lasts for 2s, Stationary Grating for 2s, and Moving Grating for 4s.

2.2.1.2 - Anesthetized SC deactivation (project 1)

The anesthetized superior colliculus project (project planning, cat training, cryoloop implantation, and data recording) was performed in full collaboration with Boris Ebisch. Raw data from this project was used for the doctoral thesis of Boris Ebisch (Ebisch 2008). The same raw data was reanalyzed with Matlab scripts custom wrote by this author for this thesis.

In brief, three cats were trained on a visual perimetry task. After a short training involving a few weeks, the cats were implanted with bilateral cryoloops (described in 2.3) over the superior colliculus. After recovery from surgery, the cats

were tested in the visual perimerty to confirm that ipsilateral SC deactivation induced a contralateral visual hemineglet. Each cat was then anesthetized for an acute experiment lasting 4-7 days. The visual stimulus was a square-wave grating as described in section 2.2.1.1. Electrophysiolological recordings were made in primary visual cortex using a 32-electrode Eckhorn-Matrix (Eckhorn & Thomas 1993).

2.2.1.3 - Anesthetized pMS deactivation (project 2)

The anesthetized pMS project was performed, beyond cryoloop implantation and minimal advising by this author, by Boris Ebisch and Kirsten Geider and became Kirsten Geider's diploma thesis (Geider 2008) and a part of Boris Ebisch's doctoral thesis (Ebisch 2008). Data from this project was reanalyzed using Matlab scripts coded by this author specifically for the current thesis. Procedures for cat perimetry training, implantation, and data recording are identical to those used for the anesthetized SC project (section 2.2.1.2). The only difference between the projects is that cryoloops were placed in the pMS rather than on the SC.

2.2.1.4 - Awake pMS - passive viewing (project 3)

Since visual neglect is a brain-state involving an awake animal, awake recording techniques were developed for this thesis to assess activity in primary visual cortex during passive viewing of a square-wave visual stimulus (section 2.2.1.1) while the pMS of 3 cats was both active and inactive.

Specifically, prior to electrophysiological recording, 3 cats were trained on the passive viewing task. Training involved placing the cat in a cat restraint bag (KV Pet,

USA). The bag was loose-fitting and allowed the cat to sit comfortably in the sphinx position with the head and tail mobile outside the bag. The cat was then placed in front of the visual stimulus (section 2.2.1.1). It was given drops of milk (Wiskas, Germany) when it sat quietly and looked at the stimulus. When the cat achieved a stage where it could sit quietly in the cat restraint bag with the stimulus running, a headholder was implanted (see 2.3.1). Ten days after headholder implantation, the headholder was fixed to a sterotaxic frame which compelled the cat to look at the stimulus monitor. This was repeated daily with increasing fixation times until the cat could sit quietly with its head immobilized for 45 min, a time window that allowed for stimulus presentation while the pMS was active, inactive, and then re-activated. Since eye-movements in the cat are very limited (Evinger & Fuchs 1978), and the stimulus was the same at any point on the monitor, eye-movements could largely be disregarded for this task.

2.2.2 - Visual perimetry (project 4)

Three cats were trained on the visual perimetry task. A human handler sat behind the cat and guided the cats head so that it looked in the middle of a 180° half-circle visual perimetry. To initiate the beginning of a trial, an LED lit-up in the middle of the 180° half-circle. The LED would remain on, and 1.8s later a second LED lit-up at one of 12 peripheral locations (fig 2.2). The LEDs were placed 15° visually apart with six LED targets on each side of the central fixation point. The cat was trained to immediately reorient its attention at the onset of the 2LED. It would approach the 2LED and receive a high incentive food reward.

Reorientation to the 2LED was assessed by both the cat handler from behind the cat and from the person controlling the stimulus and food reward from the front of the cat. Rapid reorientation to the 2LED, even if it was 15 visual degrees removed from the central fixation 1LED, was done with head movements. This is the case because cat eye movements are very limited (Evinger & Fuchs 1978). The small mass of the cat head makes head movements bioenergetically efficient than they are in larger mammals like humans (Blakemore & Donaghy 1980), and head movements allow visual and auditory maps in the cat brain to maintain a close co-registration (Haris et

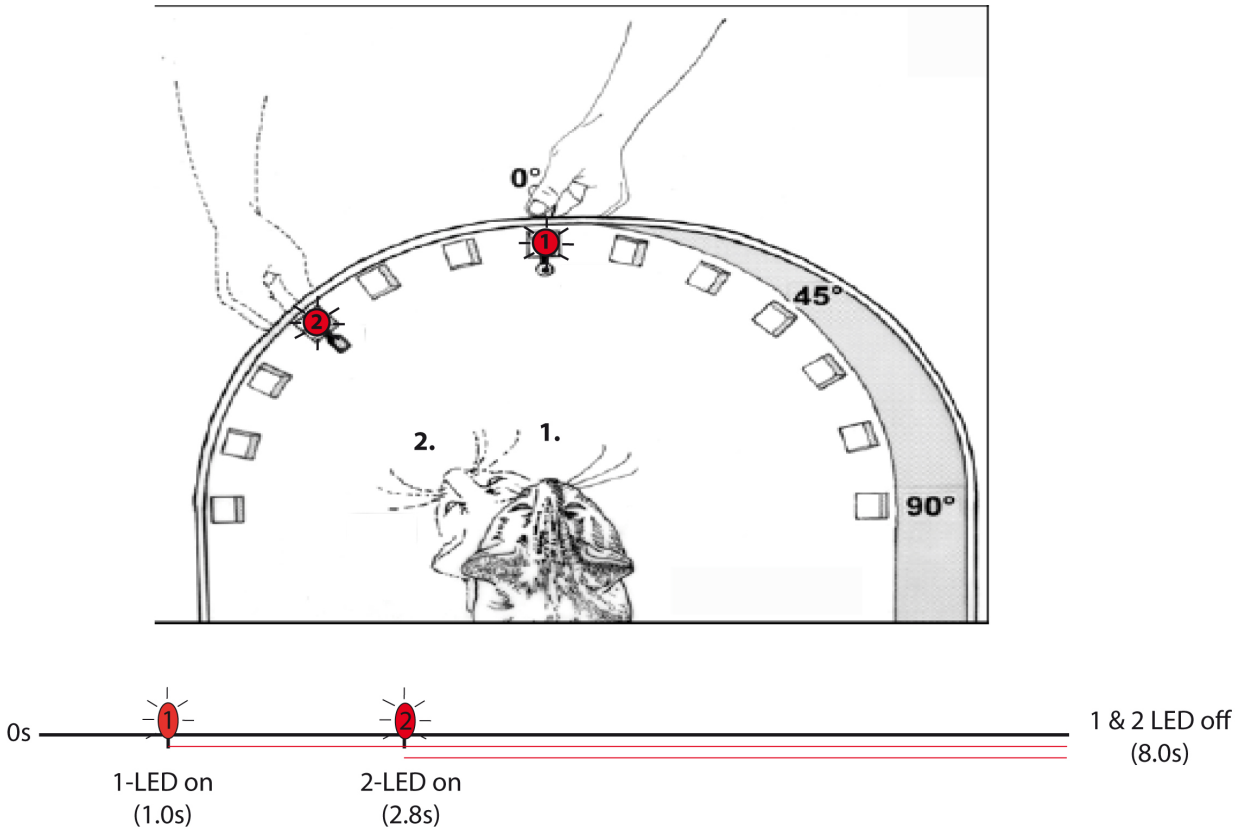

Fig 2.2 - the Perimetry task. Electrophysiological recording began at 0s. A trial was initiated 1s later by the illumination of an LED at 0 visual degrees. 1.8 seconds after the first LED, a second LED lit-up at one of many potential peripheral locations. The cat was trained to reorient its attention to the peripheral LED, approach it, and receive a high-incentive food reward. If the peripheral LED was not attended, the cat was trained to approach the central LED and receive a low-incentive food reward. Both LEDs remained illuminated for the duration of the trial. (modified from Lomber 2001)

al 1980). If the cat did not register the 2LED, as was the case during visual neglect, it was trained to approach the 1LED and receive a low-incentive reward in the form of a piece of dry cat food. If the cat responded to the 2LED, but with a time delay, no food reward was given.

Though the cats appeared to enjoy the task, to keep them motivated for up to 100 trials per day, they were given access to as much food as they wanted for just 1 hour a day after training Monday through Thursday. Food access was unrestricted on Friday afternoon and the weekends, when there was no training. Cats were trained on the perimetry task to a behavioral criterion of 80% correct (fig 2.3).

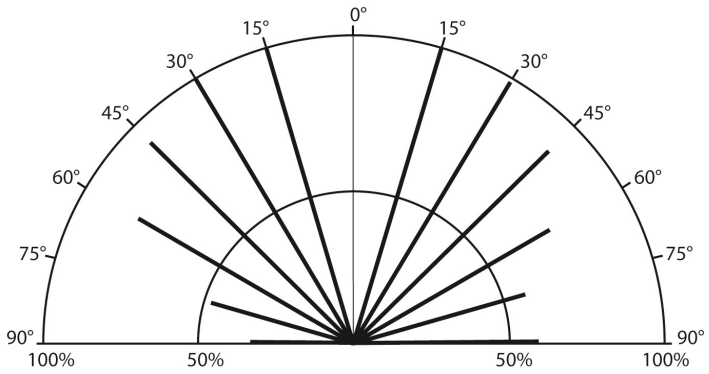

Fig 2.3 - polar plot of behavioral data. The polar plot has the same outline as that of the perimetry apparatus. Starting at the center of the plot and extending towards the locus of each visual stimuli, as indicated by the degree markings on the outside of the outer semicircle, are dark bars that summarize behavioral performance. A performance of 50% correct and 100% correct is shown by the inner and outer semicircles, respectively.

2.2.2.1 - Perimetry Task- potential behavioral outcomes

All behavioral outcomes within a recording session were classified relative to the hemisphere where the pMS was deactivated. Though there were twelve potential behavioral outcomes which can be bundled into three pMS or SC deactivation phases (pMS/SC-active, pMS/SC inactive, and pMS/SC re-activated), with each deactivation

phase containing attended and unattended stimuli in the visual hemifield ipsilateral or contralateral to pMS deactivation, only six behavioral outcomes were analyzed in this thesis work (fig 2.4). These six behavioral outcomes are:

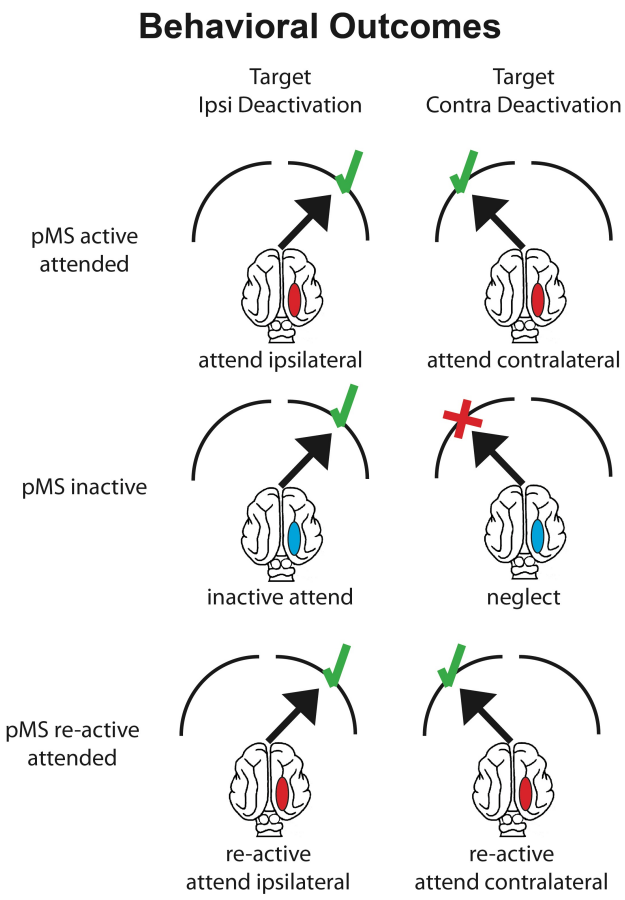

fig 2.4 – six behavioral outcomes for the perimetry task (project 4). Behavioral outcomes were defined relative to the location where pMS was deactivated in the course of a recording secession. The colored oval on the brain represents pMS as active (red) or inactive (blue). The two quarter circles in front of each brain represent visual targets as either ipsilateral (left column) or contralateral (right column) to pMS inactivation. A green check-mark indicates the visual target was attended. A red X represents a visual target that was not attended.

The top two behavioral outcomes are for pMS active and the visual target attended. The middle row shows pMS inactive. In the case of unilateral pMS inactivation, the visual targets ipsilateral to deactivation are attended (middle left icon) while the visual targets contralateral to inactivation are neglected (middle right icon). The bottom row is the same at the top with the pMS bilaterally warm and the stimulus attended.

1) Attend-Ipsi: bilateral pMS active, targets ipsi-deactivation, attended

2) Attend-Contra: bilateral pMS active, targets contra-deactivation, attended

3) Neglect: unilateral pMS inactive, targets ipsi-deactivation, not attended

4) Inactive-Attend: unilateral pMS inactive, targets contra-deactivation, attended

5) Re-active Attend-Ipsi: bilateral pMS Re-active, targets ipsi-deactivation, attended

6) Re-active Attend-Contra: bilateral pMS Re-active, targets contra-deactivation, attended

2.3 - Cryoloop implantation

In order to investigate the interaction between the pMS/SC and primary visual cortex, cryoloops were implanted in the pMS sulcus or on the dorsal aspect of the SC. As first described by Salsbury and Horel in 1983, when the loops are cooled, surrounding neural activity is suppressed. Manufacture and implantation of chronically implanted cryoloops is well described in Lomber et al. 1999. The temperature gradient increases 10°C per mm distance from the cryoloop (Lomber et al. 1996), which means that thermal deactivation is quite localized.

2.3.1 - The cryoloop

The cryoloops were formed using stainless steel tubing (.635mm outer diameter x .33mm inner diameter). The tubing was hand-formed with pliers to form an appropriate shape for the dorsal SC or pMS sulcus (fig 3.2). At the union of the loop, a thermocouple, made by twisting a copper and constantan wire together, was soldiered to the steel tubing. The thermocouple was attached to a subminiature connector (SMP-T, Omega Engineering®) to which a digital thermometer (Model HH25TC, Omega Engineering) could be attached. From the union of the loop to the thermometer plug, the methanol inlet/outlet tubes and thermocouple wire were wrapped in a heat-shrink Teflon tube to thermally insulate them from the environment. A threaded metal cylinder was placed over the inlet and outlet tubing to which a protective cap could be screwed. Dental acrylic was used to bind the plug, metal tubing, and threaded

cylinder together. Finally, the ends of the tubing were cut leaving a 3mm length exposed to which plastic tubing could be attached.

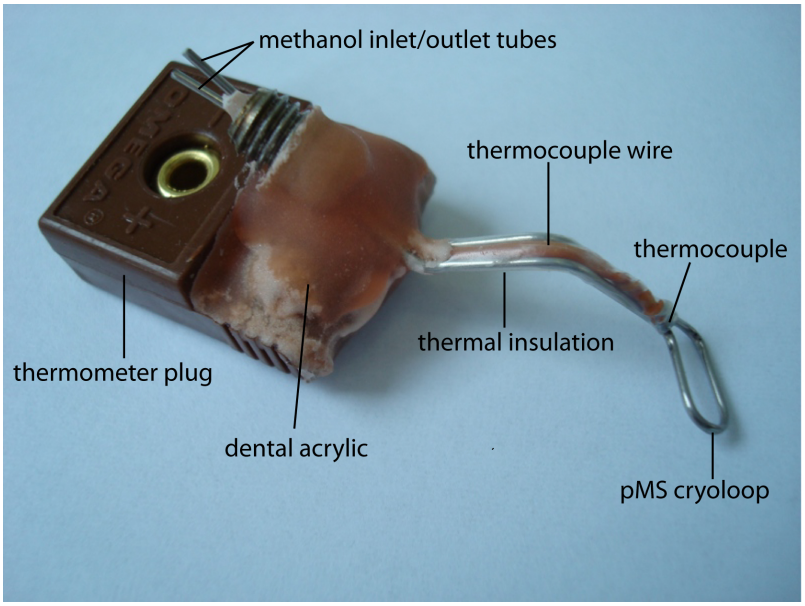

Fig 2.5 – the cryoloop. The shape of the loop itself (labeled here: pMS cryoloop) is shaped to conform to the area which is to be implanted. A thermocouple is placed at the union of the loop to monitor temperature at the locus of cooling. Metal tubing between the loop and the thermometer plug are thermally insulated. Dental acrylic binds the various components together. Plastic tubing can be attached to the methanol inlet/outlet tubes. The thermometer plug allows for a temperature-readout of the thermocouple measurements.

2.3.2 - Cooling system

The system to control the temperature of the cryoloop included a methanol reservoir, plastic tubing and a pump as described in Lomber et al 1999. The speed with which the methanol was pumped determined the temperature of the cryoloop thereby controlling pMS cortex deactivation.

2.4 - Electrodes

Electrophysiological recordings in the awake cats (projects 3 & 4) were made with Plextrode® Floating Microelectrode Arrays (FMAs) from the firm Plexon Inc. (Dallas, USA). The FMA consisted of 14 platinum-iridium electrodes attached to a 2mm^2 ceramic substrate (fig 2.6). One of the 14 electrodes was a reference electrode

with a resistance of 5kΩ and another was a ground electrode. The remaining 12 electrodes were for recording neural signals and had alternating lengths of 1.0 and 1.5mm, were spaced .40mm from each other, and had a resistance of 1MΩ. The bundle of electrode wires exited the ceramic backing and were connected to a Plexon omnetics® connector through a gold-colored wire.

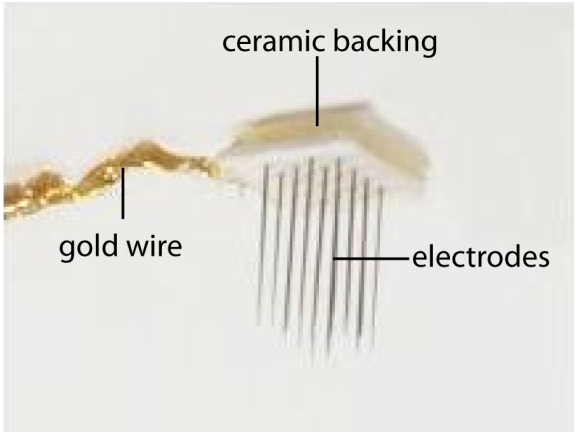

Fig 2.6 – Floating Microelectrode Array (FMA).

2.3.0 - Surgeries

The surgeries were completed in multiple phases for both the Arena and Passive Viewing tasks. Cats involved in the Perimetry task (Project 4) required two surgeries. The cryoloop implantation was followed by a 2 week period where it was confirmed that the cat had a complete contralateral visual hemineglect during unilateral pMS deactivation. By staying vigilant in the days immediately following implantation for circling, a behavior where the cat ignores contralesional visual stimuli and consistently turns in the ispilesional direction, it was also confirmed that no lesion had been induced by implantation. During cryoloop implantation a headholder was also

implanted and a craniotomy was made over the prospective implantation site of the FMAs. The craniotomy for the FMA's was covered with a titanium ring (inner diameter 20mm) and a Plexiglas lid that could be easily removed for FMA implantation. The second surgery only involved removing the Plexiglas cover and implanting the FMA, thus stress to the cat and trauma to neural tissue were minimized for the second surgery.

For the Awake Passive Viewing task (Project 3), the cryoloop and FMA implantations were similarly separated into two surgeries. However, due to the need for head fixation during the Passive Viewing task, the headholder was implanted in a seperate procedure before either the cryoloops or FMAs were implanted.

The goal for both the awake-Passive Viewing and Perimetry tasks was to implant the FMAs in well-trained cats and with minimal surgical trauma so that electrophysiological recording could start ~1-2 days after implantation.

2.3.1 - Surgery initiation

Surgeries for both anesthetized and awake projects were initiated by an intramuscular injection of ketaminhydrocloride 10mg/kg bodyweight and xylazinhydrochloride (Rompun® 2%) 1mg/kg bodyweight. Ketamin was applied to block NMDA transmission while Rompun acts as a muscle relaxer and analgesic. Atropinesulfate .1mg/kg bodyweight was also administered to prevent circulatory disturbances.

Cats were then intubated and maintained on a mixture of 70% N_20, 30% O_2, and 1.0-1.3% Halothane. The respiration pump (models 665 or 683, Harvard Apparatus, USA) was set to approximately 15 cycles/min at a volume of 50ml-60ml per cycle. Respiration pressure and exhaled CO_2 was continuously monitored (DASH 3000, GE Healthcare, Germany). Endtidal CO_2 concentration was maintained at 3%.

The cat was placed in a sterotaxic device as described by Horsly and Clarke. Body temperature was maintained through a heating pad placed under the cat whose temperature was controlled through feedback provided by a rectal thermometer. The EKG was monitored by two needles placed on either side of the thorax which fed into a differential amplifier (AM502, Tektronix®, USA) and could be visualized on an oscilloscope. A venous catheter was inserted which supplied the cat continuously with physiological saline solution (0.9% at 3ml/s) and provided fast route to administer medications in the case an emergency were to have arisen.

2.3.2 - Headholder implantation

After the cat was placed in the stereotaxic frame and was stably anesthetized, as indicated by a stable heart rate and the level of Halothane exhaled, sterile operating room conditions were introduced. A midline incision was made on the top of the skull behind the eyes and the skin and muscle were retracted. Approximately seven small titanium screws were implanted above the frontal sinus and a headholder was attached to the screws with dental cement (Paladur®, Heraeus Kulzer GmbH, Germany). For cats involved in project 3, surgery was concluded and post surgical procedures were performed (see section 2.3.5). For cats involved in the anesthetized

(projects 1 & 2) and Perimetry (project 4) tasks, cryoloops were also implanted in the same surgery as the headholder.

2.3.3 – SC cryoloop implantation

Implantation of the SC cryoloop was accomplished by making two craniotomies on either side of the midline immediately anterior to the junction of the bony tentorium and the skull. The cat was infused for ~40min with 60ml/h mannitol (Mannit-Solution 20%, Serag-Wiessner, Germany). This slightly dehydrated the cortex and allowed the SC to be visualized by retracting the posterior aspect of the cerebral cortex. At the base of the bony tentorium, the SC could be visualized and the cryoloop placed on its superficial aspect. Titanium screws were inserted in the skull above the cerebellum and the cryoloop was fixed to the skull with dental cement.

2.3.3.1 – pMS cryoloop implantation

Immediately after retracting the muscle, the pMS sulcus was often visible through the skull bone. This, along with the sterotaxic coordinates P3-A9 and L10-L16, were used to find the location of the pMS sulcus. The ring was centered on the midline at A3. The outline of the base ring (see above) was also marked on the skull. The chamber was used to make the subsequent implantation of the FMAs, which was performed ~2 weeks after cryoloop implantation, easier to perform and less traumatic for the cat.

After marking the location of all craniotomies, a small craionotomy was made over both pMS sulci and the bone was removed. The dura mater over the sulcus was

retracted and the arachnoid opened. Cooling probes were carefully implanted in the sulcus with one end of the cooling loop at the anterior bend of the sulcus. Small titanium screws were placed in the skull lateral to the pMS craniotomy and dental acrylic was used to bind the cryoloop to the screws. Following cryoloop implantation, the craniotomy was filled with gelfoam and dental acrylic was used to cover it. Upon successful implantation and mounting of one cryoloop with dental acrylic, the other pMS was implanted (fig 2.7).

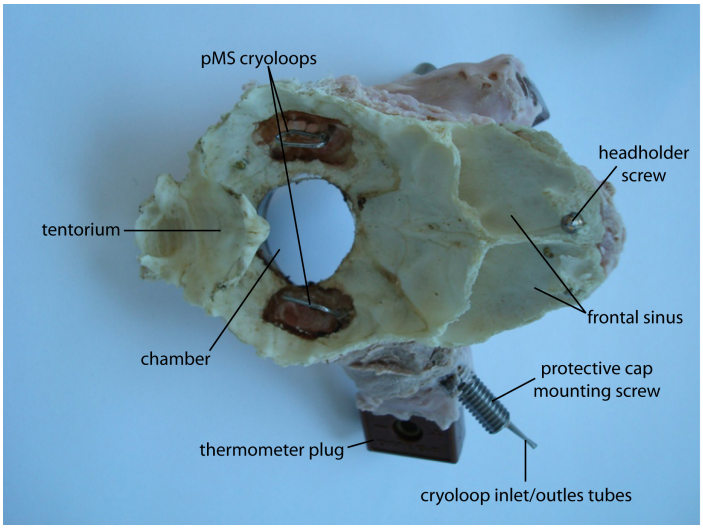

fig 2.7 – implant, bottom view. The anterior of the implant is to the right where the frontal sinus is. Craniotomies for the chamber and pMS probes are evident. Two pMS cryoloops are evident without the surround neural tissue

2.3.4 – Base ring implantation

To make future implantation of FMAs easier, a metal base ring was implanted over area 17/18. A round craniotomy was made with a diameter of radius of 10mm centered at the midline and a3. The base ring was placed over this and fixed to the skull with titanium screws and dental acrylic (fig 2.8). A clear Plexiglas cover was custom made to fit snugly over the base ring and was tightly sealed with wax and fixed with dental acrylic. The middle of the cover had a small screw that could be removed

to allow administration of antibiotics and to alleviate brain pressure in case of infection. The surgery was then brought to an end and post surgical measures were performed as described in section 2.3.5

2.3.5 - FMA implantation

Before FMA implantation, for cats involved in both the Passive Viewing and Perimetry tasks, it was confirmed that the cryoloops induced a visual hemineglect in the perimetry. The cats involved in the Passive viewing task were only briefly trained and tested on the Perimetry task. Confirmation was made that targets contralateral to unilateral pMS deactivation were neglected in the Perimetry. Only after confirming the function of the cryoloops and confirming that the cats could perform either the Perimetry task or the Passive Viewing task with ease during pMS or SC deactivation, were the FMAs finally implanted.

To begin the FMA implantation surgery, cats were anesthetized and placed in a sterotaxic frame as described in section 2.3.1. Instead of inserting earbars, eyebars, and a palate clamp, the cats head was fixed with the headholder. The omnetics® (Plexon, Dallas, USA) connector encased in a metal casing was fixed to the implant lateral to the chamber with dental acrylic. The thin layer of dental acrylic placed on the base ring Plexiglas cover was then was carefully drilled away from the rim of the chamber and the lid removed. Using a combination of the sterotaxic location of the area 17/18 boarder, landmarks in the brain, and avoidance of blood vessels, the FMA's, which were attached to the omnetics® connector by a 2cm long gold wire, were then maneuvered into position over the cortex using suction to a vacuum insertion tool

(Plexon, Dallas, USA). 38°C physiological saline was then administered to the FMA to remove the sucrose that protected the electrode tips. Upon insertion in cortex, a small amount of tissue glue was administered to hold the array in place. The wires connecting the FMA to the omnetics® connector were placed in one of the base ring exits. After the FMA was implanted in each of the two hemispheres, the Plexiglas cover was snapped into place on the chamber and sealed with dental acrylic (fig 2.8). Following bilateral implantation and while still under anesthesia, receptive fields were mapped to confirm that the FMAs were indeed implanted in the central visual field.

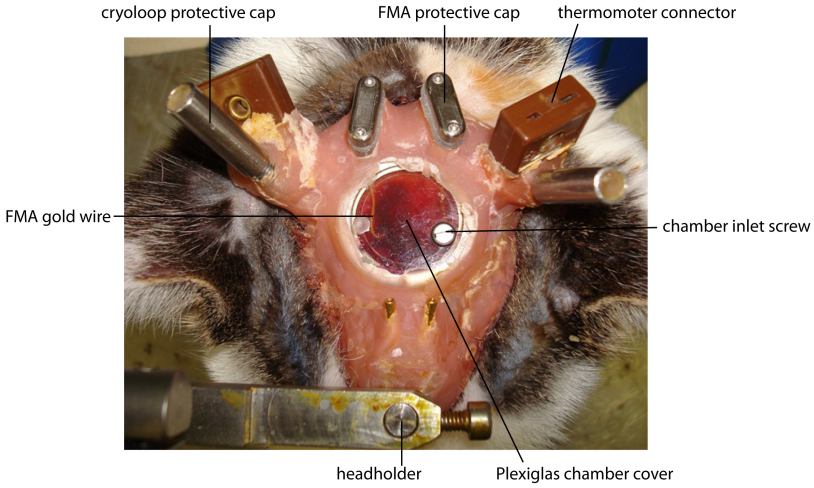

Fig 2.8 – implant, top view. This is how an implant looked following all surgical procedures. The headholder is located anterior over the frontal sinus. The poster medial region has the connectors for the FMAs. The lateral posterior region has the pMS cryoloops while the central region of the implant contains the chamber. A gold wire connecting an FMA to an omnetics connector is visible through the Plexiglas chamber cover.

2.3.6 - Post surgery care

At the close of surgery, to compensate for loss of fluids, the cats received 10ml 10% glucose and 10ml Tutofusin®K10 (Baxter, Germany) subcutaneously. The long-acting broadband antibiotic cefovecin (Convenia, Pfizer, Germany) 8mg/kg bodyweight injected subcutaneously was also administered. In the case of the cats involved in the awake recordings (project 3 & 4), the chamber was filled with clear agar and chloramphenicol (Kemicetine, Pfarmacia, UK) to help prevent infection. As an analgesic, carprofen (Rimadyl, Pfizer, Germany) .1ml/kg body weight was

administered subcutaneously on the day of the surgery and on each of the two following days.

2.4 - Electrophysiological set-up and data acquisition

The anesthetized recordings (projects 1&2) were performed with a 32-electrode Eckhorn-Matrix (Eckhorn & Thomas 1993). The signal was preamplified 20x then sent to the main amplifier (MCP-Plus, Alpha Omega Engineering, Israel). To this end, a recording chamber was mounted on top of the base ring.

The electrophysiological set-up for both the Awake Passive Viewing (project 3) and the Perimetry task (project 4) was the same, but different from projects 1 & 2. From the omnetics® connector on the implant, a 20x gain preamplifier was attached (fig 2.9). As the preamplifier easily came unplugged, a small ring of dental cement was put around the preamplifier which enabled it to be screwed to the implant during recording. Approximately 2 meters of cable separated the preamplifier from the main amplifier (MCP-Plus, Alpha Omega Engineering, Israel).

The data acquisition chain starting at the MCP-Plus is the same for all four projects. The MCP further amplified the signal another 100 times for a total signal amplification of 10,000. The main amplifier also performed a high-pass filtering of 800-5000Hz. A separate filter (built by the Max Planck Institute for Brain Research) received the raw unfiltered neural signal from the main amplifier and performed a low-pass filtering of 0-800Hz. The low-pass and high-pass signals were then sent to the analogue to digital (AD) converters (power 1401 and Power 1401 mk II, Cambridge Electronic Design Limited, UK). The low-pass signal was digitized at 2,000hz and

became the digital LFP signal. The high-pass signal was digitized at 22,000hz and became the digital spike signal. The AD-converters were controlled by the data acquisition software Spike2 (version 4.01, Cambridge Electronic Design Limited, UK).

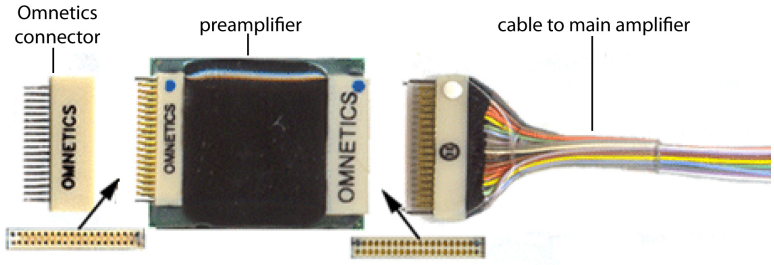

Fig 2.9 – Plexon preamplifier. The omnetics connector (left) was fixed in the implant with dental acrylic. The preamplifier (middle) amplified the signal 20x directly at the implant. A Plexon cable (right) transmitted the 20x amplified signal to the main amplifier.

A trigger was sent to Spike2, the acquisition software, from the stimulus computer at the beginning of each Passive Viewing (projects 1-3) or the Perimetry task trail. The trigger initiated an 8s long data acquisition period by Spike2. The 8s data acquisition period was punctuated by two time stamps. The stimulus computer for the Passive Viewing task sent a TTL pulse to Spike2 at the transition of the stimulus from gray screen to static grating and another TTL pulse at the transition from static grating to moving grating. The TTL pulses were similarly sent from the stimulation apparatus for the Perimetry task to Spike 2 at the onset of the first LED and another at the onset of the second, peripheral, LED. These TTL pulses set a precise time stamp in Spike2 which allowed for the creation of different time windows around which different data analysis windows could be created.

2.5 - ERP

Event related potentials (ERPs) are present in the network-reorganization stage immediately following a change in external stimulus. There were two ERPs for the Passive Viewing Task: ERP1 resulted from a change in gray screen to static grating and ERP2 resulted from a change in static grating to moving grating. The Perimetry task also had two ERPs: ERP1 followed the first LED and ERP2 following the second LED. These potentials were labeled 'P' for positive, 'N' for the negative. The 1) area under the curve between the portions of the curve more extreme than voltage=0 and the peak amplitude and 2) latency of the peak amplitude were computed. These two metrics, area-under-the-curve and latency, were compared between pMS-active, pMS-inactive, and pMS-re-active conditions.

For the Passive Viewing task, the area under the curve for ERP1 and ERP2 for the pMS active condition was set at 100. The change in the area when pMS was deactivated and then re-activated was expressed as a percent change relative to pMS active. Comparisons were done within ERP1 and again within ERP2. Latency changes in the peak amplitude of ERP1 and ERP2 were similarly normalized to the pMS-active condition.

Perimetry-task ERP baseline activity was defined as trials where the pMS had yet to be deactivated (pMS-active) and the cat reacted to the 2LED. This baseline activity was compared to Inactive-Attend, Neglect, and Re-active-Attend trials (see diagram of behavioral outcomes, fig 2.4).

All comparisons for both the Passive Viewing and Perimetry tasks were performed within each electrode. As signal-to-noise was poor in the awake animal,

the generation of a clear ERP required averaging across all recording days. Therefore an n of only 3, one for each for the three cats, was possible. Standard-error-of-the-mean bars were placed on the ERP graphs to signify how reliable the result was between cats.

2.6 - LFP

The local field potential (LFP) signal was separated into different frequency bands by applying a Fourier transform (FT) for induced activity (Tallon-Baudry and Bertrand 1999), and assessing the power of each frequency band. The frequency bands were defined as follows: delta 1-3Hz, theta 4-8Hz, alpha 9-14Hz, beta 15-21Hz, gamma1 22-48Hz, and gamma2 52-90Hz. Induced activity is defined on the computational level as the place where the FT is performed relative to raw-signal averaging. As opposed to Evoked activity, where the FT is performed after averaging of multiple trials to yield stimulus-locked activity, induced activity is the product of performing a FT for each trial then averaging the resulting FT vectors across trials. Induced power, being the result of a spectral analysis of each individual trial, contains not only evoked, stimulus-locked power, but also power components from ongoing activity that may not be the result of time-locked changes in the visual stimulus.

For the Passive Viewing task, the FT analysis window (AW) was either: 1) 1000ms - for the gray screen, static grating, and moving grating, or 2) 250ms - for the time periods immediately following the change from gray to static gating and the change from static to moving grating (fig 2.10). Delta-band activity could not be computed for the 250ms AWs due to the nature of the FT algorithm. Perimetry task FT

analysis windows were 250ms long and were constructed in the 250ms immediately before and immediately after both the 1LED and the 2LED (fig 2.11).

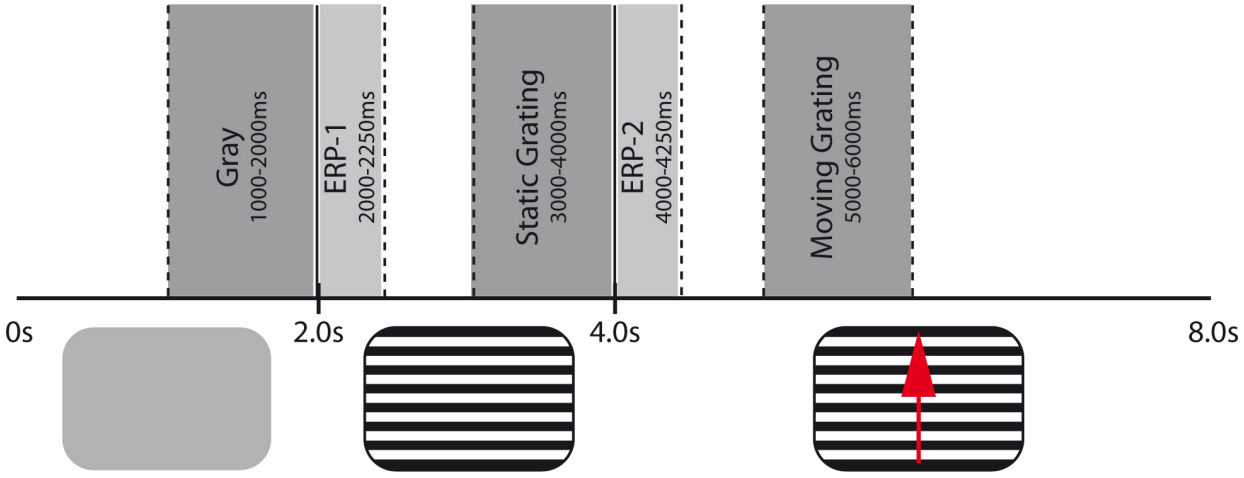

Fig 2.10 – Passive Viewing task analysis windows (AWs). Five AWs were created. Three AWs – 'Gray', 'Static Grating', and 'Moving grating' - were 1000ms in length. Two AWs – 'ERP-1', and 'ERP-2' – were 250ms in length.

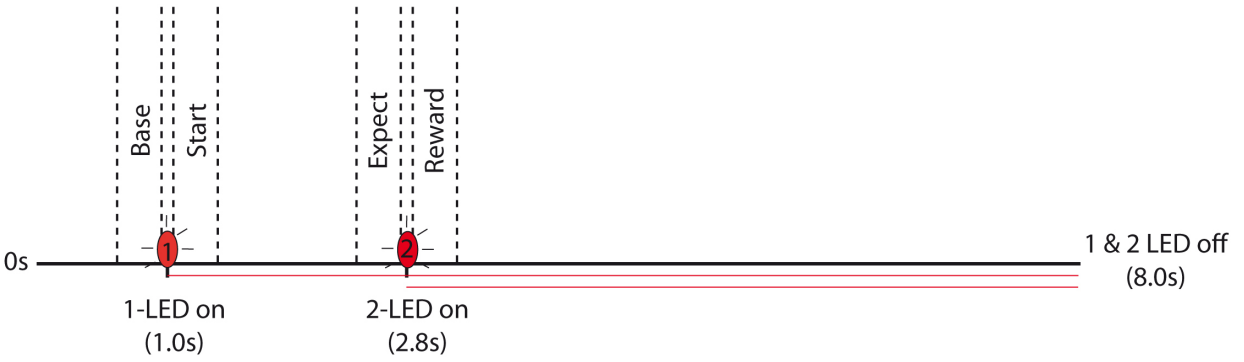

Fig 2.11 – Perimetry task analysis windows (AWs). Four AWs of 250ms length were created. The Base AW was the 250ms immediately preceding the onset of the 1LED. The Start AW was the 250ms immediately following the 1LED. The Expect AW was the 250ms immediately preceding the onset of the 2LED while the Reward AW was the 250ms immediately after the onset of the 2LED.

2.6.1 – Between cooling condition normalization (analysis 1)

Analysis 1 normalized LFP power for the pMS/SC inactive and re-active conditions to the pMS/SC active condition. For the perimetry task, baseline was defined as the trials where the pMS was active and the stimulus was attended to. Passive viewing task baseline was the trials where pMS or SC was active before being inactivated and then re-activated. The normalization was performed as such: 1) a FT was made on each trial within each AW. 2) Power within each frequency band was summed to create a single power value for each FB. 3) Within each FB, power was averaged across trials for each deactivation condition in the Passive Viewing task, or within behavioral outcome in the Perimetry task. 4) It was assessed whether the baseline power value or the experimental-condition (Inactive or Re-active) power value was larger. 5) The smaller value was divided by the larger value yielding a number between 0 and 1. 6) One was subtracted from the resulting value and that number was multiplied by 100. The end value was the amount, expressed as a percent, by which the larger power value was bigger than the smaller value. 7) If baseline (pMS active) power was greater than the experimental-condition power, as assessed in step 4, the percent change was multiplied by -1.

This final percent change value is the number that appears in the results section. A positive value expresses the amount in percent that power in the experimental-condition exceeded baseline (pMS active) power. A negative value expressed the amount that experimental power was less than the baseline power. The need to switch the position of the numerator and denominator in step 4 arises from

the fact that a simple percent change computation ([experimental condition / baseline] * 100) where the numerator and denominator are fixed, can yield an infinite increase, but only a finite decrease in power, with zero as a lower bound. Moreover, in the absence of dynamically altering the numerator and denominator as in step 5, a +50% and -50% change in power are not equivalent measures when the absolute value is taken, which shows the measure to be nonlinear. By placing the experimental-condition value in the denominator when it is larger, and then multiplying the end result by negative one, reductions in the experimental-condition power relative to baseline can be given values with negative infinity as a lower bound rather than zero.

2.6.2 – Between analysis window normalization (analysis 2)

Analysis 2 normalized LFP power by using the initial analysis window in each task, Gray for the Passive viewing, and Base for the Perimetry task, as the baseline power value. This normalization allowed for the assessment of power changes within a trial. By normalizing within a trial, changes in power already present in the Grey or Base AW, changes due to cooling or motivational state, could be controlled for. This analysis was performed exactly as in Analysis 1, with the exception that the initial AW within each trial was the baseline measurement rather than the initial pMS/SC-Active condition. The numerator and denominator in the percent change calculation were similarly dynamically chosen.

The resulting graphs show the power changes in the 1) Passive Viewing task with respect to the Gray analysis window for the ERP-1, Static Grating, ERP-2, and Moving Grating AWs, and in the 2) Perimetry task with respect to the Base AW for the Start,

Expectation, and Reward AWs. Positive values indicate the percent increase in power over baseline, while negative values indicate the amount that baseline power exceeded power in the respective AW.

2.6.3 - Statistics

For both Analysis 1 and Analysis 2 calculations, the Kolmogorov-Smirnov test was first used to confirm that the distributions were normally distributed. The distributions were indeed normally distributed in all cases with a p-value exceeding 0.01.

2.6.3.1 – Analysis 1 statistics

To test weather power changes during Inactive and Re-active phases were significantly different from Active, two criteria were set: 1) all cats must have had power changes of the same sign relative to Active (all cats had an increase in power or all had a decrease), and 2) Each cat had to individually pass a 1-tail t-test with $p<.05$. Only if all of the cats had a value less than .05 was the statistical criterion met.

In a similar fashion, it was tested weather power in the Inactive condition was different from the Re-active condition. As above, the direction of change had to be the same for all cats, and the change had to be significant for each cat individually ($p<.05$ 1-tail T-test).

2.6.3.2 - Analysis 2 statistics

The Analysis 2 normalization tested first if the stimulus caused any change in power relative to baseline (Gray-AW for Passive Viewing, Base-AW the Perimetry task)

for the Active condition. Thus, a red asterisk (for Active) was given to a frequency band if all three cats individually had a value larger or all three cats had a value smaller than baseline. The significance of the change for each cat had be more extreme than p= .05 using a 1-tail T-test. Second, a test was made to ascertain if the Inactive (blue open squares in the figures) and Re-active (green open squares) conditions caused changes in Analysis 2 power relative to the Analysis 2 Active power. Significance was achieved, as described in the Analysis 1 Statistics section, if all three cats had an increase in power or all three cats had a decrease in power relative to the Active condition. The changes relative to warm for each individual cat had to be more extreme than p=.05 using a 1-tail T-test.

2.7 - Perfusion

At the end of experiments, the cats were first anesthetized with ketamine, then sacrificed with an intravenous injection of 200 mg/per kg bodyweight of sodium pentobarbital (Narcoren®, Merial, Germany). Upon cardiac arrest, the cats were transcardially perfused with a buffered paraformaldehyde solution. The perfusion solution was then switched to 4% paraformaldehyde in saline phosphate buffer. The cat was perfused with this solution for approximately 15min. Following perfusion, the brain was carefully removed for further histological examination.

.2M phosphate buffer (PB)	
$Na_2HPO_4 \cdot 2\ H_20$	28.8g
$Na_2HPO_4 \cdot H_20$	5.2g
distilled H_20	1000ml

Saline Phosphate Buffer Solution (.9% NaCl in 0.1M phosphate buffer, pH 7.4)	
Distilled H_20	1000ml
NaCl	18g
.2M PB	1000ml

Fixative (4% Paraformaldehyde in phosphate buffer, pH 7.4)	
Paraformaldehyde	80g
NaOH	few drops
Distilled H_20	1000ml
.2 M PB	1000ml

2.8 - Histology

To determine the state of cortex following cryoloop implantation and cortical deactivation, a Nissl stain was applied. The Nissl stain dyes ribonucleotides in the cell nucleus and rough endoplasmic reticulum which leads to a differential staining of gray and white matter.

Coronal slices of the cortex were made which revealed the health of the tissue that had been adjacent to the cryoloop. The histological process began with blocking the brain, a term for isolating the brain area of histological interest by removing unneeded brain tissue and leaving a flat plane along which the brain can be sectioned, which was in our case the coronal plane. In order to remove water which could damage tissue upon freezing, the tissue block was allowed to soak in a 20% sucrose solution until the tissue sank to the bottom of the solution thus indicating that the tissue had been fully immersed with the solution. The tissue was frozen to a cryotom (Autocut 2040, reichert-Jung, Germany) and 50μm thick sections were made and stored on a phosphate buffer solution. Sections were then mounted on poly-L-lysine coated slides and left to dry. In order to achieve a more intensive staining, slides where moved through alcohol baths of descending concentration then incubated in a disulfide solution to block aldehyde groups of the fixative. After staining, sections were differentiated and dehydrated in an ascending alcohol series. Upon drying, cover slips were placed over the sections.

Nissl Stain Protocol	
100% ethyl alcohol	2min
96% ethyl alcohol	2min
70% ethyl alcohol	2min
Distilled H_2O	2min
50% potassium disulfide solution	12-15min
Distilled H_2O	wash
1.5% cresyl violet solution (in acetate buffer)	1-2min
.2M acetate buffer (pH 4.6)	2min
70% ethyl alcohol	2min
96% ethyl alcohol	2min
100% ethyl alcohol	2 x 2min
Histoclear®	3 x 2min
Mounting sections with Histomount®	

Results

3.1 - Behavioral results

Perimetry testing was done on cats involved in both the Passive Viewing and the Perimetry tasks to assess the efficacy of the cryoloops in inducing neglect. Orienting proficiency was unchanged from the unimplanted cat to the implanted cryoloop-inactive cat. Moreover, unilateral deactivation of SC or pMS cortex yielded a robust neglect of contralateral space in all cats.

3.1.2 - Perimetry task behavioral data

Polar plots (figs 3.1 & 3.2) clearly reveal the orienting performance of the cats involved in the Perimetry task (project 4) before, during, and after deactivation. Cats 2 and 3 were also involved in the Passive Viewing task. Icons of the implanted brain are below the polar plots. An oval over pMS cortex is shaded red for active cortex and blue for inactive. The first column of polar plots is for the baseline condition (red), before pMS cortex was deactivated. The second column is for the trials where pMS cortex was unilaterally deactivated, indicated by the blue color. The last column at the right also marked in red is for recording secessions where pMS cortex was allowed to rewarm and behavioral performance returned to baseline. Figure 3.1 is for the recording sessions where the left pMS was inactivated and the cat neglected right

visual hemispace. Figure 3.2 shows recording sessions where the right pMS was inactivated and left visual hemispace was neglected.

Cat 1 had only one functional cryoloop, the left pMS cryoloop, and is therefore not featured in figure 3.2. Cat 3 rarely performed into the pMS Re-active phase. As such, the recording session for cat 3 was ended after completion of sufficient pMS Inactive trials. Therefore there is no pMS re-activated polar plot for cat 3.

One should note that performance in the non-neglect hemifield at 90° drastically improved during unilateral pMS deactivation. It similarly improved for cats 2 & 3 at 90° in the non-neglected hemifield. As there is no clear explanation for the improvement°, all trials at 90° left and right of the cat for the deactivation phases: Baseline, pMS Inactive, and pMS Re-active were removed from electrophysiological analysis. Furthermore, behavioral targets near the midline were opportunities for the cats to behaviorally respond to stimuli in a way that made it unclear weather the behavioral reaction was immediate or the product of visual searching by the cat. The lab slang label we gave this behavior was 'cheating'. To keep potential cheating out of the electrophysiological analysis, targets at bilateral 15° were removed for all cats from the electrophysiological analysis. The best performing cat and the best at cheating, cat 1, had bilateral target 30° additionally removed.

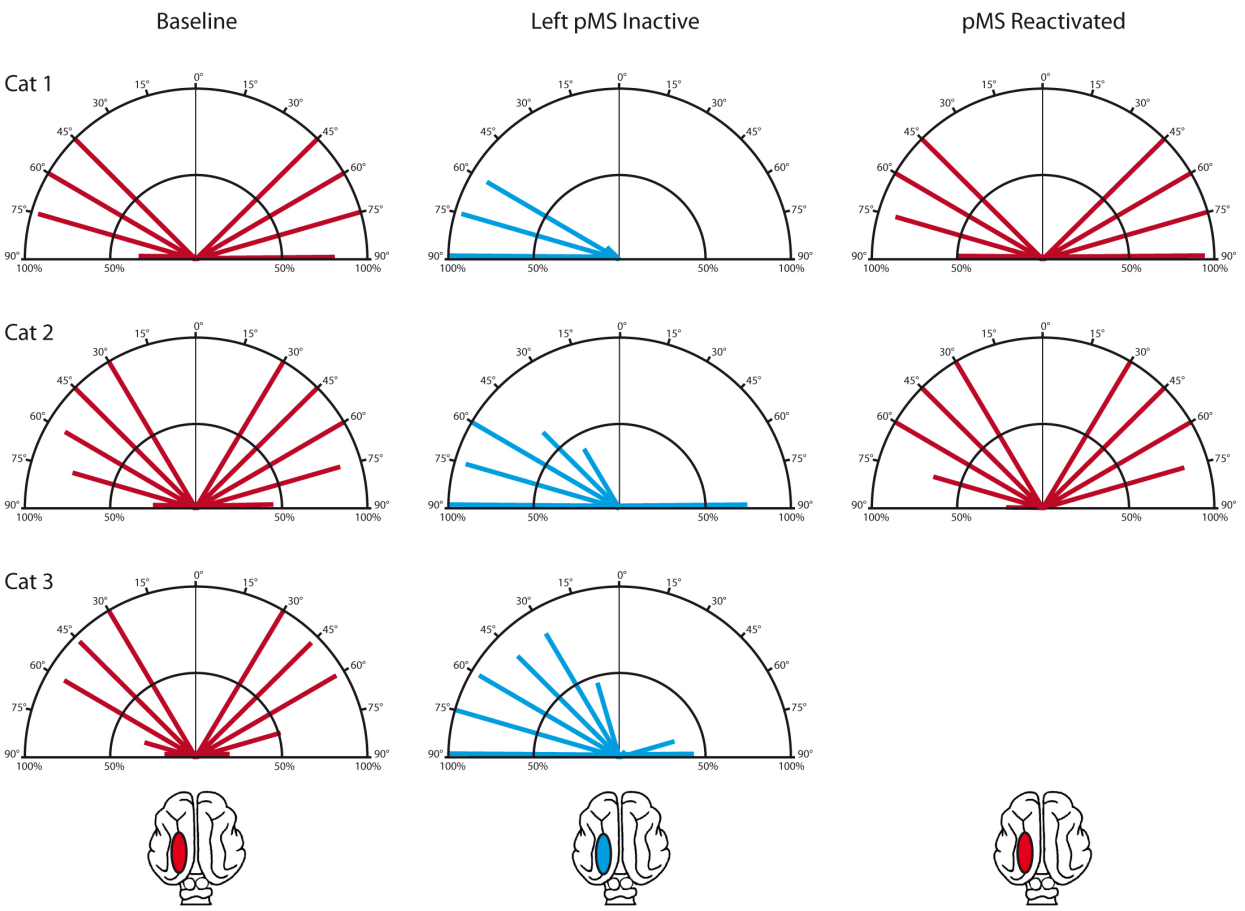

Figure 3.1 – polar plots for recording sessions where the right pMS was deactivated. Each plot contains the location of each visual stimulus as indicated by the labels on the outside of the semicircle. Starting at the focus of the semicircle and extending to each behavioral locus is a bar which indicates behavioral performance. The x-axis has labels for 50% and 100% of the trials attended. Each row of polar plots represents the summed behavioral performance for each of the three cats involved in the perimetry task. The left column of polar plots (red) is for baseline activity, the middle column (blue) is for pMS deactivation trials, and the right column (also red) is for pMS re-activated. Cat 3 did not perform into the pMS re-activated phase. The polar plots clearly show that deactivation of the left pMS cortex results in a profound contralateral neglect. The pMS re-activation phase reveals no deficit in behavior relative to baseline. Central position 15° for cats 2 & 3 and positions 15° and 30° for cat1 were excluded because the cats would scan for the central stimuli thus contaminating a clear delineation between the left and right visual hemifields.

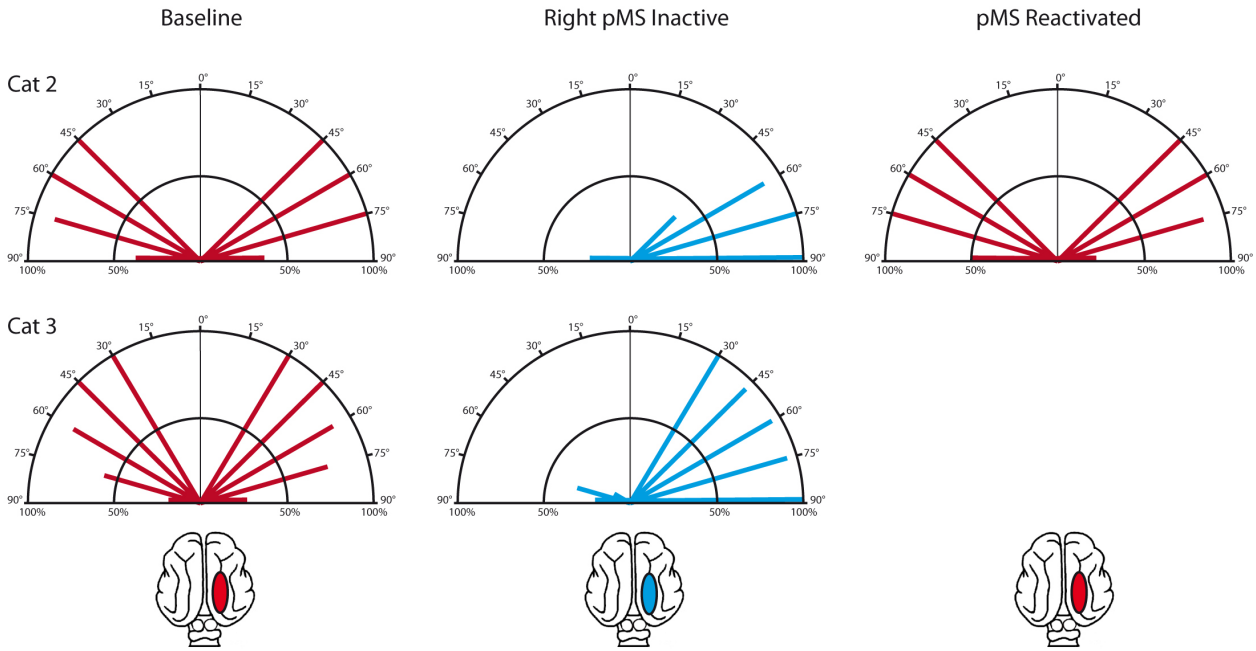

Figure 3.2 – polar plots for recording sessions where the left pMS was deactivated. Only data from cats 2 and 3 are shown as cat 1 did not have a functional right pMS cryoloop. Behavioral results for right pMS deactivation mirror the results for left pMS deactivation

3.2 – SC results (project 1)

The results of SC cooling during the anesthetized Passive Viewing task are shown in figure 3.3 for the Analysis 1 normalization, and figure 3.4 for the Analysis 2 normalization. The layout of both fig 3.3 and fig 3.4 are the same, with the top row showing recording from the hemisphere ipsilateral to SC cooling (cat1 n=1680, cat2 n=671, cat3 n=2352), the middle row showing recording contralateral to cooling (cat1 n=1680, cat2 n=671, cat3 n=2352), and the bottom row showing recording during bilateral cooling (cat2 n=168, cat3 n=504). Across the top of both figs 3.3 and 3.4 are the analysis windows in milliseconds. At the bottom of the figures are icons of the stimulus that was shown at each analysis windows. Within each sub-plot the

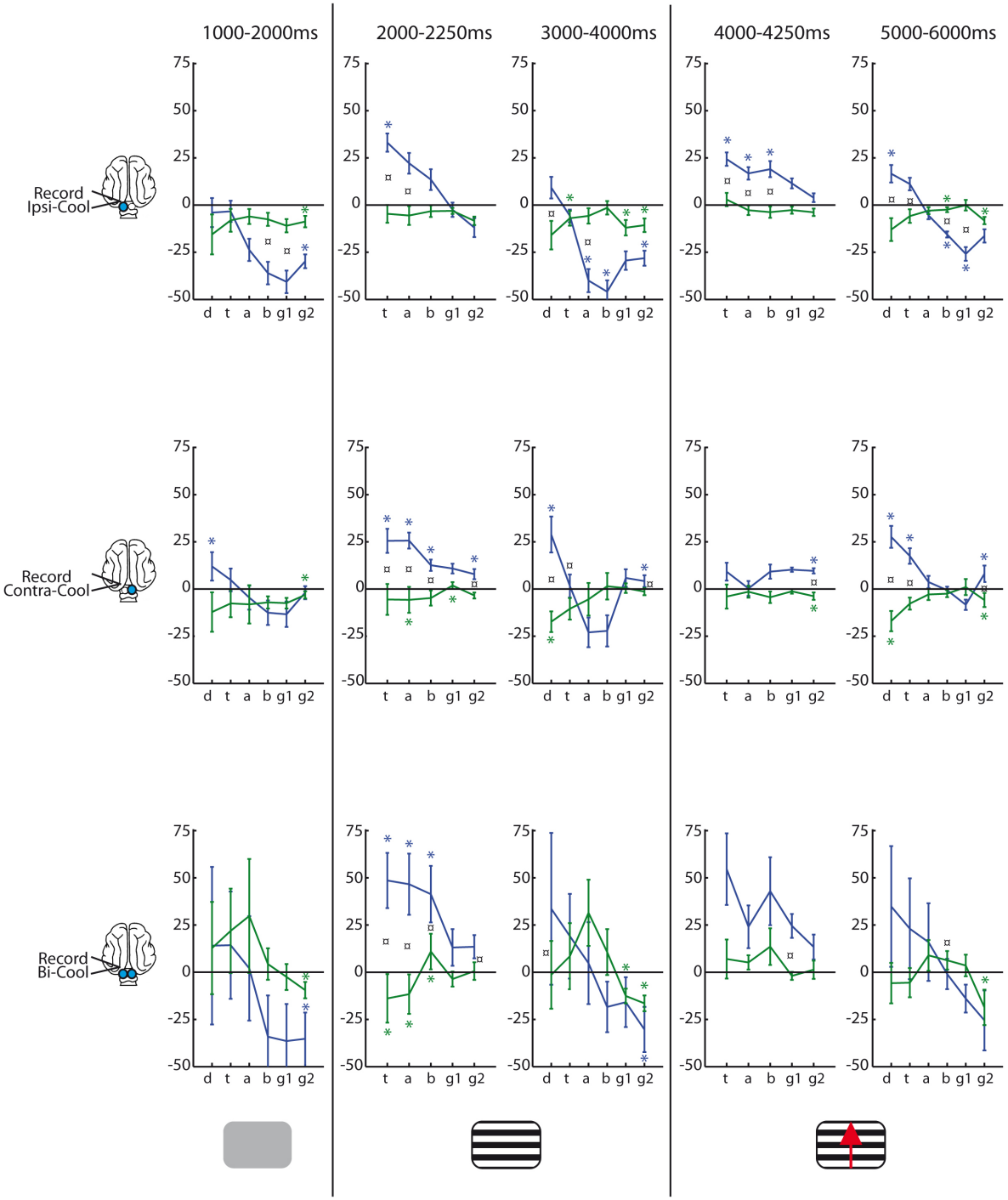

Fig 3.3 – Analysis 1, anesthetized SC inactivation. The top row is deactivation ipsilateral to the electrodes, the middle row contralateral, and the bottom row bilateral to deactivation. The blue trace is for SC Inactive and green is SC Re-active. The stimulus phase is indicated at the bottom of the figure. Analysis windows are indicated in ms at the top. The long vertical lines between the stimulus icons indicate a stimulus change. The bottom of each subplot has the frequency bands: d (delta), t (theta), a (alpha), b (beta), g1 (gamma1), and g2 (gamma2). The y-axis positive values are the percent increase in power relative to SC Active. Negative values are the amount by which Inactive and Re-active power was less than SC Active power. An asterisks indicates that each individual cat of the three cats surpassed the significance threshold (one-tail t-test, $p<.05$)

frequency bands are listed on the x-axis: delta (d), theta (t), alpha (a), beta (b), gamma1 (g1), and gamma2 (g2). Percent change relative to SC-Active is marked on the y-axis. Positive values show the percent increase in power for the Inactive condition (blue) and Re-active (green) relative to SC Active. Negative values, negative by convention, represent the percent by which Active power was greater than Inactive or Re-active power (see 2.6.1 for computation).

3.2.1 - SC results, analysis 1, ipsilateral deactivation

Ipsilateral SC deactivation led to a general decrease of high frequency oscillations in the one second long 'steady-state' AWs: Grey, Static Grating, and Moving Grating. The Moving Grating AW showed an additional increase in delta oscillations during cooling. The AWs following stimulus change, ERP-1 and ERP-2, show an increase

	1000-2000ms	2000-2250ms	3000-4000ms	4000-4250ms	5000-6000ms
Delta	- -	33.1%, p<3.3E-16 -	- -	24.3%, p<3.7E-15 -	16.6%, p<0.048 -
Theta	- -	- -	- -6.9% p<0.003	16.8%, p<5.28E-13 -	- -
Alpha	- -	- -	-40.0%, p<3.6E-15 -	19.0%, p<7.4E-03 -	- -
Beta	- -	- -	-45.9%, p<1.9E-13 -	- -	-15.6%, p<4.0E-10 -2.4%, p<0.009
Gamma1	- -	- -	- -12.0%, p<0.004	- -	-25.9%, p<2.5E-07 -
Gamma2	-29.8%, p<0.002 -8.7%, p<1.52E-05	- -	-28.1%, p<7.4E-06 -10.7%, p<3.9E-06	- -	- -8.2%, p<0.018

Table 1: ipsilateral SC deactivation, Analysis 1. The SC was deactivated (blue) or reactivated (green) ipsilateral to recording electrodes. Percent change in power relative to SC Active (from fig 3.3 - top) was listed if all three cats surpassed significance criterion. The listed p-value is the value associated with the power change that was the least significant of the three cats. Dashes represent values that did not exceed significance criterion and were thus not listed.

in low-frequency oscillations. Re-activating the SC showed an almost complete reversion of power to the Active condition. Table 1 lists the percent change values that met the criterion for statistical significance. The associated p-value in the table is the least significant p-value of the three cats that were tested. At the top of each column is the time period for each of the five AWs.

3.2.1.2 SC results, analysis 1, cool contralateral

SC deactivation contralateral to recording did not cause the decrease in gamma oscillations seen in ipsilateral deactivation. On-the-contrary, all AWs except Grey showed a cooling-induced increase in gamma2 oscillatory power. Low-frequency power during the inactive condition increased for all AWs except ERP-2. As with

	1000-2000ms	2000-2250ms	3000-4000ms	4000-4250ms	5000-6000ms
Delta	12%, p< .03	-	28.9%, p< 0.0002	-	27.6%, p<1.7E-05
	-	-	-17.3%, p<0.03	-	-16.9%, p<0.015
Theta	-	25.5%, p<3.0E-08	-	-	17.5%, p<0.001
	-	-	-	-	-
Alpha	-	25.6%, p<1.1E-15	-	-	-
	-	-5.7%, p<0.008	-	-	-
Beta	-	12.6, p<1.2E-06	-	-	-
	-	-	-	-	-
Gamma1	-	-	-	-	-
	-	1.9%, p<0.003	-	-	-
Gamma2	-	7.9%, p<1.33E-02	4.2%, p<0.008	9.6%, p<1.3E-04	8.1%, p<2.4E-05
	-3.1%, p<.03	-	-	-3.8%, p<4.4E-05	-5.8%, p<0.0006

Table 2: contralateral deactivation, Analysis 1. The SC was deactivated (in blue) or reactivated (in green) contralateral to recording electrodes. The percent change in power relative to SC Active (from fig 3.3-middle) were listed if all three cats surpassed significance criterion. The listed p-value is the value associated with the power change that was the least significant of the three cats. Dashes represent values that did not exceed significance criterion and were thus not listed.

ipsilateral deactivation, allowing the contralateral SC to rewarm led to a reversion to SC Active values. Table 2 summarizes significant power changes and their associated p-values. As mentioned, the p-values are the least significant value of the three values computed from the three individual cats.

3.2.1.3 - SC results, analysis 1, bilateral deactivation

Despite only deactivating the SC bilaterally in two cats, rather than three as was done for ipsi- and contra-Inactive, few power changes approached statistical significance. Since any single cat not reaching significance excluded a data point from being significant, less cats make it easier to fulfill significance criterion. However, few data points pass this criterion for bilateral deactivation. Data for bilateral deactivation was noisier than for unilateral cooling. Data points that did reach significance were: 1) a decrease in gamma2 oscillations in the AW Grey and AW Static

	1000-2000ms	2000-2250ms	3000-4000ms	4000-4250ms	5000-6000ms
Delta	-	48.6%, p<5.0E-16	-	-	-
	-	-13.8%, p<1.6E-08	-	-	-
Theta	-	46.6%, p<5.0E-16	-	-	-
	-	-11.6%, p<9.3E-03	-	-	-
Alpha	-	41.4%, p<1.1E-10	-	-	-
	-	11.1%, p<5.3E-03	-	-	-
Beta	-	-	-	-	-
	-	-	-	-	-
Gamma1	-	-	-	-	-
	-	-	-12.5%, p<0.0005	-	-
Gamma2	-35.2%, p<0.002	-	-30%, p< .008	-	-
	-9.5%, p<0.03	-	-16.4%, p<3.8E-14	-	-18.6%, p<5.2E-05

Table 3: bilateral deactivation, Analysis 1. The SC was deactivated (in blue) or reactivated (in green) bilateral to recording electrodes. Percent change in power relative to SC Active (from fig 3.3-bottom) were listed if all three cats surpassed significance criterion. The listed p-value is the value associated with the power change that was the least significant of the three cats. Dashes represent values that did not exceed significance criterion and were thus not listed.

Grating, but not AW Moving Grating, and 2) an increase in low frequency oscillations the ERP-1 AW. Re-activation led largely to a reversion to SC active levels. Table 3 lists significant values and their associated p-values.

3.2.2 SC Results, Analysis 2

The Analysis 2 normalization for SC deactivation is shown in figure 3.4. Only four AWs are shown because AW Gray was used to normalize power (see 2.6.2). To review section 2.6.2, values in Fig 3.4 are normalized within trial to a time point that occurred no more than 5 seconds earlier, in AW Gray. The graphs reflect how the cortex reacts to the stimulus within each trial and within cooling condition. Red asterisks indicate a significant change in power during the SC Active condition relative to AW-Grey. The open blue (Inactive) and green (Re-active) squares indicate Inactive and Re-active values that are statistically different from the SC warm values that were also derived from Analysis 1 . To simplify the text, significant values were moved to tables. The SC inactive and SC re-active values listed in the tables are 1) significantly different from SC active values, and 2) the change in power, within cooling condition, relative to AW-Grey. So while the Inactive and Re-active values listed in the charts are significantly different from Active, the Active value from the table needs to be subtracted from the Inactive or Re-active value to get the change in power relative to Active. Associated p-values for Inactive and Reactive are the probability that their values are different from SC Active. An additional graph with Warm values subtracted from the Inactive and Re-active values was not made to economize on graphs.

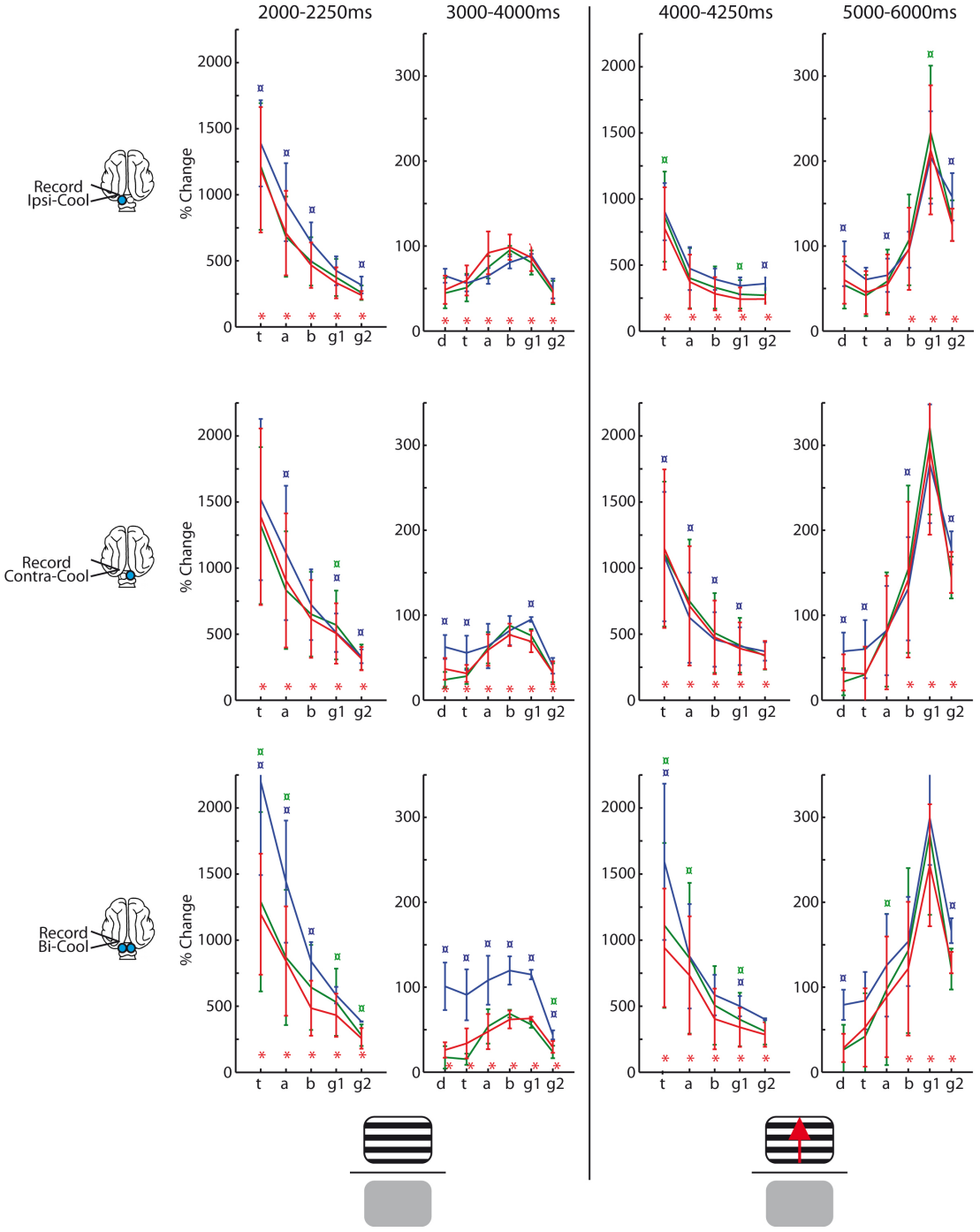

Fig 3.4 – SC inactivation, Analysis 2. The top row is ipsilateral deactivation data, the middle row contralateral, and the bottom row bilateral deactivation. Red represents SC Active, blue is SC Inactive, and green is SC Re-active. The analysis time window is given in ms at the top of the figure. The icons at the bottom of the figure indicate stimulus phase (static or moving grating) divided by the gray screen that appeared at the beginning of a trial. The long vertical line between the stimulus icons indicate a stimulus change. The bottom of each subplot has the frequency bands: d (delta), t (theta), a (alpha), b (beta), g1 (gamma1), and g2 (gamma2). The y-axis values are the percent increase of power over baseline (gray screen). Red asterisks indicate a significant change in power over the baseline (gray screen) time period. The blue (SC Inactive) and green (SC Re-Active) boxes indicate a power-change value significantly different from SC Active (red line). The computation for SC Active (red line), SC Inactive (blue line), and SC Re-active (green line), was the same. Only the statistical comparison (grating v gray screen for SC Active [red asterisks], SC Active v SC Inactive or SC Re-active [blue or green box]) was different.

The stimulus caused a significant increase in power during the Active condition for all frequency bands in the ERP-1, Static Grating, and ERP-2 AWs. The moving grating caused a high-frequency bump in power for the beta, gamma1, and gamma2 frequency bands. Lower-frequency delta, theta, and alpha power bands were unaffected in the Moving Grating AW.

3.2.2.1 – SC Analysis 2, Cool Ipsilateral

	2000-2250ms	3000-4000ms	4000-4250ms	5000-6000ms
Delta		49%, p< 6.9e-5 - -		- 79%, p< .002 -
Theta	1189%, p< 2.0e-171 1388%, p< .03 -	59%, p< 3.1e-293 - -	777%, p<2.8e-122 - 866%, p< .004	- - -
Alpha	710%, p< 1.7e-141 944%, p< .002 -	92%, p< 3.1e-293 - -	373%, p< 3.4e-111 - -	- 66%, p< .002 -
Beta	467%, p< 4.7e-187 642%, p< 4.7e-187 -	99%, p< 2.5e-143 - -	283, p< 1.3e-159 - -	97%, p< 3.0e-190 - -
Gamma1	334%, p< 3.1e-293 - -	86%, p< 1.5e-207 - -	242%, p< 8.1e-232 - 279%, p< 8.1e-232	213%, p< 8.6e-286 - 299%, p< .01
Gamma2	240%, p< 1.5e-285 317%, p< 1.5e-285 -	49%, p< 1.7e-216 - -	242, p< 1.0e-199 359%, p<1.0e-199 -	125%, p< 4.0e-229 158%, p< 3.7e-6 -

Table 4: SC ipsilateral to recording electrodes, Analysis 2. Active is red, Inactive is blue, Re-active is green. Changes in power for the different stimulus phases relative to the gray screen stimulus phase were listed if values reached significance. Dashes are placed for data points where at least one of the three cats did not surpass the significance threshold. Significance criterion were met if each of the three cats individually passed p<.05 on a 1-tail t-test. The least significant value from the three cats is listed. The t-test was performed for SC-warm (red values) relative to 0, and for SC-incative (blue values) and SC-reactive (green values) relative to SC-warm. Red values thus represent significant power changes relative to the gray screen stimulus, while blue and green values are power changes for Inactive and Re-active that were significantly different from SC-active power changes. There are no values for delta in the 2000-2250ms and 4000-4250ms AW's because a Fourier transform for 250ms for frequencies below 4Hz is not possible.

In response to ipsilateral SC deactivation, primary visual cortex was generally more responsive to a change in stimulation. AW ERP-1 showed a power increase in theta, alphabet, beta, and gamma2 over and above Active power. AW Static Grating showed no change in power for Inactive. AW ERP-2 showed an increase in Gamma2 power. The AW Moving Grating had a cooling induced power increase in the low frequencies and gamma2. In all AWs Rewarm led to a reversion of power values to Warm levels. (Table 4)

3.2.2.2 – SC Analysis 2, Cool Contralateral

	2000-2250ms	3000-4000ms	4000-4250ms	5000-6000ms
Delta		37%, p< 2.4e-9 63%, p< .005 -		- 58%, p< .005 -
Theta	1388%, p< 2.3e-92 - -	31%, p< 1.2e-318 56%, p< .004 -	1147%, p< 5.3e-96 1087%, p< .02 -	- 60%, p< 1.9e-4 -
Alpha	906%, p< 3.2e-129 1115%, p< .002 -	59%, p< 1.2e-318 - -	714%, p< 1.1e-115 625%, p< 6.3e-6 -	- - -
Beta	615%, p< 3.4e-114 - -	77%, p< 7.1e-68 - -	476%, p< 1.2e.318 460%, p< .0003 -	142%, p< 1.8e-116 131%, p< 4.9e-7 -
Gamma1	505%, p< 9.2e-150 511%, p< 2.8e-6 569%, p< 6.5e-4	69%, p< 5.4e-100 95%, p< .009 -	392%, p< 4.1e-155 409%, p< .002 -	297%, p< 4.9e-152 - -
Gamma2	315%, p< 4.6e-167 333%, p< .005 -	32%, p< 1.1e-101 - -	342%, p< 7.0e-312 - -	150%, p< 1.2e-318 179%, p< .004 -

Table 5: SC deactivation contralateral to recording electrodes, Analysis 2. Active is red, Inactive is blue, Re-active is green. An in-depth figure legend is in table 4.

In contrast to ipsilateral cooling, contralateral SC cooling led cortex to react more strongly to the Static Grating in the low and gamma1 frequency bands. ERP-2 gamma2 power was not affected by contralateral cooling, unlike ipsilateral cooling (Table 5).

3.2.2.3 – SC Analysis 2, Cool Bilateral

Bilateral SC deactivation led to primary visual cortex reacting more strongly to visual stimulation as compared to the SC Warm condition. The shape of the SC bilateral cool curves is the same shape as the ipsilateral and bilateral curves, but

	2000-2250ms	3000-4000ms	4000-4250ms	5000-6000ms
Delta		26%, p< .002 101%, p<4.8e-6 -		- 79%, p< 2.5e-6 -
Theta	1196%, p< 6.0e-52 2198%, p< 2.4e-15 1291%, p< .002	34%, p< .003 91%, p< 1.7e-7 -	942%, p< 2.4e-50 1593%, p< 6.3e-10 1112, p< .04	- - -
Alpha	842%, p< 8.4 e-67 1443%, p< 1.2e-13 869%, p< 3.9e-6	48%, p< 3.3e-10 108%, p< 1.6e-9 -	733%, p< 6.9e-58 - 863%, p< 4.9e-4	- - 97%, p< .04
Beta	485%, p< 3.3e-70 839%, p< 1.2e-7 -	62%, p< 3.0e-31 120%, p< 5.7e-12 -	403%, p< 2.9e-60 - -	122%, p< 5.9e-5 - -
Gamma1	432%, p< 7.0e-105 - 530%, p< 3.9e-4	63%, p< 4.1e-40 115%, p< 1.4e-13 -	340%, p< 5.6e-80 501%, p< .01 399%, p< .02	244%, p< 1.3e-67 - -
Gamma2	257%, p< 6.3e-91 - 281%, p< .04	30%, p< 5.7e-50 44%, p< 6.2e-4 24%, p< .03	286%, p< 5.6e-97 - -	129%, p< 5.2e-60 167%, p< 6.9e-6 -

Table 6: SC deactivation bilateral to recording electrodes, Analysis 2. Active is red, Inactive is blue, Re-active is green. An in-depth figure legend is in table 4.

shifted upwards, particularly for the ERP1 and Static Grating AWs. The easier significance criterion parameters, with just two cats bilaterally cooled, did not however lead to an increase in significant data points for the ERP2 and Moving Grating AWs. This is presumably due to an increase in LFP noise resulting from bilateral removal of SC input.

3.3 – Anesthetized pMS (Project 2)

The results from pMS deactivation have the same layout as the SC deactivation results. The only difference is the location of cooling, pMS rather than SC. Ipsilateral pMS deactivation had the following number of trials: cat1 n=1176, cat2 n=1344, cat3 n=1680; contralateral deactivation had: cat1 n=2184, cat2 n=840, cat3 n=1680 trials; and bilateral deactivation had: cat1 n=2016, cat2 n=2184, cat3 n=2016 trials.

3.3.1 Anesthetized pMS – Analysis 1

Inactivating pMS had a strongly lateralized effect on oscillatory activity. Similar to SC cooling, high frequency gamma activity was drastically reduced during ipsilateral pMS deactivation. In contrast to SC deactivation, low frequency activity was also reduced. Contralateral pMS inactivation had no effect or yielded even a slight increase in power relative to Active. Thus, the gamma trend for ipsilateral and contralateral cooling is similar for SC and pMS deactivation, with the primary visual cortex responsible for the neglect hemifield having a reduction in gamma power while

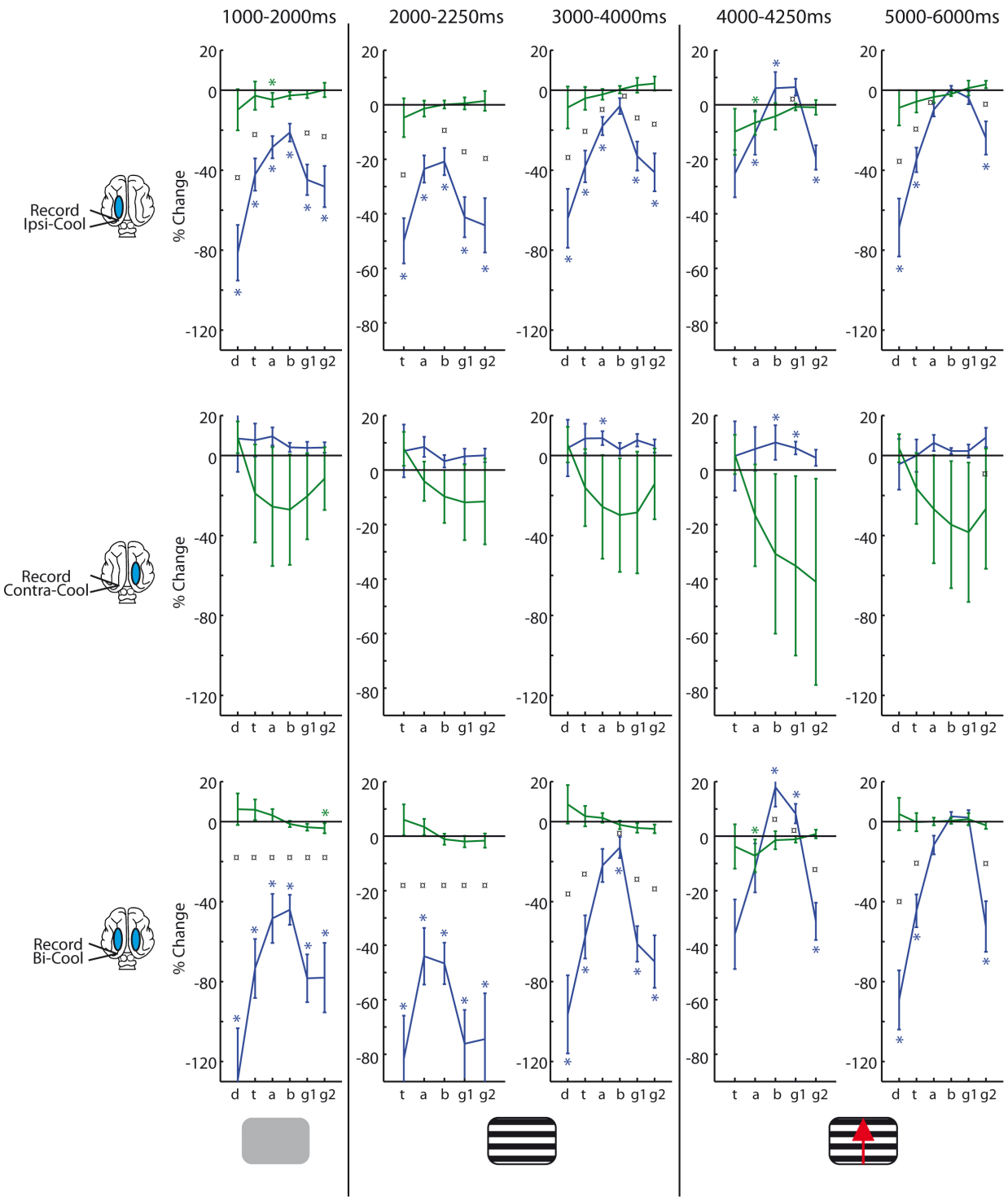

Fig 3.5 – Analysis 1, anesthetized pMS inactivation. The top row is deactivation ipsilateral to the electrodes, the middle row contralateral, and the bottom row bilateral to deactivation. The blue trace is for pMS Inactive and green is pMS Re-active. The stimulus phase is indicated at the bottom of the figure. Analysis windows are indicated in ms at the top. The long vertical lines between the stimulus icons indicate a stimulus change. The bottom of each subplot has the frequency bands: d (delta), t (theta), a (alpha), b (beta), g1 (gamma1), and g2 (gamma2). The y-axis positive values are the percent increase in power relative to pMS Active. Negative values are the amount by which Inactive and Re-active power was less than pMS Active power. An asterisks indicates that each individual cat of the three cats surpassed the significance threshold (one-tail t-test, $p<.05$)

the hemisphere responsible for the intact visual hemifield had an increase in gamma. Bilateral pMS cooling, rather than being a summation of ipsi and contralateral deactivation effects, showed a pattern resembling ipsilateral pMS deactivation, but with the deactivation-induced power-decreases amplified.

3.3.1.1 Ipsilateral pMS Cooling

Data points that met significance criterion are listed in table 7. In the Grey screen AW, before stimulus onset, all frequency-bands showed a reduction in power with delta and gamma frequency bands particularly affected. This pattern continues through the ERP-1 and Static Grating AWs. The AW ERP-2, where the grating starts moving, is not strongly affected by cooling beyond a 19% decrease in gamma2 oscillations. The AW Moving Grating power changes resemble AW Gray, with a

	1000-2000ms	2000-2250ms	3000-4000ms	4000-4250ms	5000-6000ms
Delta	-81%, p< 3.3e-16 -		-64%, p< 3.3e-16 -		-69%, p< 3.3e-16 -
Theta	-42%, p< 3.3e-16 -	-50%, p< 3.3e-16 -	-38%, p< 3.3e-16 -	- -7%, p< 8.1e-7	-35%. p< 3.3e-16 -
Alpha	-28%, p< .02 -5%, p< .02	34%, p< 3.3e-16 -	-18%, p< 4.8e-5 -	-10%, p< 5.4e-12 -	- -
Beta	-21%, p< .0006 -	-21%, p< .005 -	- -	6%, p< -.02 -	- -
Gamma1	-45%, p<1.1e-16 -	-41%, p< 3.0e-14 -	-33%, p< 3.8e-12 -	- -	- -
Gamma2	-48%, p< .02 -	-44%, p< 5.0e-13 -	-41%, p<.03 -	-19%, p< 2.0e-5 -	-24%, p<.02 -

Table 7: Anesthetized pMS deactivation ipsilateral to recording electrodes, Analysis 1. The pMS was deactivated (blue) or reactivated (green) ipsilateral to recording electrodes. Percent change in power relative to pMS Active (from fig 3.5 - top) was listed if all three cats surpassed significance criterion. The listed p-value is the value associated with the power change that was the least significant of the three cats. Dashes represent values that did not exceed significance criterion and were thus not listed.

reduction in gamma2 power as well as low-frequency delta and theta power. Rewarming pMS led to a clear reversion to pMS Warm values.

3.3.1.2 Contralateral pMS Cooling

Cooling of contralateral pMS tended to make oscillatory power increase, but few data points reached significance (table 8). Rewarming pMS caused a power decrease, but the trend did not reach significance.

	1000-2000ms	2000-2250ms	3000-4000ms	4000-4250ms	5000-6000ms
Delta	-		-		-
	-		-		-
Theta	-	-	-	-	-
	-	-	-	-	-
Alpha	-	-	9%, p< .0012	10%, p< .02	-
	-	-	-	-	-
Beta	-	-	-	8%, p< .0001	-
	-	-	-	-	-
Gamma1	-	-	-	-	-
	-	-	-	-	-
Gamma2	-	-	-	-	-
	-	-	-	-	-

Table 8: Anesthetized pMS deactivation contralateral to recording electrodes, Analysis 1. Inactive is blue. The pMS was deactivated (blue) or reactivated (green dashes) contralateral to recording electrodes. Percent change in power relative to pMS Active (from fig 3.5 - middle) was listed if all three cats surpassed significance criterion. The listed p-value is the value associated with the power change that was the least significant of the three cats. Dashes represent values that did not exceed significance criterion and were thus not listed.

3.3.1.3 Bilateral pMS Deactivation

Bilateral deactivation of pMS yielded a clear amplification of ipsilateral cooling effects (table 9). Rewarming of bilateral pMS, as in other cooling conditions, caused power values to return to Warm levels.

	1000-2000ms	2000-2250ms	3000-4000ms	4000-4250ms	5000-6000ms
Delta	-129%, p<3.3e-16 -		-96%, p< 3.3e-16 -		-89%, p< 3.3e-16 -
Theta	-73%, p< 3.3e-16 -	-82%, p< 3.3e-16 -	-58%, p< 3.3e-16 -	- -	-45%, p< 3.3e-16 -
Alpha	-48%, p< .03 -	-44%, p< 3.3e-16 -	- -	- -7%, p< 1.2e-6	- -
Beta	-44%, p< 3.3e-16 -	-47%, p< .001 -	-13%, p< .0006 -	18%, p< 3.3e-16 -	- -
Gamma1	-78%, p< 3.3e-16 -	-76%, p< 3.3e-16 -	-61%, p< 3.3e-16 -	8%, p< 1.2e-7 -	- -
Gamma2	-78%, p< 1.4e-11 -3%, p< .015	-74%, p< 3.3e-16 -	-70%, p< 3.3e-16 -	-31%, p< .04 -	-52%, p< 2.4e-6 -

Table 9: Anesthetized pMS deactivation bilateral to recording electrodes, Analysis 1. Inactive is blue, Re-active is green. The pMS was deactivated (blue) or reactivated (green) bilateral to recording electrodes. Percent change in power relative to pMS Active (from fig 3.5 - bottom) was listed if all three cats surpassed significance criterion. The listed p-value is the value associated with the power change that was the least significant of the three cats. Dashes represent values that did not exceed significance criterion and were thus not listed.

3.3.2 Anesthetized pMS, Analysis2

The pMS Active condition shows the high-frequency gamma-bump for the Moving Grating that the SC graph also shows. Significant stimulus-induced changes in the SC Active condition are depicted with a red asterisk.

First, it should be noted that though absolute power in each frequency band may change for pMS Inactive relative to Active, the change of each frequency band relative to the neighboring frequency bands is relatively constant. In other words, the shape of the graphs for Active and Inactive are very similar.

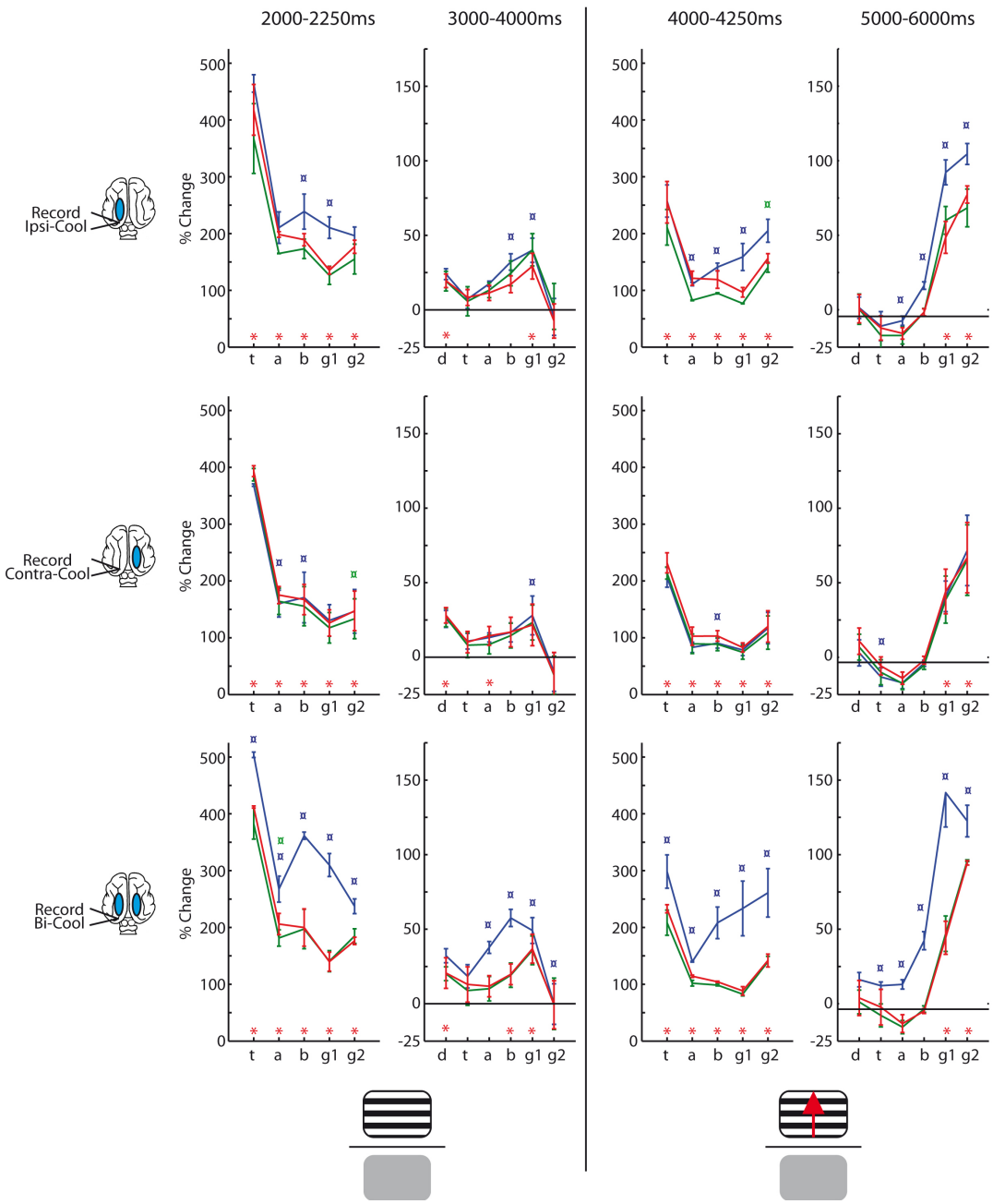

Fig 3.6 – anesthetized pMS inactivation, Analysis 2. The top row is ipsilateral deactivation data, the middle row contralateral, and the bottom row bilateral deactivation. Red represents pMS Active, blue is pMS Inactive, and green is pMS Re-active. The analysis time window is given in ms at the top of the figure. The icons at the bottom of the figure indicate stimulus phase (static or moving grating) divided by the gray screen that appeared at the beginning of a trial. The long vertical line between the stimulus icons indicate a stimulus change. The bottom of each subplot has the frequency bands: d (delta), t (theta), a (alpha), b (beta), g1 (gamma1), and g2 (gamma2). The y-axis values are the percent increase of power over baseline (gray screen). Red asterisks indicate a significant change in power over the baseline (gray screen) time period. The blue (pMS Inactive) and green (pMS Re-Active) boxes indicate a power-change value significantly different from pMS Active (red line). The computation for pMS Active (red line), pMS Inactive (blue line), and pMS Re-active (green line), was the same. Only the statistical comparison (grating v gray screen for SC Active [red asterisks], SC Active v pMS Inactive or pMS Re-active [blue or green box]) was different.

As with SC deactivation, cooling ipsilateral pMS causes primary visual cortex to react more strongly to the grating stimulus relative to the pre stimulus time period (fig 3.6, top row). It is important to keep in mind that, similar to ipsilateral SC deactivation, the pMS Analysis 2 normalization accounts for a deficit in power already in the Grey AW as a result of ipsilateral pMS deactivation. Thus, the greater increase in power resulting from the stimulus onset for the Inactive condition may reflect a

	2000-2250ms	3000-4000ms	4000-4250ms	5000-6000ms
Delta		16%, p< 1.8e-8 - -		- - -
Theta	418%, p< 8.5e-239 - -	- - -	255%, p< 1.0e-323 - -	- - -
Alpha	198%, p< 1.0e-323 - -	- - -	121%, p< 1.0e-323 111%, p< .0006 -	- -3%, p< .02 -
Beta	189%, p< 1.0e-323 239%, p< .001 -	- 26%, p< .002 -	119%, p< .003 141%, p< .003 -	- 20%, p< 5.3e-9 -
Gamma1	135%, p< 2.5e-182 210%, p< .0008 -	23%, p< 1.0e-323 32%, p< .007 -	97%, p< .002 158%, p< .002 -	51%, p< 1.0e-323 93%, p< .01 -
Gamma2	176%, p< 1.1e-314 - -	- - -	156%, p< 3.3E-250 - 141%, p< 1.0e-323	79%, p< 1.4e-220 106%, p< 3.6e-13 -

Table 10: anesthetized pMS ipsilateral to recording electrodes, Analysis 2. Active is red, Inactive is blue, Re-active is green. Values from fig 3.6 top. Changes in power for the different stimulus phases relative to the gray screen stimulus phase were listed if values surpassed significance criterion. Significance criterion were met if each of the three cats individually passed p<.05 on a 1-tail t-test. Dashes are placed for data points where at least one of the three cats did not surpass significance. The least significant value from the three cats is listed. The t-test was performed for pMS-warm (red values) relative to 0, and for pMS-incative (blue values) and pMS-reactive (green values) relative to pMS-warm. Red values thus represent significant power changes that a stimulus induced relative to the gray screen stimulus, while blue and green values are power changes for Inactive and Re-active that were significantly different from pMS-active power changes. There are no values for delta in the 2000-2250ms and 4000-4250ms AW's because a Fourier transform for 250ms for frequencies below 4Hz cannot be performed.

primary visual cortex responding to the stimulus like it responds in the Active condition, but starting with a baseline power deficit in the pre stimulus time period.

Contralateral pMS cooling led to no change in power. This is to be expected as Analysis-1 showed no difference between Active and Inactive conditions for this cooling location.

3.3.2.1 Analysis2 - pMS Ipsilateral Deactivation

Ipsilateral pMS deactivation for analysis 2 caused an increase in high-frequency oscillations when compared to pMS Active values. The beta and gamma1 frequency bands showed an increase in power for all four AWs. The Moving Grating AW showed an additional significant increase Gamma2 over pMS warm (table 10).

3.3.2.2 Analysis2 - pMS Contralateral Deactivation

Analysis2 revealed minimal effect of contralateral pMS cooling on stimulus-induced power changes. (table 11)

	2000-2250ms	3000-4000ms	4000-4250ms	5000-6000ms
Delta		23%, p< 2.2e-10 - -		- - -
Theta	393%, p< 1.0e-219 - -	- - -	232%, p< 9.5e-152 - -	- -2%, p< .03 -
Alpha	175%, p< 1.6e-151 160%, p< .01 -	11%, p< .03 - -	103%, p< 1.4e-299 - -	- - -
Beta	167%, p< 1.4e-299 171%, p< .02 -	- - -	103%, p< 1.4e-299 91%, p< .02 -	- - -
Gamma1	126%, p< 5.3e-163 - -	- 22%, p< .01 -	83%, p< 4.0e-130 - -	45%, p< 1.4e-299 - -
Gamma2	147%, p< 1.9e-169 - 134%, p< .001	- - -	120%, p< 8.6e-150 - -	67%, p< 1.4e-299 - -

Table 11: anesthetized pMS contralateral to recording electrodes, Analysis 2. Active is red, Inactive is blue, Re-active is green. Values from fig 3.6 - middle. For figure legend details, see table 10.

3.3.2.3 Analysis2 - pMS Bilateral Deactivation

Bilateral pMS deactivation showed effects resembling ipsilateral pMS deactivation for analysis 2, but amplified. This finding is congruous with the large loss of power caused by bilateral pMS cooling in AW-Grey for Analysis 1. With the exception of the delta band in the static grating AW, all frequency bands in all AWs had

an increase in normalized power for Inactive relative to Active. Re-active values returned to Active levels. (table 12)

	2000-2250ms	3000-4000ms	4000-4250ms	5000-6000ms
Delta		16%, p< .004 - -		- - -
Theta	412%, p< 1.4e-299 504%, p< 6.5e-8 -	- - -	233%, p< 1.4e-299 298%, p< 5.0e-5 -	- 10%, p< .03 -
Alpha	206%, p< 1.4e-299 267%, p< 7.1e-9 181%, p< .001	- 30%, p< 3.5e-15 -	114%, p< 1.4e-299 140%, p< 9.1e-6 -	- 11%, p< 5.3e-7 -
Beta	200%, p< 1.4e-299 361%, p< 3.5e-15 -	16%, p< 1.4e-299 46%, p< 3.5e-15 -	104%, p< 1.4e-299 208%, p< 3.5e-15 -	- 40%, p< 3.5e-15 -
Gamma1	140%, p< 1.4e-299 310%, p< 3.5e-15 -	30%, p< 1.4e-299 39%, p< 4.6e-9 -	88%, p< 1.4e-299 233%, p< 3.5e-15 -	47%, p< 1.4e-299 140%, p< 3.5e-15 -
Gamma2	176%, p< 1.4e-299 237%, p< 1.0e-12 -	- -0.2%, p< .004 -	142%, p< 1.4e-299 261%, p< 3.5e-15 -	96%, p< 1.4e-299 121%, p< .001 -

Table 12: anesthetized pMS bilateral to recording electrodes, Analysis 2. Active is red, Inactive is blue, Re-active is green. Values from fig 3.6 - bottom. For figure legend details, see table 10.

3.4 – Awake pMS Results (Project 3)

With the exception of bilateral cooling, which was not performed in the awake cat, the results from awake pMS deactivation have the same layout as the anesthetized pMS deactivation. Ipsilateral pMS deactivation had the following number of trials: cat1 n=278, cat2 n=524, cat3 n=447, while contralateral deactivation had the following number of trials: cat1 n=278, cat2 n=98, cat3 n=447. The smaller number of

trials for contralateral cooling relative to ipsilateral cooling, 98 vs 524 trials, for cat 2 is due to a malfunction in one recording array in the early phase of the experiment.

The only data points that passed significance criterion, the same criterion used for the anesthetized projects, was the beta band for grey screen and ERP-1. There was a general trend for a reduction in ipsilateral Cool power in all analysis windows,

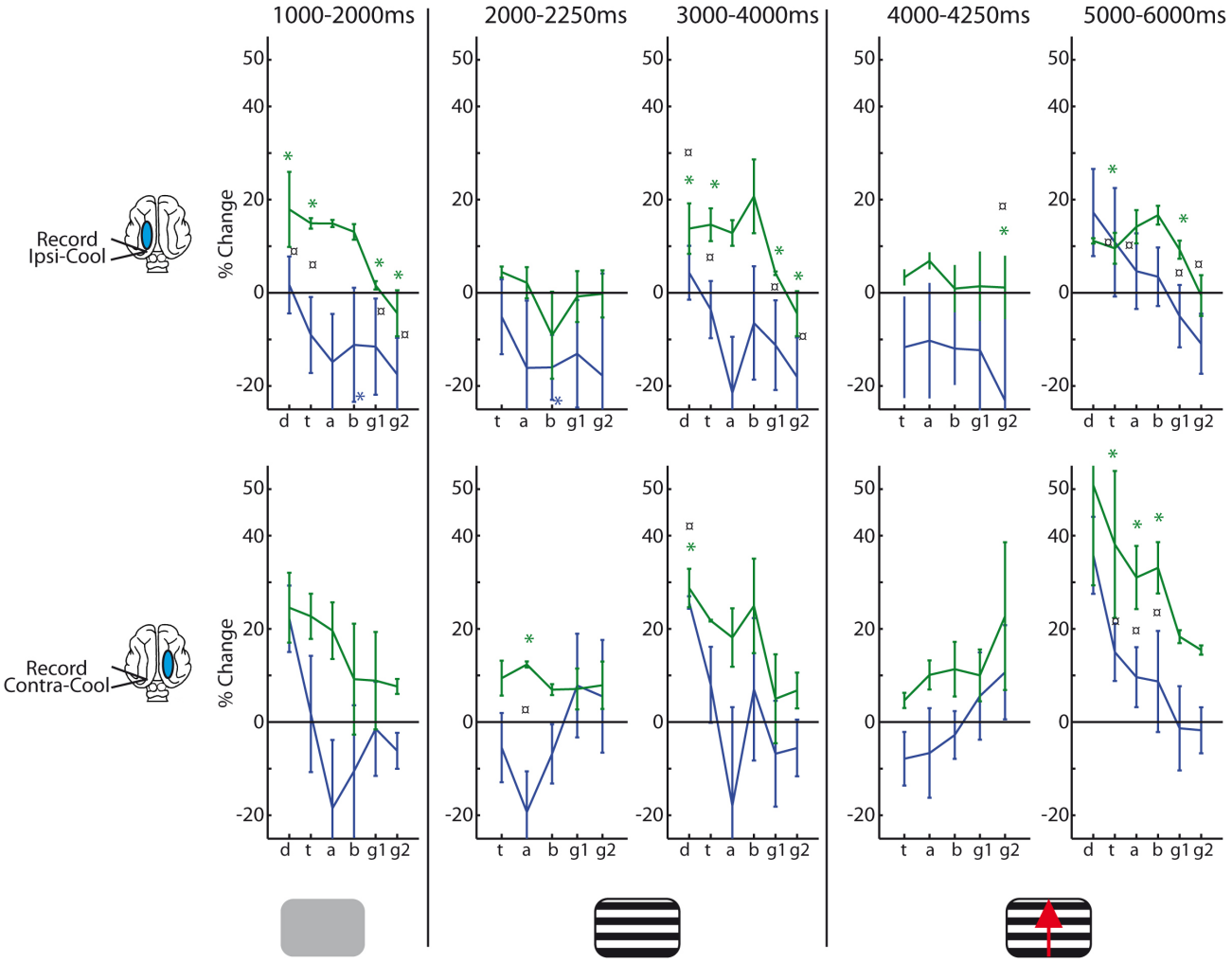

Fig 3.7 – awake pMS inactivation, Analysis 1. The top row is deactivation ipsilateral to the electrodes and the bottom row contralateral to deactivation. The blue trace is for pMS Inactive and green is pMS Re-active. The stimulus phase is indicated at the bottom of the figure. Analysis windows are indicated in ms at the top. The long vertical lines between the stimulus icons indicate a stimulus change. The bottom of each subplot has the frequency bands: d (delta), t (theta), a (alpha), b (beta), g1 (gamma1), and g2 (gamma2). The y-axis positive values are the percent change in Inactive and Re-active power relative to SC Active power. An asterisks indicates that each individual cat of the three cats surpassed the significance threshold (one-tail t-test, $p<.05$)

with a particularly strong trend in gamma1 and gamma2. Inactivation-induced curves seem to resemble each other for the ipsilateral and contralateral cooling conditions for AWs Gray, Static Grating and Moving Grating, with the caveat that the contralateral curve is shifted in the positive direction relative to the ipsilateral curve.

If the gamma1 and gamma2 inactivation induced power changes for the ERP-1 and ERP-2 AWs are compared between ipsi and contralateral cooling, a trend towards a power imbalance can be discerned. The gamma power ipsilateral to cooling is largely decreased for ERP-1 and ERP-2, the 250ms AWs immediately following stimulus change that are involved in orienting behavior in the visual perimetry task, while gamma power following contralateral cooling has a trend to increase. This interhemispheric gamma imbalance was strongly significant in two of the three cats (Gamma1: cat2 = $p < 9.1 \times 10^{-216}$, cat 3 = $p < 9.1 \times 10^{-175}$ & Gamma2: cat2 = $p < 9.1 \times$

	1000-2000ms	2000-2250ms	3000-4000ms	4000-4250ms	5000-6000ms
Delta	- 18%, p< .03		- 14%, p< .04		- -
Theta	- 15%, p< .0003	- -	- 15%, p< .02	- -	- 10%, p< .003
Alpha	- -	- -	- -	- -	- -
Beta	-11%, p< .05 -	-16%, p< .01 -	- -	- -	- -
Gamma1	- 2%, p< .003	- -	- 4%, p< .01	- -	- 9%, p< .001
Gamma2	- 4%, p< .02	- -	- -4%, p< .02	- 1%, p< .04	- -

Table 12: Analysis 1, awake pMS ipsilateral to recording electrodes. The pMS was deactivated (blue) or reactivated (green) ipsilateral to recording electrodes. Percent change in power relative to pMS Active (from fig 3.7 - top) was listed if all three cats surpassed significance criterion. The listed p-value is the value associated with the power change that was the least significant of the three cats. Dashes represent values that did not exceed significance criterion and were thus not listed.

	1000-2000ms	2000-2250ms	3000-4000ms	4000-4250ms	5000-6000ms
Delta	- -		- 29%, p< .03		- -
Theta	- -	- -	- -	- -	- 38%, p< .01
Alpha	- -	- 12%, p< .03	- -	- -	- 31%, p< .05
Beta	- -	- -	- -	- -	- 33%, p< .03
Gamma1	- -	- -	- -	- -	- -
Gamma2	-	- -	- -	- -	- -

Table 13: awake pMS contralateral to recording electrodes, Analysis 1. The pMS was deactivated (blue dashes) or reactivated (green) contralateral to recording electrodes. Percent change in power relative to pMS Active (from fig 3.7 - bottom) was listed if all three cats surpassed significance criterion. The listed p-value is the value associated with the power change that was the least significant of the three cats. Dashes represent values that did not exceed significance criterion and were thus not listed.

10^{-216} , cat3 = $p < 9.1 \times 10^{-216}$). These p-values, more extreme than 1.0×10^{-175}, are highly significant in the two cats. Cat 1 did not reach significance however. A good explanation for the difference between cat 1 and the last two cats, is the very low motivation of cat 1. It was always on the verge of sleeping during the passive viewing task, would get very excited without warning during the Passive Viewing task, and never achieved the rewarm part of the Perimetry task. In the cat colony, it startled easily and often hid itself from the other cats. It is thus likely that the data from cat 1 in the passive viewing task, where no behavior was required of the animal, and minimal assessment of internal state of the animal could be made, can be regarded as an outlier. The data points for cat 1 in the passive viewing task may be more reflective of the internal state of the cat, than the external visual stimulus

3.4.1 Awake pMS, Analysis2

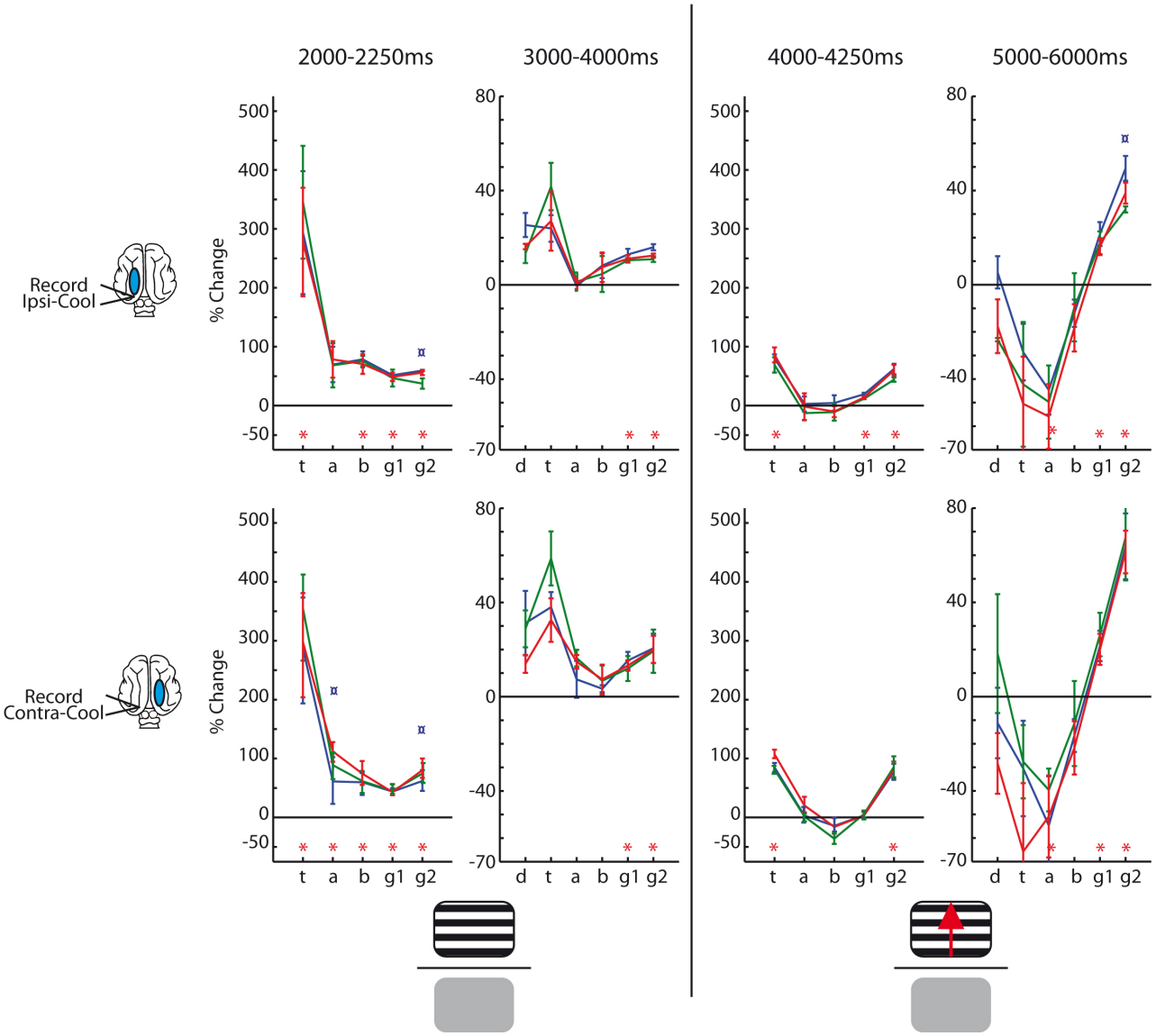

Fig 3.8 – awake pMS inactivation, Analysis 2. The top row is ipsilateral deactivation data and the middle row contralateral deactivation. Red represents pMS Active, blue is pMS Inactive, and green is pMS Re-active. The analysis time window is given in ms at the top of the figure. The icons at the bottom of the figure indicate stimulus phase (static or moving grating) divided by the gray screen that appeared at the beginning of a trial. The long vertical line between the stimulus icons indicate a stimulus change. The bottom of each subplot has the frequency bands: d (delta), t (theta), a (alpha), b (beta), g1 (gamma1), and g2 (gamma2). The y-axis values are the percent increase of power over baseline (gray screen). Red asterisks indicate a significant change in power over the baseline (gray screen) time period. The blue (pMS Inactive) and green (pMS Re-Active) boxes indicate a power-change value significantly different from pMS Active (red line). The computation for pMS Active (red line), pMS Inactive (blue line), and pMS Re-active (green line), was the same. Only the statistical comparison (grating v gray screen for SC Active [red asterisks], SC Active v pMS Inactive or pMS Re-active [blue or green box]) was different.

Analysis 2 yielded a largely similar result for the pMS Active condition for Awake (project 3) when compared to Anesthetized (Project 2) states. As with the anesthetized figure, the red asterisks show significant stimulus-induced changes in power (fig 3.8, tables 14 & 15). Differences between anesthetized and awake recordings exist in 1) the amplitude of changes, with the awake animal having less extreme stimulus-induced changes than anesthetized, 2) an increase in gamma2 for

	2000-2250ms	3000-4000ms	4000-4250ms	5000-6000ms
Delta		-		-
		-		-
		-		-
Theta	278%, p< 4.6e-91	-	86%, p< 6.8e-13	-
	-	-	-	-
	-	-	-	-
Alpha	-	-	-	-50%, p< 3.6e-9
	-	-	-	-
	-	-	-	-
Beta	71% p< 3.1e-5	-	-	-
	-	-	-	-
	-	-	-	-
Gamma1	49%, p< 9.8e-69	11%, p< 3.9e-8	14%, p< .0006	16%, p< 9.3e-11
	-	-	-	-
	-	-	-	-
Gamma2	56%, p< 2.0e-60	12%, p< 4.5e-9	60%, p< 1.5e-55	39%, p< 2.9e-76
	60%. p< .04	-	-	49%, p<, .01
	-	-	-	-

Table 14: awake pMS ipsilateral to recording electrodes, Analysis 2. Active is red, Inactive is blue, Re-active is green. Values are from fig 3.8 top. Changes in power for the different stimulus phases relative to the gray screen stimulus phase were listed if values surpassed significance criterion. Significance criterion were met if each of the three cats individually passed p<.05 on a 1-tail t-test. Dashes are placed for data points where at least one of the three cats did not surpass significance. The least significant value from the three cats is listed. The t-test was performed for pMS-warm (red values) relative to 0, and for pMS-incative (blue values) and pMS-reactive (green values) relative to pMS-warm. Red values thus represent significant power changes that a stimulus induced relative to the gray screen stimulus, while blue and green values are power changes for Inactive and Re-active that were significantly different from SC-active power changes. There are no values for delta in the 2000-2250ms and 4000-4250ms AW's because a Fourier transform for 250ms for frequencies below 4Hz cannot be performed.

the Static-grating AW for awake vs. no change in the anesthetized cat, and 3) a larger decrease in low frequencies (significant for alpha) in the Moving Grating AW for awake cats.

Changes for the Inactive recording condition relative to Active were negligible for both ipsilateral and contralateral cooling for Analysis 2. This is different from Analysis 2 power increases in the anesthetized Inactive condition. It could be that the effects of cooling are masked by ongoing activity in the awake animal. Awake Re-active values, as with the anesthetized cat, were unchanged from Active.

	2000-2250ms	3000-4000ms	4000-4250ms	5000-6000ms
Delta		-		-
		-		-
		-		-
Theta	294%, p< 4.0e-20	-	103%, p< 1.1e-5	-
	64%, p< .003	-	-	-
	-	-	-	-
Alpha	115%, p< .003	-	-	-51%, p< 3.6e-9
	-	-	-	-
	-	-	-	-
Beta	74%, p< 3.4e-7	-	-	-
	-	-	-	-
	-	-	-	-
Gamma1	43%, p< 6.6e-13	13%, p< .003	-	20%, p< 9.2e-11
	-	-	-	-
	-	-	-	-
Gamma2	77%, p< 3.0e-19	20%, p< 1.4e-8	80%, p< 2.8e-20	61%, p< 2.0e-6
	62%, p< .01	-	-	-
	-	-	-	-

Table 15: awake pMS contralateral to recording electrodes, Analysis 2. Active is red, Inactive is blue, Re-active is green. Values from fig 3.8 - bottom. For figure legend details, see table 14.

3.4.3 Awake pMS - ERP Results

Following the two stimulus changes in the passive viewing task, the waveform in the LFP data was averaged across trials for each of the Active, Inactive, and Reactive conditions. The area between voltage=0 and the initial positive deflection immediately following stimulus change, and the area between voltage=0 and the negative deflection following the positive deflection, were ascertained. The time point in milliseconds where the voltage peaked in the positive deflection and where it peaked in the negative deflection were also computed. This was done for each cat for Active, for Inactive, and again for Re-active. The results of this analysis are shown in

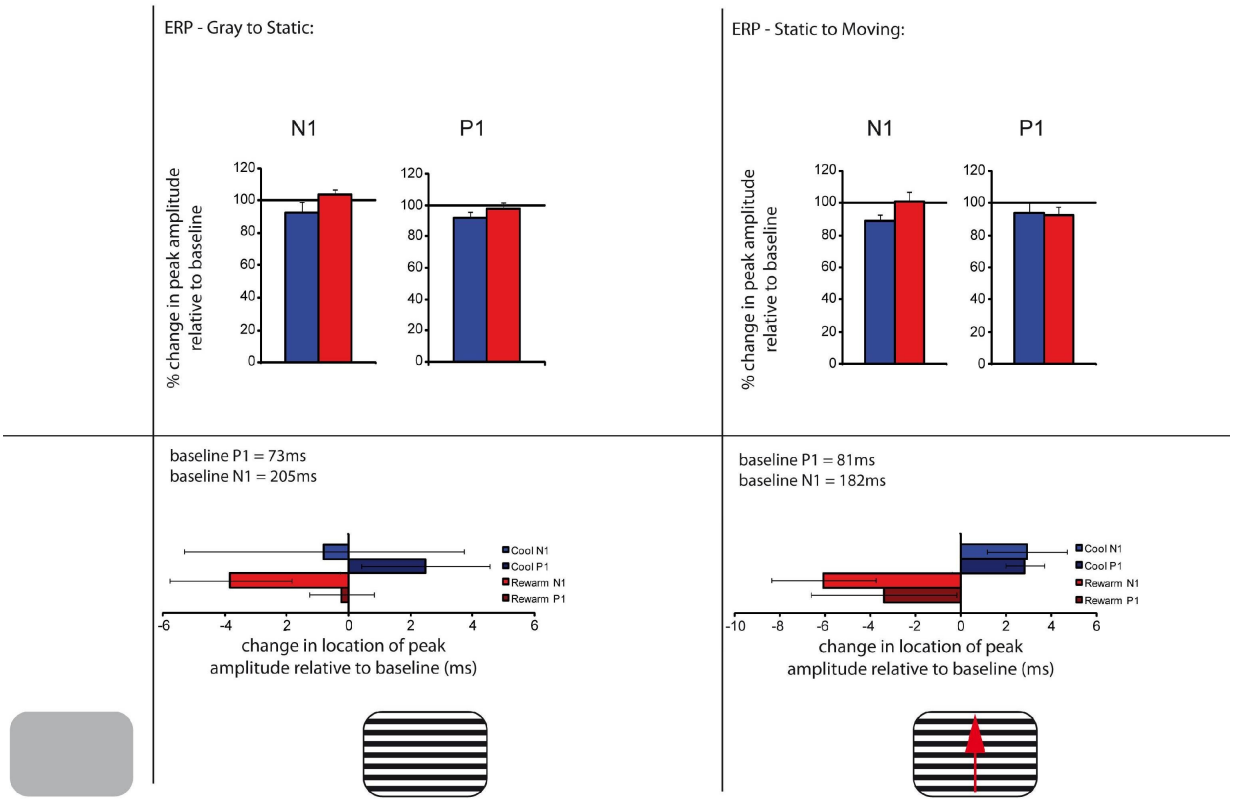

Fig 3.9 – awake pMS inactivation, ERP analysis. Stimulus icons are at the bottom of the figure. The vertical lines indicate change in the stimulus. The ERP analysis assesses change in area under the curve for the N and P peaks relative to pMS Active for the Inactive and Re-active conditions, upper part of the figure. The lower part of the figure displays changes in the latency of the peaks relative to pMS Active. Red depicts pME rewarm data, blue shows pMS inactive data

fig 3.9. The error bars on the graphs are standard error of the mean for the three cats. The 100% value on the y-axis for the area under the curve analysis is the value for Active. On the time axis at the bottom of the figure, zero is the time for the Active peak. The Inactive and Re-active peaks are expressed as millisecond deviations from Active, with positive values indicating a time point after the Active value. Active time values are on the figure. Active grey-to-static-grating ERP had a positive peak at 73ms and a negative peak at 205ms. Warm static-to-moving-grating had a positive value of 81ms and a negative value of 182ms.

Take-home points from the awake pMS ERP analysis are: 1) cooling reduces the amplitude of the positive and negative peaks for both grey-to-static-grating and static-to-moving-grating of ~15%. 2) Re-active amplitude values return to Active values with the exception of the P deflection for static-to-moving-grating which stays at Inactive levels. 3) The time of peak amplitude of both positive and negative peaks is little changed between Warm, Cool, and Rewarm.

3.4 Perimetry (Project 4)

Electrophysiological recording in cat while performing a visual perimetry task with cortical cooling is a new paradigm. Therefore, Analysis 2 (fig 3.10), where the analysis windows Start, Expectation, and Reward, are normalized to Baseline activity, will be shown before Analysis 1 (fig 3.11). This allows for an overview of how the cat primary visual cortex responds to the Perimetry stimulus. The number of trials for each behavioral outcome are as follows: attend contralateral: cat1 n= 76, cat2 n=124, cat3 n=51; attend ipsilateral: cat1 n= 70, cat2 n=134, cat3 n=56; Inactive attend: cat1

n=183 , cat2 n=160, cat3 n=125; Neglect: cat1 n=120 , cat2 n=160, cat3 n=95; Re-active ipsilateral: cat1 n=42 , cat2 n=58; Re-active contralateral: cat1 n= 46, cat2 n=60

3.4.1 Perimetry – Analysis2

Analysis 2 provides an overview of how activity changes in response to the stimulus: pMS active - stimulus attended (fig 3.10, top), pMS inactive - ipsilateral stimulus attended/contralateral stimulus neglected (fig 3.10, middle), and pMS re-active - stimulus attended (fig 3.10, bottom). As it was unknown in which hemifield the 2LED stimulus would appear, trials pre Reward AW were averaged, thereby doubling the number of trials pre 2LED relative to post 2LED. Following the vertical line indicating 2LED onset in figure 3.10, two behavioral outcomes were possible: 1) stimulus contralateral to the pMS which was eventually cooled and 2) stimulus ipsilateral to the pMS that was eventually cooled. The icons above the graphs following the 2LED icon indicate: if the pMS was active (red) or inactive (blue), where the stimulus appeared (left or right hemifield), and if the stimulus was attended-to (green check) or neglected (red 'X'). The standard error of the mean for the three cats is represented by the error bars. Criterion for significance, where the asterisks are, is the same as previously described. To review, all three cats had to have a power change in the same direction relative to baseline and all changes had to be more significant that $p < .05$. Significant data points are placed in color coded tables for: pMS active (red, table 16), pMS inactive (blue, table 17), and pMS re-active (green,

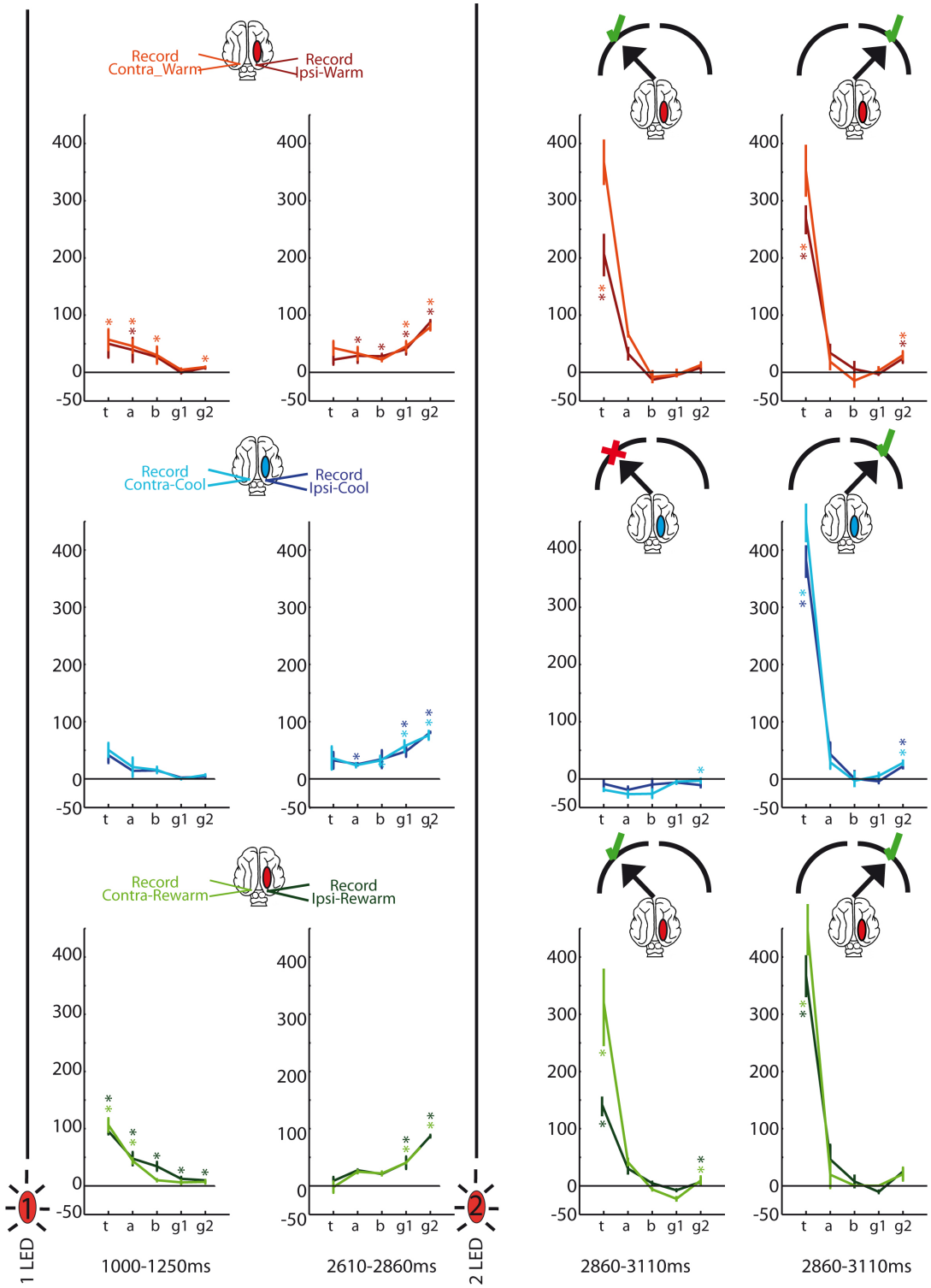

Fig 3.10 – Perimetry Analysis 2. The top row is pMS Active, the middle row pMS Inactive, and the bottom row pMS Re-active. The long vertical lines extending from LED1 and LED2 indicate the time point of the respective LED onset. Icons over the subplots post LED2 indicate the cooling state of the pMS (blue inactive, red active) and the behavioral response of the cat in the perimetry (either perimetry left or right response). The bottom of each subplot has the frequency bands: d (delta), t (theta), a (alpha), b (beta), g1 (gamma1), and g2 (gamma2). The y-axis values are the change in power relative to pre 1LED power levels. Asterisks indicate a significant change in power relative to baseline, pre 1LED. (1-tail t-test, $p<.05$ for each individual cat)

table 18).

General trends in the data for all cooling conditions include: 1) an increase in low frequency and gamma2 power in the Start AW, 2) an increase in gamma1 and gamma 2 power in the Expectation AW, 3) and increase in theta and gamma2 power in the Reward AW when the stimulus was attended. The AW Reward for Neglect, showed a reduction in power relative to AW Base.

3.4.1.1 Perimetry – Analysis2 – pMS Active

The cooling condition pMS active, showed an increase in theta, alpha, beta, and gamma2 power for the contralateral hemisphere (light red) and a similar trend for the

	1000-1250ms	2610-2860ms	Contra 2860-3110ms	Ipsi 2860-3110ms
Theta	58%, p< .048	-	361%, p< 1.2e-9	359%, p< 7.3e-11
	-	-	208%, p< 5.7e-9	271%, p< 3.8e-6
Alpha	46%, p< .0051	-	-	-
	40%, p< .009	29%, p< .02	-	-
Beta	30%, p< .014	-	-	-
	-	28%, p< .037	-	-
Gamma1	-	45%, p< 3.4e-8	-	-
	-	41%, p< 3.5e-6	-	-
Gamma2	10%, p< .0035	79%, p< 1.4e-36	-	23%, p< 1.8e-9
	-	-88%, p< 1.1e-27	-	16%, p< 1.8e-3

Table 16: Perimetry task pMS Active, Analysis 2. Light red represents electrodes contralateral to the pMS. Dark red represents electrodes ipsilateral to the pMS. Values are from fig 3.10 top. Changes in power for the different stimulus phases relative to pre 1LED were listed if values surpassed significance criterion. Significance criterion were met if each of the three cats individually passed p<.05 on a 1-tail t-test. Dashes are placed for data points where at least one of the three cats did not surpass significance. The least significant value from the three cats is listed. The t-test was performed for post 1LED values relative to pre 1LED.

ipsilateral hemisphere (dark red) with a significant increase in alpha power only (Table 16). The Expect AW had a significant increase in bilateral gamma 1 and gamma 2 power. When the stimulus associated with a reward and a behavior occurred, 2LED, theta power had a significant increase for both ipsilateral and contralateral stimuli. Gamma2 also showed an increase for both stimuli, but only power changes for ipsilateral stimuli reached significance.

3.4.1.2 Perimetry – Analysis2 – pMS Inactive

Similar to pMS active, there was an increase in low-frequency power for AW Start, but it failed to reach significance. The Expectation AW had a power change similar to pMS Active with Gamma1 and Gamma2 power significantly increasing bilaterally to levels similar to pMS Active (table 17). The Reward AW showed a similar

	1000-1250ms	2610-2860ms	Contra 2860-3110ms	Ipsi 2860-3110ms
Theta	- -	- -	- -	483%, p<7.3e-11 389%, p< 3.7e-6
Alpha	- -	- 26%, p< .002	- -	- -
Beta	- -	- -	- -	- -
Gamma1	- -	55%, p< 3.3e-16 48%, p< 2.2e-92	- -	- -
Gamma2	- -	75%, p< 4.5e-63 81%, p< 4.6e-54	-2%, p< .037 -	36%, p<, 1.8e-9 22%, p< 1.8e-3

Table 17: Perimetry task pMS Inactive, Analysis 2. Light blue represents electrodes contralateral to the pMS. Dark blue represents electrodes ipsilateral to the pMS. Values are from fig 3.10 middle. Changes in power for the different stimulus phases relative to pre 1LED were listed if values surpassed significance criterion. Significance criterion were met if each of the three cats individually passed p<.05 on a 1-tail t-test. Dashes are placed for data points where at least one of the three cats did not surpass significance. The least significant value from the three cats is listed. The t-test was performed for post 1LED values relative to pre 1LED.

power profile to pMS Active when the stimulus was attended, but when the stimulus was neglected, there was no change from Baseline power and even a 2% decrease in gamma2 power for the hemisphere contralateral to pMS deactivation. The notable part of this lack of power change, is that the 'expectation profile' with gamma power elevated in the Expectation AW, is no longer present in the Reward AW for neglected stimuli. The expectation-profile is absent despite a mere 250ms time-shift between Expectation and Reward AWs (there was no time delay between the end of AW Expect and the beginning of AW Reward).

3.4.1.3 Perimetry – Analysis2 – pMS Re-active

At the end of each recording secession, the pMS was allowed to rewarm. This was used as a control to see if neural activity returned to baseline, pMS Active, levels in tandem with the return of behavioral performance. Cat3, as mention in the Awake Passive Viewing task, did not continue performing this long each day. Therefore, the pMS Rewarm data and associated significance values come from only 2 cats.

Rewarm values largely returned to their pMS Warm values. The Expectation-profile in AW Expectation, was still present. A notable difference from Inactive – attend contralateral is the significant increase, following the decrease during neglect, of gamma 2, which bilaterally increased by 15% over baseline in the Re-active – attend contralateral condition. Gamma2 power for Re-active – attend contralateral was no longer significant, but still showed a non-significant increase in power of ~15%.

	1000-1250ms	2610-2860ms	Contra 2860-3110ms	Ipsi 2860-3110ms
Theta	106%, p< 6.0e-8 95%, p< 2.8e-5	- -	335%, p< 2.3e-6 144%, p< 7.2e-5	491%, p< .0009 387%, p< .002
Alpha	43%, p< 1.4e-5 48%, p< .01	- -	- -	- -
Beta	- 34%, p< .01	- -	- -	- -
Gamma1	- 13%, p< .04	41%, p< 3.1e-9 41%, p< 6.8e-6	- -	- -
Gamma2	- 10%, p< .03	86%, p< 6.0e-29 87%, p< 9.1e-26	15%, p< .039 15%, p< 4.5e-5	- -

Table 18: Perimetry task pMS Re-active, Analysis 2. Light green represents electrodes contralateral to the pMS. Dark green represents electrodes ipsilateral to the pMS. Values are from fig 3.10 bottom. Changes in power for the different stimulus phases relative to pre 1LED were listed if values surpassed significance criterion. Significance criterion were met if each of the three cats individually passed p<.05 on a 1-tail t-test. Dashes are placed for data points where at least one of the three cats did not surpass significance. The least significant value from the three cats is listed. The t-test was performed for post 1LED values relative to pre 1LED.

3.4.2 Perimetry – Analysis1

Analysis 1 compared the change in power in all four AWs for pMS inactive and pMS Re-active relative to pMS Active (fig 3.11). The only significant changes in power occurred in the Reward AW for neglected stimuli. Theta, alpha, and gamma2 showed a bilateral decrease in power. Power changes and associated p-values are shown in table 19.

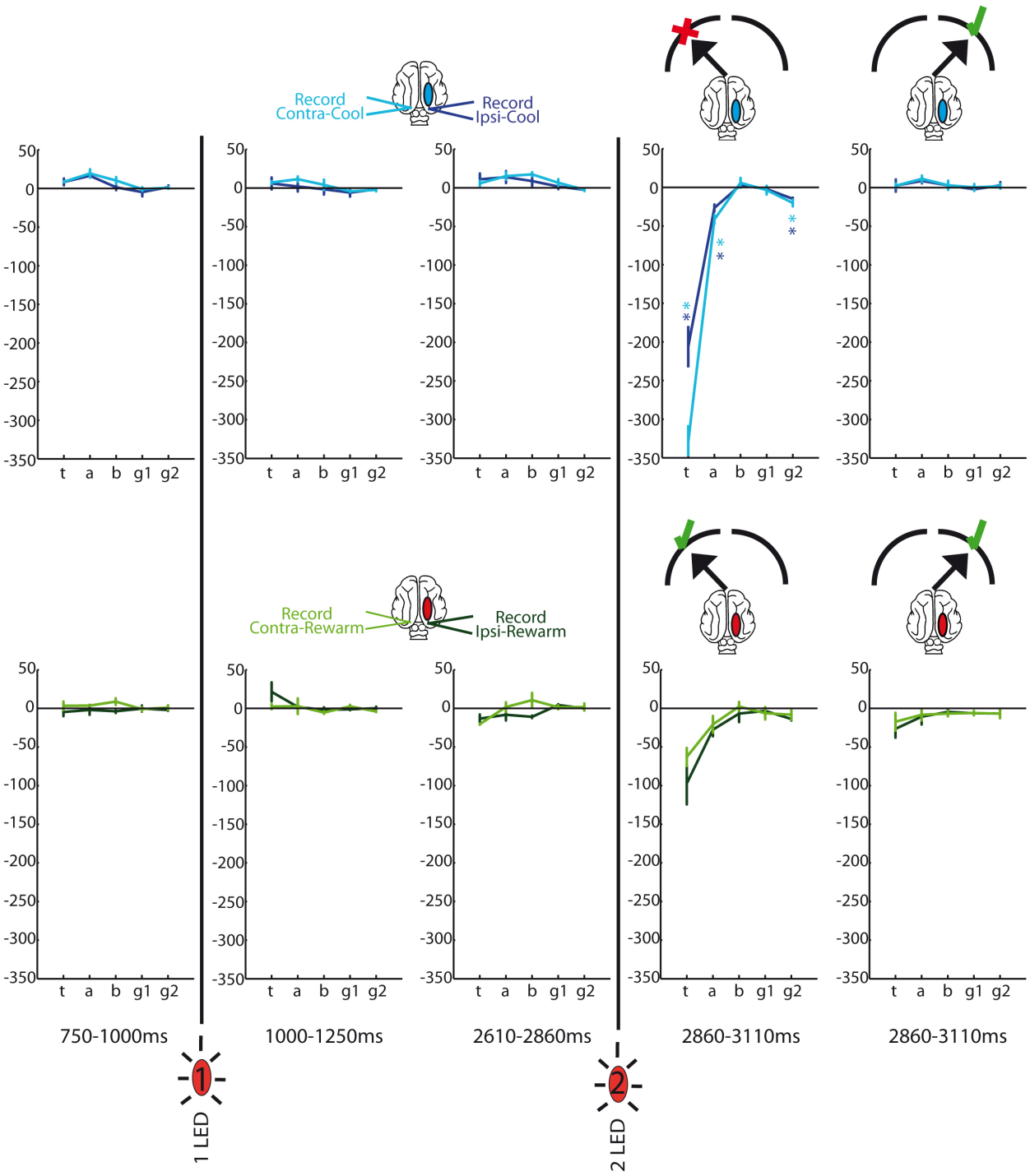

Fig 3.11 – Perimetry Analysis 1. The top row is pMS Inactive, and the bottom row pMS Re-active. The long vertical lines extending from LED1 and LED2 indicate the time point of the respective LED onset. Icons over the subplots post LED2 indicate the cooling state of the pMS and the behavioral response of the cat. The bottom of each subplot has the frequency bands: d (delta), t (theta), a (alpha), b (beta), g1 (gamma1), and g2 (gamma2). The y-axis positive values are the percent increase of power over pre LED1 activity within the respective pMS cooling state. Negative values are the amount by which pre LED1 power was greater than pMS Inactive or Re-active power. Note the significant bilateral decrease in power for the post-LED2 neglect condition.

	750-1000ms	1000-1250ms	2610-2860ms	Contra 2860-3110ms	Ipsi 2860-3110ms
Theta	-	-	-	-342%, p< 9.9e-12	-
	-	-	-	-210%, p< 4.5e-7	-
Alpha	-	-	-	-49% p< .05	-
	-	-	-	-26%, p< ..033	-
Beta	-	-	-	-	-
	-	-	-	-	-
Gamma1	-	-	-	-	-
	-	-	-	-	-
Gamma2	-	-	-	-20%, p< .02	-
	-	-	-	-14%, p< .01	-

Table 19: Perimetry task pMS Inactive, Analysis 1. Light blue represents electrodes contralateral to the pMS. Dark blue represents electrodes ipsilateral to the pMS. Percent change in power relative to pMS Active (from fig 3.11 - top) was listed if all three cats surpassed significance criterion. The listed p-value is the value associated with the power change that was the least significant of the three cats. Dashes represent values that did not exceed significance criterion and were thus not listed.

3.4.2 Perimetry – ERP analysis

The average waveform from trials within cat and behavioral-cocktail following LED-1 and LED-2 onset was made. Figure 3.12 shows the latency of the ERP following the onset of LED-1 and following the onset of LED-2. The time point of the negative peak and the time point of the positive peak were computed. As the time values for both hemispheres were statistically undifferentiable for each other, the ERP values from the left and right array were combined. The first negative, N, peak following LED-1 was ~167ms following LED-1 onset, while the positive, P, peak was ~215ms after LED-1 onset (fig 3.12). Following LED-2 the N-peak was at ~90ms. The reason for this earlier occurrence is presumably due to attentional effects induced by LED-1. LED-1 indicated to the cat that a peripheral stimulus, LED-2, would occur in 1.8s after LED-1 lit-up. The two time values for the N-peak following LED-2 are for visual targets

contralateral to future pMS deactivation, 88ms in dark green, and targets ipsilateral to future pMS deactivation, 108ms in light green.

Not only were the peaks earlier for LED-2 relative to LED-1, ~48% earlier for the N-peak, but the amplitude of two peaks following LED-2 were much larger than for LED-1. The N-peak for LED-2 increased over the LED-1 peak ~230% for ipsilateral targets, and ~2200% for contralateral targets. The P-peak increased ~1800% for

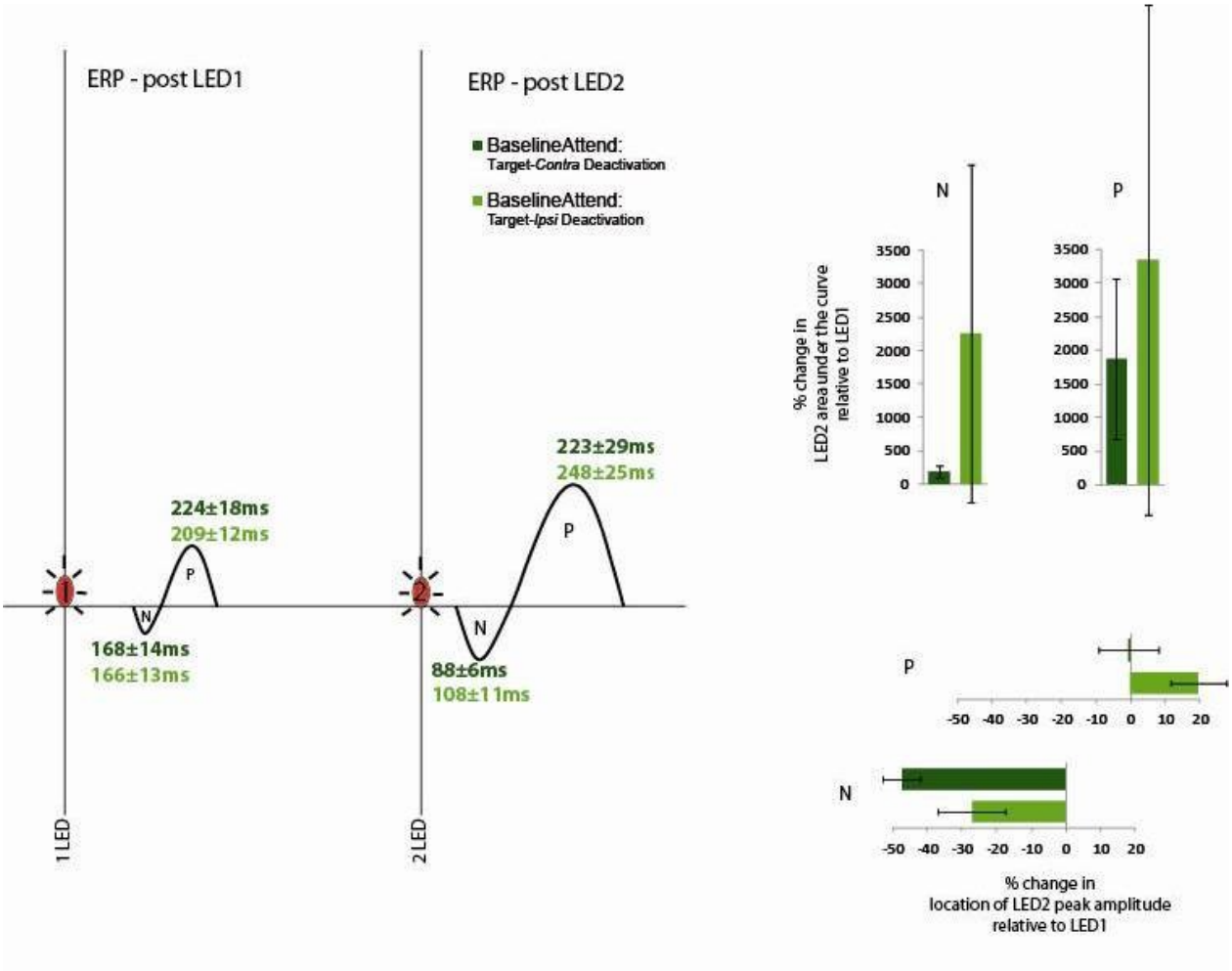

Fig 3.12 – Perimetry ERP- pMS Active, baseline analysis. Stimulus icons in the middle of the figure with the associated vertical lines indicate LED1 and LED2 onset. The ERP analysis assesses the latency of ERP peaks during pMS Active conditions with associated SEM for the 3 cats. Area under the curve and latency for the N and P peaks was normalized for LED2 relative to LED1 (right side of figure). Note the earlier onset of the N peak post 2LED, as-well-as the increase in amplitude for the N and P peaks post 2LED. This occurs despite the stronger visual saliency of the centrally place LED1 relative to the position of the 2LED in the lateral visual hemifield.

ipsilateral and ~3300% for contralateral targets. The error bars are the SEM for the three cats. Their large size conceals the fact all three cats had an increase in area-under-the-curve of more than 200%. Thus the priming that LED-1 provided to the LED-2 ERP was a robust phenomenon.

3.4.2.2 Perimetry ERP - Between Cooling Conditions

Changes in latency and area-under-the-curve were assessed relative to the pMS Active-stimulus attended behavioral outcome. Changes for Neglect and Inactive-attend were assessed (marked in blue in fig 3.13), as-well-as changes for Re-active - attend contralateral and Re-active-attend ipsilateral (marked in red in fig 3.13). Values for ERP-1 were averaged for 2LED ipsilateral and 2LED contralateral trials. This averaging was done because there was no indication to the cat, prior to LED-2 onset, in which hemifield LED-2 would appear.

Deactivating pMS led to a ~30% decrease in the N and P peak following LED-1. Reactivating pMS let to an increase to the N peak of 39% over pMS Warm, while the P-peak remained close to the pMS Cool value, 23% below the pMS Warm value. The latencies of the peaks increased by around 8ms for both Cool and Rewarm.

The striking aspect of this ERP analysis is the almost absence an ERP for the Neglect post LED-2 trials. The N-peak decreased 91% from the Active-stimulus attended value and the P-peak decreased by 96% (fig 3.13, dark blue). The Inactive-stimulus attended values were on par with Active-stimulus attended or even slightly

increased (fig 3.13, light blue). Re-activating the pMS led to a return of values to Active-stimulus attended values.

Latency changes were minimal for Inactive and Re-active. Since the ERP-2 amplitude of the neglected stimuli was so drastically diminished, changes in ERP latency were difficult to assess.

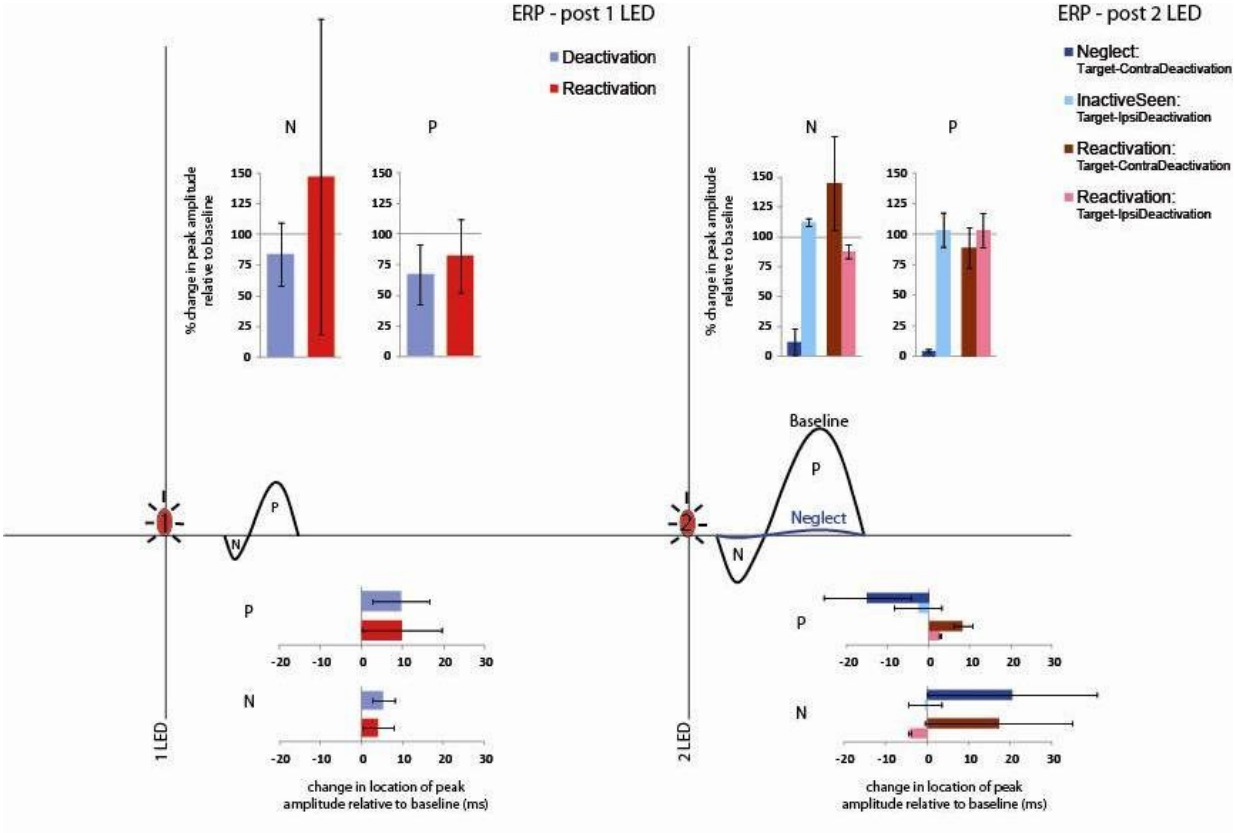

Fig 3.13 – Perimetry ERP - pMS Inactive/Re-active analysis. Stimulus icons in the middle of the figure with the associated vertical lines indicate LED1 and LED2 onset. Changes in area under the curve relative to pMS Active-Attend are shown at the top of the figure. Latency changes relative to pMS Active-Attend are shown at the bottom. Note the drastic reduction in amplitude for the Neglect condition. Error bars are SEM for the three cats.

Discussion

4.1 – Results: points of discussion

The perimetry task (project 4) had a couple of experimental caveats: 1) the ERP2 latency difference between the two visual hemifields in figure 3.12, and 2) reaction time measurements.

The two time values for the ERP N-peak following LED-2 are for visual targets contralateral to future pMS deactivation, 88ms in dark green, and targets ipsilateral to future pMS deactivation, 108ms in light green (fig 4.1). As cooling the left or right pMS required attaching plastic tubing to deliver the chilled methanol to the cryoloop, as-well-as attaching a plug to the thermocouple that monitored probe temperature, there was a small imbalance in forces on the head that was dependent on the side of the cortex that was being deactivated. This potential pull on the head by cryoloop cables is consistent with the earlier occurrence of ERP2 when the 2LED visual target was contralateral to the pMS-cryoloop that had the methanol tubing and thermometer cable attached.

Unfortunately reaction time during project 4 was not measured. Analysis could be improved by using the onset of the behavioral reaction to LED2 as the reference point for creating the Reward AW rather than the onset of LED2 stimulus. Different cats had different motivational levels and motivation changed between days. Since gamma oscillations in response to the stimulus could be very transient, using the reaction time would improve signal-to-noise for the gamma signal by helping to place

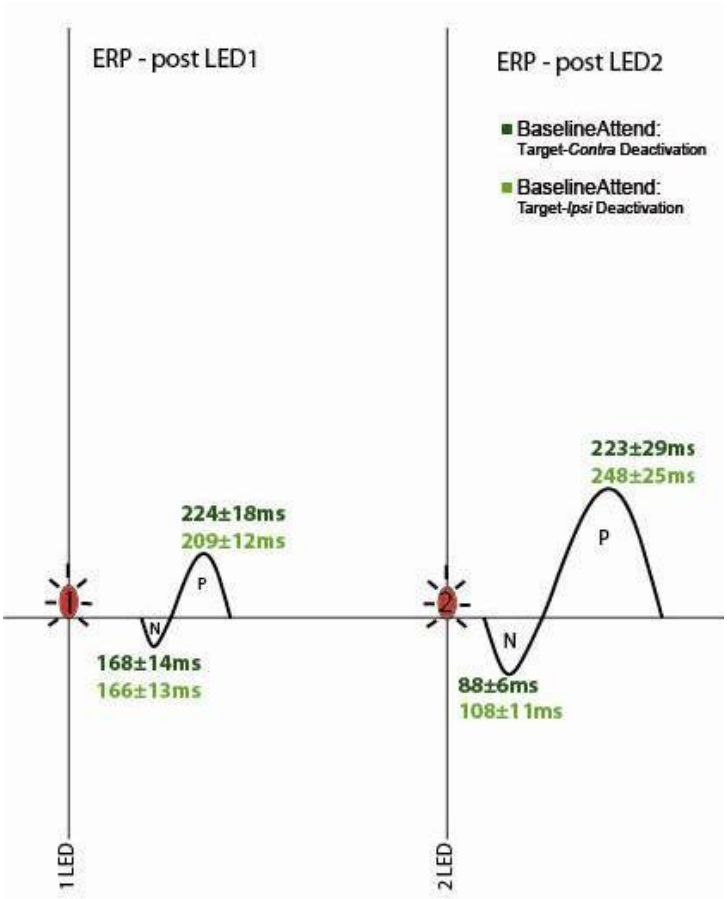

Fig 4.1 (replicated from fig 3.12, where timing and amplitude differences are quantified) - the N-peak following 2LED is much earlier than the N-peak following 1LED. Moreover, the latency for the N-peak following 2LED is different for stimuli ipsilateral to attached cryoloop (methanol tubing and thermometer cable) versus stimuli contralateral to attached cryoloop. This likely creates the 20ms difference between the visual hemifields in peak latency for post 2LED N-peak.

the analysis window more precisely. Moreover, it would increase signal to noise for theta oscillations and help to clarify the interplay between theta and gamma in response to LED2. A lack of reaction time measurements in the current data set does not however jeopardize the current findings; rather the presence of a reaction time reference point could only improve signal-to-noise ratio and thus the experimental findings.

A broad-band noise occurs in the LFP signal ~350ms post LED2 onset. This is almost certainly the head movement of the cat when it identifies the location of LED2. The noise confirms that the signal analyzed in the Reward AW, the 250ms immediately following LED2 onset, contains no movement artifacts because the first motor action a cat made during a trial was to orient to LED2, thus generation the

broadband noise. It can be concluded that head-movement noise at ~350ms is the first behavioral reaction to 2LED, not eye movements, because cat eye movements are very limited (Evinger & Fuchs 1978). The small mass of the cat head makes head movements bioenergetically efficient (Blakemore & Donaghy 1980) and head movements allow visual and auditory maps to maintain a close co-registration (Haris et al 1980).

4.2 – Results summary

A brief summary of the results is as follows: as mentioned, all electrophysiological recordings in all four projects were made from the area 17/18 boarder. Unilateral cooling of the SC in the anesthetized cat (project 1) leads to an ipsi-cool decrease in gamma oscillations in primary visual cortexes and a contra-cool increase (fig 3.3). Unilateral cooling of the pMS during passive viewing in the anesthetized cat (project 2) leads to an ipsi-cool decrease in gamma oscillations as-well-as an ipsi-cool decrease in low frequency delta and theta oscillations while contralateral pMS cooling has the tendency to slightly increase power in all frequency bands (fig 3.5). Unilateral cooling of the pMS in the awake cat during passive viewing (project 3) leads to a statistically insignificant imbalance in gamma oscillations between the hemispheres, with cooling causing an ipsi-cool reduction in gamma power relative to the contra-cool hemisphere (fig 3.7). The statistical insignificance of the effect is presumably due to much stronger ongoing activity in the awake cat relative to the anesthetized. Unilateral pMS cooling while performing a visual perimetry task

(project 4) leads to a bilateral loss of theta and gamma power for neglected stimuli relative to warm-seen stimuli (fig 3.11). The clear commonality between all four projects is the loss of gamma power for cooling-related unilateral visual hemineglect. Deactivation of pMS but not the SC leads to a theta reduction.

4.3 – Awake Behaving Data

Since project 4 probes neglect using electrophysiological recordings in the awake behaving animal, it will be the starting point for the discussion. Figure 4.2 shows the effects on oscillatory power as a result of pMS inactivation. The Reward analysis window (AW) immediately following onset of LED2 shows a statistically significant drop in bilateral theta and gamma for each of the three cats when stimuli were neglected, while stimuli that were attended ipsilateral to pMS cooling led to no significant change in power. This means that the loss of theta and gamma power are not simply associated with pMS inactivation, but rather the loss of power occurs only when stimuli are neglected. To further underscore this point, AWs prior to LED2 onset, when a behavioral response had yet to be made, show no change in pMS inactive power relative to pMS active. Loss of theta and gamma power comes only in the Reward AW when a behavioral response was to be made, but was not made due to pMS-deactivation induced hemineglect.

Changes in oscillatory power relative to pre LED1 onset (analysis 2) for pMS active, inactive, and re-active conditions (fig 4.3) reveal a large increase in theta and gamma power for attended stimuli in the post LED2 onset, Reward AW. This resembles

an amplification of the low-frequency and gamma power increase following LED1 onset. While the central (foveal) location of LED1, versus the peripherally placed LED2, would suggest a higher visual saliency for LED1, this higher saliency is not observed in the electrophysiological signal. On the contrary, oscillatory power is

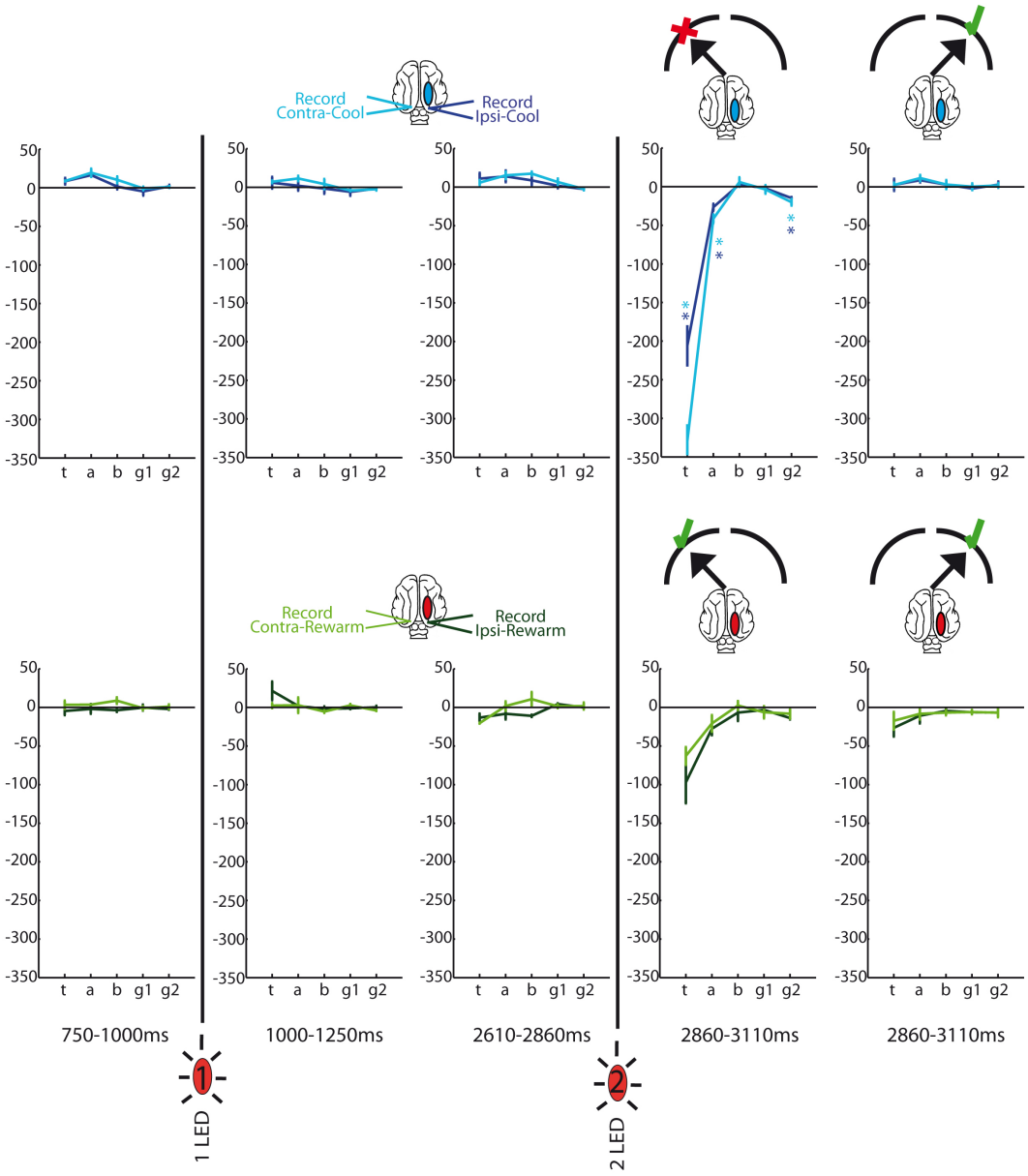

Fig 4.2 (replicated from fig 3.11) - changes in power for pMS inactive and re-active relative to pMS active. The top row is inactive (blue) and the bottom row is re-active (green). There is a significant drop in theta, alpha and gamma power for neglected stimuli. All other time points during pMS inactivation show no change in power from the pMS Active condition. Re-activation showed no difference relative to pMS Active

amplified following LED2 relative to LED1, an amplification mimicked in the ERP (see fig 4.2). This amplification is likely due to the 1) behavioral relevance of LED2 and 2) the peripheral location of LED2 necessitating a reorienting of attention which requires more brain power. Though LED1 was place centrally in the visual field, it merely started a trial, while the peripherally placed LED2 signaled a high-incentive food reward.

Figure 4.3 also shows and expectancy profile in the AW immediately before LED2 onset. The profile is characterized by a significant increase in gamma1 and gamma 2 power. The expectancy profile was present for pMS active, inactive, and re-active condition. Expectancy has been shown to lead to an increase in gamma power (Neuenschwander et al 2008). The Reward AW, following LED2 onset, shows a reduction in gamma power relative to the expectation phase for attended stimuli, though gamma power still remained above pre LED1 levels.

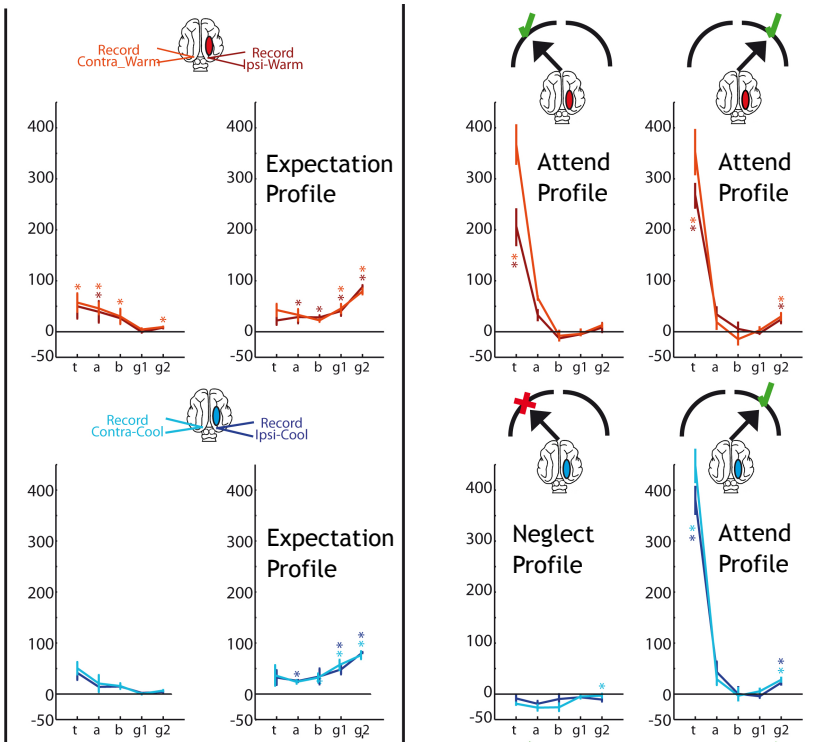

Fig 4.3 (replicated from fig 3.10 which contains the rewarm data) - The two long vertical lines are LED1 and LED2. The power profile right before the middle vertical line (LED2) is the expectation profile. Following LED2 the red graph has the attend profile and the blue flat graph has the Neglect profile. The lighter and darker tones within color represent electrode arrays contralateral and ipsilateral to the pMS cryoloop respectively.

In trials where LED2 was neglected, there was no power change relative to pre LED1 (fig 4.3-Neglect Profile). The notable part of this lack of power change, is that the expectation profile, with gamma power elevated in the Expectation AW located immediately before 2LED onset, is no longer present in the Reward AW for neglected stimuli. The expectation profile is absent despite a mere 250ms time-shift between Expectation and Reward AWs (there was no time delay between the end of AW Expect and the beginning of AW Reward). Moreover, when a stimulus was neglected, the cat continued to wait for a stimulus to appear. It remained alert, with its body still, head pointed right at LED1, and tail flipping back and forth as if it were hunting for the stimulus. Due to this short 250ms time difference and the continued waiting for the 2LED, it seems unlikely that an internal clock signaled to visual cortex to stop expecting a stimulus, and thereby extinguish the expectancy profile in the electrophysiological signal. An alternative likelihood is that the stimulus entered the visual processing network triggering a network state-change. However, this state-change did not translate into awareness of the 2LED. The neglect activity profile is neither an 'expectation profile' seen in in the Expect AW, nor is it an 'attend profile' apparent in the the Reward AW with elevated theta and gamma power (fig 4.3 - attend profile). Rather, the activity profile is flat, suggesting an in-between network state. As mentioned in the introduction, neglected visual stimuli in human neglect patients are indeed processed, but just in unforeseen ways. The activity profile for neglected stimuli could reflect this phenomenon in cats.

4.4 – Gamma, Theta, and Neglect

In light of evidence that there is an electrophysiological trace but no behavioral response to neglected stimuli, the difference between the attend and neglect electrophysiology profile, namely the theta and gamma power reductions, is the likely candidate for a mechanistic explanation for the attentional failure. Gamma, but not theta power was reduced when the SC was deactivated in project 1 while gamma as-well-as theta were reduced in the anesthetized pMS deactivations in project 2. As described in the introduction, multiple network nodes are involved in neglect (fig4.6) and gamma oscillations are an efficient way to offer communication windows through which the network nodes can send fast, high-fidelity signals in the form of spikes to each other (Vicente et al, 2008). Increases in theta power are often associated with an increase in gamma power, and though theta oscillations are primarily associated

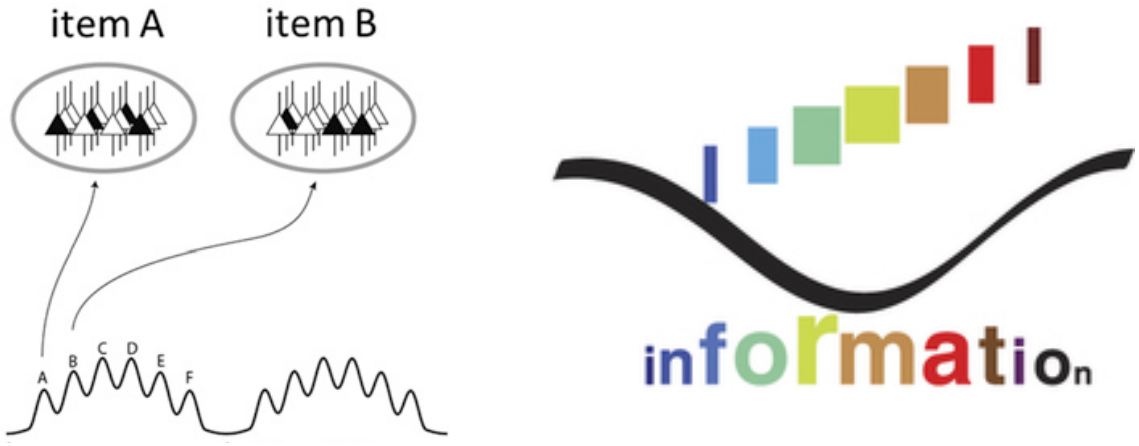

fig 4.5 - left: gamma oscillations are depicted riding on top of a theta oscillation. Item A is represented in gamma peak 'A' by the simultaneous firing of a neural ensemble represented in black. Item B is represented in gamma peak B by a different neural ensemble (reprinted from Penttonen et al 1998). right: the different colors represent different gamma cycles. A different letter is represented in each cycle thus keeping an organized transmission of the word 'information'. (reprinted from Buzsaki & Moser 2013)

with the hippocampus, gamma and theta power work in concert in multiple brain areas (Lisman & Jensen, 2013) including in human primary visual cortex (Jacobs & Kahana, 2009).

Lower frequencies are associated with long range brain communication (Voss & Clark 1975, Nuñez, 1998). It could be that a global theta oscillation between cat primary visual cortex and other brain areas involved in orienting enables a higher-frequency gamma-synchrony between these disparate brain nodes, with gamma oscillations riding on top of theta oscillations. Indeed, a preliminary analysis of project 4 data reveals that when stimuli are attended post LED2 onset, the increase in theta power starts ~60ms following LED2 onset with a gamma power increasing ~50ms later.

Beyond inducing long-distance synchrony, theta is a good mechanism to separate different gamma cycle. Four to eight gamma cycles are nested in a theta cycle. As the gamma cycles rise up and over the hill of a theta cycle, the opportunity for different cell assemblies to be expressed in an ordered way arises (fig 4.4). The peak and trough of the gamma cycle are membrane fluctuations with less and more depolarization. These depolarization fluctuations provide time windows for neurons to spike with depolarization inviting spiking and polarization suppressing it. In this manner, subsequent gamma cycles create and isolate data packages whose information could be encoded in distributed simultaneously spiking neurons that fire together at the depolarized phase of the gamma cycle. Gamma oscillations thus

functions to isolate spiking data packets through subsequent oscillatory cycles which ride on a theta wave (fig 4.5).

Oscillations work as way to bind distributed neural ensembles. For the case of orienting and neglect, there are doubtless myriad structures beyond those placed in the diagram in figure 4.6. Another region not listed in the diagram whose known functions holds an uncanny likeness to the symptoms experienced by human neglect patients following parietal damage is the hippicampus. Human neglect patients not only have difficulty in orienting, but also problems when asked to describe scene from memory. The hippocampus is a place strongly involved in mapping the external environment, a capacity involved in orienting, and is also known to be involved in memory.

In a hypothesis set forward by Whitlock, Sutherland, Witter and Moser (2008), the parietal cortex takes the world-centered coordinate system present in the place and grid cells of the hippocampus and entorhinal cortex and transforms the coordinate system, with the aid of constantly updating visual information from visual corticies, into a new coordinate system that is based around the task at hand (e.g. grasping, head orienting, jumping, etc). In this hypothesis, pMS deactivation leads to a failure of the cat to create a new coordinate space based on the momentary behavioral need, namely orienting to the 2LED. The replacement of the 'expectation profile' by a 'neglect profile' in project 4 (fig 4.3) may show the failure of this transformation, with visual information present but lacking an appropriate coordinate system. Furtheremore, the close coupling shown between in pMS and SC using 2DG and

deactivation of either structure (Rushmore et al 2006) may indicate that the results seen in project 1, SC inactivation, could be the product of the effects of SC inactivation being transmitted to the pMS.

Anatomical pathways between the hippocampus include the corpus striatum (CS) which has been found to have a high level of coherence with the hippocampus

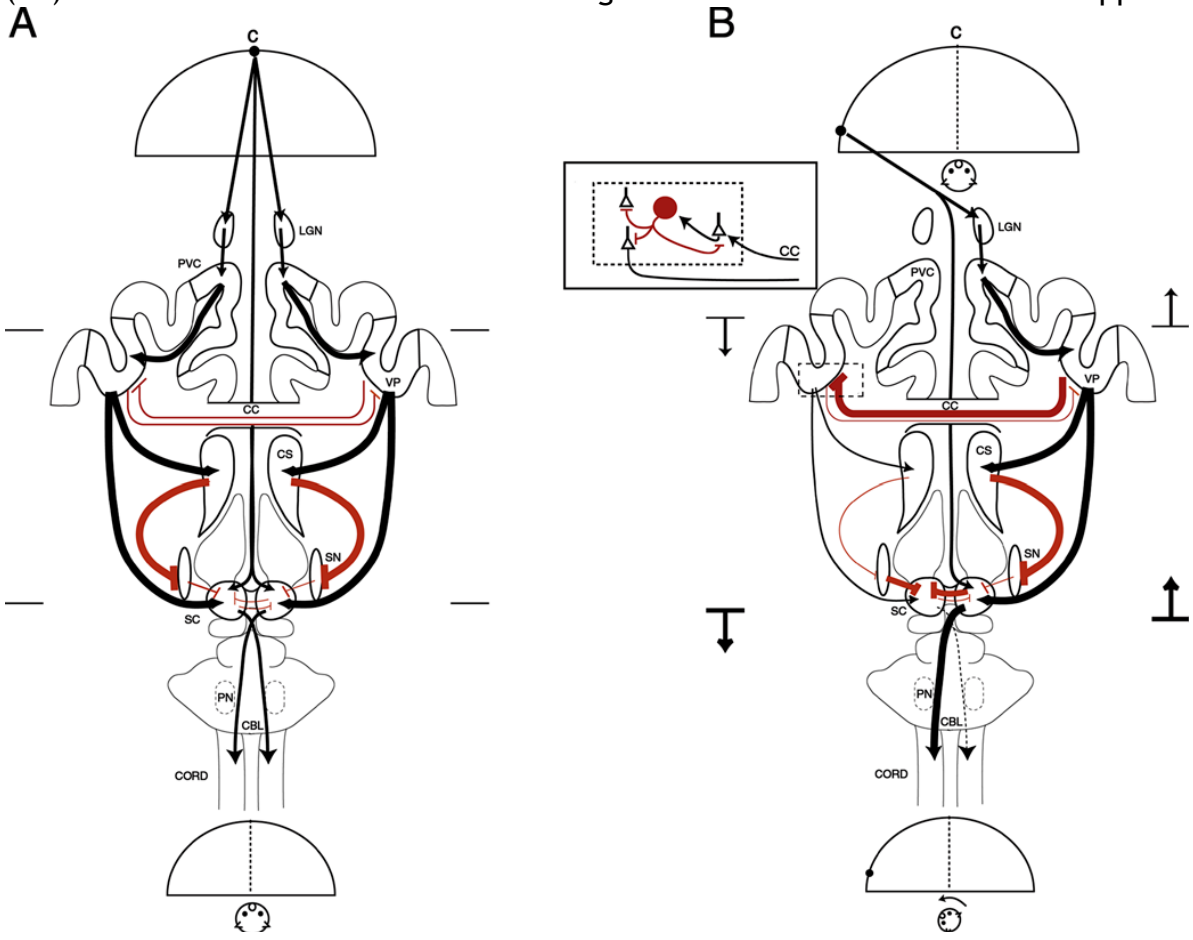

Fig 4.6 – visual orienting network of the cat. The left side, A, is the orienting network when the cat fixates in the middle of a visual perimetry. The right side, B, is the network when the cat reorients to the left. The top semicircle in both A and B is the location of the visual stimulus. Black network connections are excitatory, red are inhibitory. The inset shows corpus callosum (CC) neurons synapsing on inhibitory satellite cells. The vertical arrows in B indicate changes in activity in VP cortex (top) and the SC (bottom) for areas contralateral to stimulation (right arrows) and ipsilateral (left arrows). Abbrevations: PVC-primary visual cortex, VP-visuoparietal cortex, CBL-cerebellum, CS-corpus striatum, CBL-cerabellum, PN-pontine nuclei, SN-substantia niagra. (figure reproduced with permission from Payne & Rushmore 2004)

during periods of decision (DeCoteau et al, 2007) and is also involved in the cat orienting network (fig 4.6 - labeled 'CS'). The prefrontal cortex is also a mediator between the hippocampus and the PPC.

The hypothesis set forward that the parietal cortex transforms coordinates of the external world into goal-specific coordinated bears a likeness to the Attention to Memory hypothesis mentioned in the introduction (section 1.2). In the AtoM hypothesis, the posterior parietal cortex allocates attention to internal models and goals.

4.5 - Chronic electrode implantation (FMA's)

The FMA's showed a rapid loss of a spike signals within a few days after implantation for the awake passive viewing task (project 3), and the spike signal was exceedingly sparse for the perimetry stimulus (project 4) from the very first recording day. A spike signal was however recorded for every session. Spike sorting for either project would be difficult to impossible, but rectifying the area under the curve for the spike signal and comparing that area for different cooling conditions in project 3 or behavioral outcomes in project 4 could be a possibility.

When both analysis 1 & 2 for project 4 were performed on individual cats for individual days, the results showed no change from the first recording day to the last. Therefore, it can be said with certainty that the LFP analysis shown in this dissertation

is robust and not affected by any long-term processes associated with chronically implanted electrodes.

4.6 - Awake vs. Anesthetized recordings

The within-trial normalization (Analysis 2) used to assess stimulus-induced changes in the passive viewing projects (projects 1-3) showed the same moving-grating-induced significant increase in gamma power, a 'gamma bump', for anesthetized SC (fig 3.4 - red trace) and pMS (fig 3.6 - red trace) as-well-as awake pMS (fig 3.8 - red trace) projects. This also acts as a control for the FMA electrodes. The anesthetized projects used electrodes made for an acute preparation and spiking cells were searched for, while the FMAs were used in the awake projects and were chronically implanted. This gamma bump in both types of electrodes show that the FMA's retained their signal despite a long implantation time. The gamma bump in projects 1-3 for moving gratings also shows that anesthesia plays little role in the interplay between gamma and moving gratings.

Points of difference between the awake and anesthetized projects exist in the alpha power (red trace figs 3.4, 3.6, and 3.8) and in the power balance between hemispheres while cortex was cool (blue trace figs 3.3, 3.5, and 3.7). It is known that occipital alpha decreases with an external stimulus. This indeed happened during presentation of the moving grating for the awake preparation in project 3 (fig 3.8). When gamma power in fig 3.8 goes up, alpha goes down. Anesthetized projects 1 and 2 however show either a significant increase (project 1, fig 3.4) or an insignificant

decrease (project 2, fig 3.6) in alpha power when gamma power increases. Presumably the difference between awake and anesthetized alpha can be explained by a massive reduction of internal, stimulus independent, processing in the anesthetized preparation. However, a general reduction in broad-band oscillatory power in the anesthetized verses the awake passive viewing projects is difficult to accurately assess due to differences in electrodes and amplification chains between the projects.

Interhemispheric imbalance in cooling-induced power changes is much more pronounced in the anesthetized preparation than in the awake (figs 3.3 & 3.5 vs fig3.7). A recent Science Translational Medicine publication devised an information theoretical measure that was based on the EEG signal following a TMS pulse applied to humans during multiple stages of sleep, different types of anesthesia, and pathological locked-in or vegetative states (Casali et al 2013). The results show that anesthesia yields an information theoretical value equal to that of slow-wave sleep or a vegetative state. Under anesthesia cortical modules are presumably more isolated from each other. The interhemisphereic power imbalance resulting from cooling in project 1 (fig 3.3) and project 2 (fig 3.5) appears to confirm this hypothesis when viewing the more moderate power imbalance in the awake passive viewing data from project 3 (fig 3.7). The reduction in interhemisphereic imbalance virtually disappears in the awake behaving cat in project 4. Thus, anesthesia seems to affect internal oscillations as evidenced in the difference in alpha power and it seems to disrupt interaction between the hemispheres.

4.7 - The dream project - wrapping up loose ends

To clarify the role that gamma oscillations play in network dynamics during attention, a complicated but technically feasible dream project would be to implant FMAs bilaterally cat SC, pMS, and area 17/18. The roles of the SC and pMS in neglect could be elucidated by implanting both with cooling loops in the same animal. Though cooling both structures leads to similar behavioral outcomes, there is a marked difference in the behavioral role pMS vs SC cooling plays in the behavior on a landmark task (see section 1.3.3). It could be assessed in the perimetry task using LEDs as a stimulus while measuring reaction time weather SC cooling leads to a theta reduction as it does with pMS cooling, or whether the theta reduction is unique to pMS deactivation. A theta reduction resulting from pMS deactivation but not from SC deactivation would lend support to theories on parietal function. Oscillatory coherence in the gamma and theta range between the SC, pMS, and area 17/18 could be measured. As a side project, to assess the effects of anesthesia on recordings, the same cats used for the perimetry task could be easily trained to perform an awake passive viewing task with cooling, then as a terminal experiment, recorded under anesthesia with the same passive viewing stimulus during SC/pMS active and inactive conditions.

Refrences

1. Abramson BP & Chalupa LM (1988). Multiple pathways from the superior colliculuc to the extrageniculate visual thalamus of the cat. Journal of Comparitive Neurology. 271, 397-418, 1988.

2. Ahmed B, Anderson JC, Douglas RJ, Martin KA & Nelson JC (1994). Polyneuronal innervation of spiny stellate neurons in cat visual cortex. J. Comp. Neurol. 341, 39–49.

3. Bartolomeo P, Thiebaut de Schotten M & Doricchi F (2007). Left unilateral neglect as a disconnection syndrome. Cerebral cortex. 17, 2479-2490

4. Behan M, Lin CS & Hall WC (1987). The nigrotectal projection in the cat: an electron microscope autoradiographic study. *Neuroscience*, 21, 529–539.

5. Berman N & Jones EG (1977). A retino-pulvinar projection in the cat. Brain Res. 134, 237–248.

6. Berman R & Wurtz RH (2010). Functional Identification of a Pulvinar Path from Superior Colliculus to Cortical Area MT. J Neuroscience, 30(18), 6342– 6354.

7. Berman R & Wurtz RH (2011). Signals Conveyed in the Pulvinar Pathway from Superior Colliculus to Cortical Area MT. J Neuroscience, 31(2), 373–384.

8. Berson DM (1988). Retinal and cortical inputs to cat superior colliculus: composition, convergence and laminar specificity. *Prog Brain Res*, 75, 17–26.

9. Berson DM & McIlwain JT (1983). Visual cortical inputs to deep layers of cat's superior colliculus. *J Neurophysiol*, 50, 1143– 1155.

10. Berson DM, Isayama T & Pu M (1999). The Eta ganglion cell type of cat retina. J. Comp. Neurol., 408, 204–219.

11. Berson DM, Pu M & Famiglietti EV (1998). The zeta cell: a new ganglion cell type in cat retina. J. Comp. Neurol., 399, 269–288.

12. Bishop PO, Kozak W, Levick WR & Vakkur GJ (1962). The determination of the projection of the visual field on to the lateral geniculate nucleus in the cat. J. Physiol. (Lond.). 163, 503–539.

13. Bisiach G, Capitani E, Luzzatti C & Perani D (1981). Brain and conscious representation of outside reality. Neuropsychology. 19, 543-551.

14. Blakemore C & Donaghy M (1980). Co-ordination of head and eyes in the gaze changing behaviour of cats. J Physiol, 300, 317–335.

15. Boycott BB & Wässle H (1974). The morphological types of ganglion cells of the domestic cat's retina. J. Physiol. 240, 397–419.

16. Bowling DB & Michael CR (1984). Termination patterns of single physiologically characterized optic tract fibers in the cat's lateral geniculate nucleus. J. Neurosci. 4, 198–216.

17. Buchtel HA, Camarda R, Rizzolatti G & Scandolara C (1979). The effect of hemidecortication on the inhibitory interactions in the superior colliculus of the cat. J Comp Neurol, 184, 795–810.

18. Buhl EH & Singer W (1989). The callosal projection in cat visual cortex as revealed by a combination of retrograde tracing and intracellular injection. *Exp Brain Res*, 75, 470-476.

19. Burwell RD & Amaral DG (1998). Cortical afferents of the perirhinal, postrhinal, and entorhinal cortices of the rat. J Comp Neurol 398:179–205.

20. Buzsaki G & Moser E (2013). Memory, navigation and theta rhythm in the hippocampal-entorhinal system. Nature Neuroscience, 16, 130-138.

21. Cabeza R, Ciaramelli E, Olson IR & Moscovitch M. (2008). The parietal cortex and episodic memory: an attentional account. Nature reviews. Neuroscience, 9(8), 613–25.

22. Casali AG, Gosseries O, Rosanova M, Boly M, Sarasso S, Casali KR, Casarotto S, Bruno MA, Laureys S, Tononi G & Massimini M (2013). A Theoretically Based Index of ConsciousnessIndependent of Sensory Processing and Behavior. Science Translational Medicine. 5:198, 1-10.

23. Chalfin BR, Cheung DT, Muniz JAPC, De Lima Silveira LC & Finlay BL (2007). Scaling of Neuron Number and Volume of the Pulvinar Complex in New World Primates: Comparisons with Humans, other primates, and mammals. J Comp Neurology, 504, 265-274.

24. Churchland PS, Ramachandran VS & Sejnowski TJ (1993). A critique of pure vision. In: Largescale neuronal theories of the brain (C. Koch, and J. Davis, Eds.), pp. 23–60 Cambridge, Mass, MIT Press.

25. Ciaramelli E, Grady CL & Moscovitch M (2008). Top-down and bottom-up attention to memory: A hypothesis (AtoM) on the role of the posterior parietal cortex in memory retrieval. Neuropsychologia, 46, 1828–1851.

26. Ciaramelli E, Grady C, Levine B, Ween J & Moscovitch M (2010). Top-down and bottom-up attention to memory are dissociated in posterior parietal cortex: neuro imaging and neuropsychological evidence. The Journal of neuroscience : the official journal of the Society for Neuroscience, 30(14).

27. Csicsvari J, Jamieson B, Wise KD & Buzsáki G (2003). Mechanisms of gamma oscillationsin the hippocampus of the behaving rat. Neuron 37:311–322.

28. Cleland BG, Harding TH & Tulunay-Keesey U (1979). Visual resolution and receptive field size: examination of two kinds of cat retinal ganglion cell. Science, 205, 1015–1017.

29. Doty RW (1971). Survival of pattern vision after removal of striate cortex in the adult cat. J. Comp. Neurol. 143, 341–370.

30. Driver J & Vuilleumier P (2001). Perceptual awareness and its loss in unilateral neglect and extinction. Cognition, 79(1-2), 39–88.

31. Durmer JS & Rosenquist AC (2001). Ibotenic acid lesions in the pedunculopontine region result in recovery of visual orienting in the hemianopic cat. Neuroscience, 106, 765–81.

32. Enroth-Cugell C & Robson JG (1966). The contrast sensitivity of retinal ganglion cells of the cat. J. Physiol, 187, 517–552.

33. Evinger C & Fuchs AF (1978). Saccadic, smooth pursuit, and optokinetic eye movements of the trained cat. J Physiol, 285, 209–229.

34. Fabre-Thorpe M, Vievard A & Buser P (1986). Role of the extrageniculate pathway in visual guidance II. Effects of lesioning the pulvinar-lateral posterior thalamic complex in the cat. Exp Brain Res, 62, 596–606.

35. Fairen A & Valverde F (1980). A specialized type of neuron in the visual cortex of cat: a Golgi and electron microscope study of chandelier cells. *J Comp Neurol*, 194, 761–779.

36. Fisahn A, Pike FG, Buhl EH & Paulsen O (1998) Cholinergic induction of network oscillationsat 40 Hz in the hippocampus in vitro. Nature 394:186–189.

37. Freund TF, Martin KAC, Somogyi P & Whitteridge D (1985). Innervation of cat visual areas 17 and 18 by physiologically identified X- and Y-type thalamic afferents. I. Arborization patterns and quantitative distribution of postsynaptic elements. J. Comp. Neurol. 242, 263–274.

38. Fries P (2005). A mechanism for cognitive dynamics: neuronal communication through neuronal coherence. Trends Cogn. Sci., 9, 474–480.

39. Fries P, Nikolic D & Singer W (2007). The gamma cycle. Trends Neurosci, 30, 309–316.

40. Fries P, Womelsdorf T, Oostenveld R & Desimone R (2008). The effects of visual stimulation and selective visual attention on rhythmic neuronal synchronization in macaque area V4.J. Neurosci. 28, 4823–4835.

41. Garey LJ & Powell TPS (1967). The projection of the lateral geniculate nucleus upon the cortex in the cat. Proc. R. Soc. Lond. 169, 107–126.

42. Geisert EE (1980). Cortical projections of the lateral geniculate nucleus in the cat. J. Comp. Neurol. 190, 793–812.

43. Gilbert CD & & Wiesel TN (1979). Morphology and intracortical projections of functionally characterised neurones in the cat visual cortex. Nature 280, 120–125.

44. Gilbert CD & Kelly JP (1975). The projections of cells in different layers of the cat's visual cortex. J Comp Neurol, 163, 81–105.

45. Gilbert CD & Wiesel TN (1983). Clustered intrinsic connections in cat visual cortex. J. Neurosci. 3, 1116–1133.

46. Grant S & Shipp S (1991). Visuotopic organization of the lateral suprasylvian area and of an adjacent area of the ectosylvian gyrus of cat aortex: a physiological and connectional study. Vis Neurosci, 6, 315-338.

47. Gray CM, König P, Engel AK & Singer W (1989). Oscillatory responses in cat visual cortex exibit inter-columnar synchronization which reflects global stimulus properties. Nature, 223, 334-337.

48. Guillery RW, Geisert EE, Polley EH & Mason CA (1980). An analysis of the retinal afferents to the cat's medial interlaminar nucleus and its rostral thalamic extension, the "geniculate wing". J. Comp. Neurol. 194, 117–142.

49. Hada J & Hayashi Y (1990). Retinal X-afferents bifurcate to lateral geniculate X-cells and to the pretectum or superior colliculus in cats. Brain Res. 515, 149–154.

50. Hardy SC & Stein BE (1988). Small Lateral Suprasylvian Cortex Lesions Produce Visual Neglect and Decreased Visual Activity in the Superior Colliculus, 542, 527–542.

51. Harris LR, Blakemore C & Donaghy M (1980). Integration of visual and auditory space in the mammalian superior colliculus. Nature, 288, 56–59

52. Harting JK, Huerta MF, Hashikawa T, Weber JT & Van Lieshout DP (1988). Neuroanatomical studies of the nigrotectal projection in the cat. *J Comp Neurol*, 278, 615–631.

53. Harting JK, Updyke BV & Van Lieshout DP (1992). Corticotectal projections in the cat: anterograde transport studies of twenty-five cortical areas. J of Comp Neurology, 324, 379-414.

54. Harvey M, Milner AD & Roberts RC (1995). An investigation of hemispatial neglect using the landmark task. Brain Cogn. 27, 59-78.

55. Herculano-Houzel S, Munk MH, Neuenschw&er S & Singer W (1999). Precisely synchronized oscillatory firing patterns require electroencephalographic activation. J. Neurosci. 19, 3992–4010.

56. Hoffman K-P & Straschill M (1971). Influences of cortico-tectal and intertectal connections on visual responses in the cat's superior colliculus. *Exp Brain Res*, 12, 120–131.

57. Hughes HC (1980). Efferent Organization of the Cat Pulvinar Comp With a Note on Bilateral Claustrocortical and Reticulocortical Connections. J Comp Neurology, 193, 937-963.

58. Humphrey AL, Sur M, Uhlrich DJ & Sherman SM (1985). Termination patterns of individual X- and Y-cell axons in the visual cortex of the cat, Projections to area 18, to the 17/18 border region, and to both areas 17 and 18. J. Comp. Neurol. 233, 190–211.

59. Humphrey AL, Sur M, Uhlrich DJ & Sherman SM (1985). Termination patterns of individual X- and Y-cell axons in the visual cortex of the cat, Projections to area 18, to the 17/18 border region, and to both areas 17 and 18. J. Comp. Neurol. 233, 190–211.

60. Huppe-Gourgues F, Bickford ME, Boire D, Ptito M & Casanova C (2006). Distribution, Morphology, and Synaptic Targets of Corticothalamic Terminals in the Cat Lateral Posterior-Pulvinar Complex that Originate from the Posteromedial Lateral Suprasylvian Cortex. J Comp Neurology, 497, 847-863.

61. Hutchinson JB, Uncapher MR & Wagner AD (2009). Posterior parietal cortex and episodic retrieval: convergent and divergent effects of attention and memory. Learning & memory (Cold Spring Harbor, N.Y.), 16(6), 343–56.

62. Illing RB & Wässle H (1981). The retinal projection to the thalamus in the cat: a quantitative investigation and a comparison with the retinotectal pathway. J. Comp. Neurol. 202, 265–285.

63. Isayama T, Berson DM & Pu M (2000). Theta ganglion cell type of cat retina. *J. Comp. Neurol.*, 417, 32–48.

64. Jaehner NG, Rothkopf CA, Voegler S, Triesch J & Galuske RAW (2012). Topographic And Functional Organization Of Feedback Axons From Middle Suprasylvian Sulcus To Primary Visual Cortex In The Cat. FENS Abstract, 6, p039.38.

65. Jaehner NG (2013). Topographie kortikaler Rückprojektionen im visuellen System der Katze. doctoral thesis, Advisor: Galuske R.A.W., Technische Universität Darmstadt

66. Jiang H, Stein BE & McHaffie JG (2003). Opposing basal ganglia processes shape midbrain visuomotor activity bilaterally. Nature, 423(6943), 982–6.

67. Jiang H, Stein BE & McHaffie JG (2011). Physiological evidence for a trans-basal ganglia pathway linking extrastriate visual cortex and the superior colliculus. The Journal of physiology, 589(Pt 23), 5785–99.

68. Karnath HO, Schenkel P & Fischer B (1991). Trunk orientation as the determining factor of the `contralateral´ deficit in the neglect syndrome and as the physical

anchor of the internal representation of body orientation in space. Brain. 114 (4), 1997-2014.

69. Karnath HO, Himmelbach M & Rorden C (2002). The subcortical anatomy of human spatial neglect: putamen, caudate nucleus and pulvinar. Brain. 125(2):350-360.

70. Kelly LR, Li J, Breckinridge C & Bickford ME (2003). Ultrastructure and Synaptic Targets of Tectothalamic Terminals in the Cat Lateral Posterior Nucleus. J ok Comp Neurology, 464, 472-486.

71. Kerr KM, Agster KL, Furtak SC & Burwell RD (2007)Functional neuroanatomy of the parahippocampalregion: The lateral and medial entorhinal areas. Hippocampus17:697–708.

72. Kersten D & Mamassian P (2004). "Object perception as Bayesian inference."Annual review of psychology 55: 271-304.

73. Knill D & Richards W (1996). Perception as Bayesian inference, Cambridge University Press.

74. Kooistra C A & Heilman KM (1989). Hemispatial visual inattention masquerading as hemianopia. Neurology, 39, 1125-1172.

75. Lee I, Kim J & Lee C (1999). Anatomical characteristics and three-dimensional model of dog dorsal lateral geniculate body. The anatomical record, 256, 29-39.

76. Lisman JE & Jensen O (2013). The theta-gamma neural code. Neuron, 77, 1002-1011.

77. Lomber SG, Payne BR & Cornwell P (2001). Role of the superior colliculus in analyses of space: superficial and intermediate layer contributions to visual orienting, auditory orienting, and visuospatial discriminations during unilateral and bilateral deactivations. J. Comp Neurol, 441, 44-57.

78. Lomber SG, Payne BR, Cornwell P & Long KD (1996). Perceptual and cognitive visual functions of parietal and temporal cortices in the cat. Cerebral Cortex, 6, 673-695.

79. Lomber SG & Payne BR (1996). Removal of two halves restores the whole: Reversal of visual hemineglect during bilateral cortical or collicular inactivation in the cat. *Visual Neuroscience*, 13, 1143-1156.

80. Lomber SG & Payne BR (2001). Task-specific reversal of visual hemineglect following bilateral reversible deactivation of posterior parietal cortex: A comparison with deactivation of the superior colliculus. *Visual Neuroscience*, 18, 487-499.

81. Lomber SG, Payne BR & Cornwell P (2001). Role of the superior colliculus in analyses of space: superficial and intermediate layer contributions to visual orienting, auditory orienting, and visuospatial discriminations during unilateral and bilateral deactivations. *The Journal of Comparative Neurology*. 441, 44-57.

82. Lomber SG, Payne BR & Horel JA (1999). The cryoloop: an adaptable reversible cooling deactivation method for behavioral or electrophysiological assessment of neural function. *J. Neurosci.Methods* 86, 179-194.

83. Markov NT, Vezoli J, Chameau P, Falchier A, Quilodran R, Huissoud C, Lamy C, Misery P, Giroud P, Barone P, Dehay C, Ullman S, Knoblauch K & Kennedy H (2014b). Anatomy of Hierarchy: Feedforward and feedback pathways in macaque visual cortex. Journal of Comparative Neurology, 522, 225-259.

84. MacNeil MA, Lomber SG & Payne BR (1996). Rewiring of transcortical projections to middle suprasylvian cortex following early removal of cat areas 17 and 18. Cerebral Cortex. 6, 362-376.

85. Mann EO, Suckling JM, Hajos N, Greenfield SA & Paulsen O (2005) Perisomatic feedbackinhibition underlies cholinergically induced fast network oscillations in the rat hippocampusin vitro. Neuron 45:105–117.

86. Marshall JC & Halligan PW (1988). Blindsight and insight in visuo-spatial neglect. Nature, 336, 766-767.

87. Martin KAC & Whitteridge D (1984). Form, function and intracortical projections of spiny neurones in the striate visual cortex of the cat. J. Physiol. (Lond.) 353, 463-504.

88. Meredith MA & Stein BE (1986). Visual, auditory, and somatosensory convergence on cells in superior colliculuc result in multisensory integration. J Neurophysiology, 56, 640-662, 1986

89. McHaffie JG, Norita M, Dunning DD & Stein BE (1993). Corticotectal relationships: direct and “indirect” corticotectal pathways. *Prog Brain Res*, 95, 139–150.

90. McIlwain JT (1977). Topographic organization and convergence in corticotectal projections from areas 17, 18, and 19 in the cat. *J Neurophysiol*, 40, 189–198.

91. Merabet L, Desautels A, Minville K & Casanova C (1998). Motion integration in a thalamic visual nucleus. Nature, 396, 265-268.

92. Meredith MA & Stein BE (1986). Visual, auditory, and somatosensory convergence on cells in superior colliculus results in multisensory integration. *J Neurophysiology* 56, 640-662.

93. Mesulam M (1999). Spatial attention and neglect: parietal, frontal and cingulate contributions to the mental representation and attentional targeting of salient extrapersonal events. Philos Trans R Soc Lond B Biol Sci, 354(1387), 1325–46.

94. Molotchnikoff S & Shumikhina S (1996). The lateral posterior-pulvinar complex modulation of stimulus-dependent oscillations in the cat visual cortex. Vision Res. 36, 2037–2046.

95. Monaghan P & Shillcock R (1998). The cross-over effect in unilateral neglect. Modelling detailed data in the line-bisection task. Brain: a journal of neurology, 121 (Pt 5(1998), 907–21.

96. Mort DJ, Malhotra P, Mannan SK, Rorden C, Pambakian A, Kennard C & Husain M (2003). The anatomy of visual neglect. Brain. 126(Pt 9): 1986-1997.

97. Mozer MC, Halligan PW & Marshall JC (1997). The end of the line for a brain-damaged model of unilateral neglect. Journal of cognitive neuroscience, 9(2), 171–90.

98. Mumford D (1994). Neuronal architectures for pattern-theoretic problems. Large-scaleneuronal theories of the brain, MIT Press.Leventhal, A.G., Rodieck, R.W., and Dreher, B. (1985). Central projections of cat retinal ganglion cells. *J Comp Neurol*, 237, 216-226.

99. Munk MH, Roelfsema PR, König P, Engel AK & Singer W. (1996).Role of reticular activation in themodulation of intracortical synchronization.Science 272, 271–274.

100. Neuenschwander S & Singer W(1996). Long-range synchronizationof oscillatory light responses in the catretina and lateral geniculate nucleus.Nature, 379, 728–732.

101. Niimi K & Sprague JM (1970). Thalamo-cortical organization of the visual system in the cat. J. Comp. Neurol. 138, 219–250.

102. O'Brien BJ, Isayama T & Berson DM (1999). Light responses of morphologically identified cat ganglion cells. *Invest. Ophthalmol. Vis. Sci.*, S815.

103. Ojima H, Murakami K, & Kishi K (1996). Dual termination modes of corticothalamic fibers originating from pyramids of layers 5 and 6 in cat visual cortical area 17. Neurosci Lett, 208, 57–60.

104. Olshausen B (2010). 20 Years of Learning About Vision: Questions Answered, Questions Unanswered, and Questions Not Yet Asked, in J.M. Bower (Ed.), 20 Years of Computational Neuroscience (pp. 243 -270). New York, NY: Springer.

105. Olson IR & Berryhill M (2009). Some surprising findings on the involvement of the parietal lobe in human memory. Neurobiol Learn Mem 91, 155– 165.

106. Ouellette BG & Casanova C (2006). Overlapping visual response latency distributions in visual cortices and LP-pulvinar complex of the cat. Exp Brain Res.

107. Payne BR, Lomber SG, Geeraertst S, Van Der Gucht E & Vandenbussche E (1996). Reversible visual hemineglect. Proceedings of the National Academy of Scheinces, 93, 290-294.

108. Payne BR & Peters A (2002). The Concept of Cat Primary Visual Cortex, In B.R. Payne & A. Peters (Eds.), The Cat Primary Visual Cortex (pp. 1-129). San Diego, CA: Academic Press.

109. Palmer LA, Rosenquist AC & Tusa RJ (1978). The retinotopic orginization of lateral suprasylvian visual areas in the cat. J Cmp Neurology, 177, 237-256.

110. Payne BR & Rushmore RJ (2003). Animal models of cerebral neglect and its cancellation. The Neuroscientist : a review journal bringing neurobiology, neurology and psychiatry, 9(6).

111. Payne BR & Rushmore JR (2004). Functional circuitry underlying natural and interventional cancellation of visual neglect. *Exp Brain Res*, 154, 127-153.

112. Payne BR & Siwek DF (1991). The visual map in the corpus callosum of the cat. Cerebral Cortex 1, 173–188.

113. Penttonen M, Kamondi A, Acsady L & Buzsaki G (1998). Gamma frequency oscillation in the hippocampus of the rat: intracellular analysis in vivo. Eur. J. Neurosci. 10, 718–728

114. Peters A (1984). Chandelier cells. In: Peters A, Jones E (eds) Cerebral cortex, vol 1 (pp 361–380). New York, NY: Plenum Press.

115. Peters A & Payne BR (1993). Numerical relationships between geniculo-cortical afferents and pyramidal cell modules in cat primary visual cortex. Cerebral Cortex 3, 69–78.

116. Peters A, Payne BR & Josephson K (1990). Transcallosal nonpyramidal cell projections from visual cortex in the cat. *J Comp Neurol*, 302, 124–142

117. Peterson SE & Posner MI (2012). The Attention System of the Human Brain: 20 Years After. Annual Reviews Neuroscience, 35, 73-89.

118. Purushothamen G, Marion R, Li K & Casagrande VA (2012). Gating and control of primary visual cortex by pulvinar. Nature Neuroscience, 15(6), 905-913.

119. Rao RPN & Olshausen BA (2002). Probabilistic models of the brain: Perception and neural function, MIT Press.

120. Rowe MH & Palmer LA (1995). Spatio-temporal receptive-field structure of phasic W cells in the cat retina. Vis. Neurosci., 12, 117–139.

121. Rizzolatti G & Camarda R (1977). Influence of the presentation of remote visual stimuli on visual responses of cat area 17 and lateral suprasylvian area. *Exp Brain Res*, 29, 107–122

122. Robinson DL & Peterson SE (1992). The pulvinar and visual salience. Trends in Neuroscience, 15, 127 -132.

123. Royce GJ & Laine EJ (1984). Efferent connections of the caudate nucleus, including cortical projections of the striatum and other basal ganglia: an autoradiographic and horseradish peroxidase investigation in the cat. *J Comp Neurol*, 226, 28–49.

124. Rushmore RJ, Valero-Cabre A, Lomber SG, Hilgetag CC & Payne BR (2006). Functional circuitry underlying visual neglect. Brain, 129, 1803-1821.

125. Stone J (1983). Parallel processing in the visual system. New York, NY: Plenum Press.

126. Salsbury KG & Horel JA (1983). A cryogenic implant for producing reversible functional brain lesions. Behavior Research Methods and Instrumenatation, 433-435.

127. Sanderson KJ (1971). The projection of the visual field to the lateral geniculate and medial interlaminar nuclei in the cat. J. Comp. Neurol., 143, 101–118.

128. Sawai H, Fukuda Y & Wakakuwa K (1985). Axonal projections of X-cells to the superior colliculus and to the nucleus of the optic tract in cats. Brain Res. 341, 1–6.

129. Sharon D, Jancke D, Chavane F, Na'aman S & Grinvald A (2007). Cortical Response Field Dynamics in Cat Visual Cortex. *Cerebral Cortex*. 17, 2866 - 2877.

130. Shapley RM & Victor JD (1986). Hyperacuity in cat retinal ganglion cells. Science, 231, 999–1002.

131. Sherk H (2010). Evidence regarding the integrity of the posterior medial lateral suprasylvian visual area in the cat. J Comp Neurology, 518, 3343-3358.

132. Sherk H (1986). Location and connections of visual cortical areas in the cat's suprasylvian sulcus. J Comp Neurol, 247, 1-31.

133. Shumikhina S & Molotchnikoff S (1999). Pulvinar participates in synchronizing neural assemblies in the visual cortex, in cats. Neurosci. Lett. 272, 135–139.

134. Smith Y, Bevan MD, Shink E & Bolam JP (1998). Microcircuitry of the direct and indirect pathways of the basal ganglia. Neuroscience, 86, 353–387.

135. Sprague JM (1966). Interaction of cortex and superior colliculus in mediation of visually guided behavior in the cat. Science, 153, 1544–7.

136. Sprague JM & Meikle TH (1965). The role of the superior colliculus in visually guided behavior. Exp Neurol, 11, 115–46.

137. Stein BE (1984) Development of the superior colliculus. Ann Rev Neurosci, 7, 95-125.

138. Stein BE & Meredith MA (1991). Functional organization of the superior colliculus. In A.G. Leventhal (Ed.), *The neuronal basis of visual function* (pp 85-110). London: MacMillian.

139. Stone J (1983). Parallel processing in the visual system. The classification of retinal ganglion cells and its impact on the neurobiology of vision. Perspectives in vision research, C. Blakemore (Series Editor), New York, NY: Plenum Press.

140. Stone J & Dreher B (1973). Projection of X – and Y – cells of the cat's lateral geniculate nucleus to areas 17, and 18 of visual cortex. J. Neurophysiol. 36, 551–567.

141. Sur M, Esguera M, Garraghty PE, Kritzer MF & Sherman SM (1987). Morphology of physiologically identified retinogeniculate X- and Y-axons in the cat. J. Neurophysiol. 58, 1–32.

142. Shumikhina S & Molotchnikof S (1999). Pulvinar participates in synchronizing neural assemblies in the visual cortex, in cats. Neuroscience Letters, 272, 135-139.

143. Swisher JD, Halko MA, Merabet LB, McMains SA & Somers DC (2007). Visual topography of human intraparietal sulcus. J Neurosci 27, 5326–5337.

144. Tamamaki N, Uhlrich DJ & Sherman SM (1995). Morphology of physiologically identified retinal X and Y axons in the cat's thalamus and midbrain as revealed by intraaxonal injection of biocytin. J. Comp. Neurol. 354, 583–607.

145. Tegnér R & Levander M (1991). Through a looking glass. A new technique to demonstrate directional hypokinesia in unilateral neglect. Brain, 114, 1943-1951.

146. Tong L, Kalil RE & Spear PD (1982). Thalamic projections to visual areas of the middle suprasylvian sulcus in the cat. J Comp Neurol, 212, 103–117.

147. Troy JB (1987). Do Y geniculate neurons have greater contrast sensitivity than X geniculate neurons at all visual field locations?. Vis. Res., 27, 1733–1735.

148. Uhlhaas PJ, Pipa G, Lima B, Melloni L, Neuenschwander S, Nikolic D & Singer W. (2009). Neural synchrony in cortical networks: history, concept and current status. Frontiers in Integrative Neuroscience, 3, 17.

149. Updyke BV (1993). Organization of visual corticostriatal projections in the cat, with observations on visual projections to claustrum and amygdala. *J Comp Neurol*, 327, 159–193.

150. Vallar G (2001). Extrapersonal visual unilateral spatial neglect and its neuroanatomy. Neuroimage. 14(1 Pt 2):S52--S58.

151. Vicente R, Gollo LL, Mirasso CR, Fischer I & Pipa G (2008). Dynamical relaying can yield zero time lag neuronal synchrony despite lonconduction delays. Proc. Natl. Acad. Sci. 105, 17157–17162.

152. Vuilleumier P, Valenza N, Perrig S, Mayer E & Landis T (1999). To see better to the left when looking more to the right : effects of gaze direction and frame of spatial coordinates in unilateral neglect. Journal of the International Neuropsychology Society, 5, 75-82.

153. Waleszczyk WJ, Dec K & Hekimian AA (1993). Influence of the intertectal connection upon visual responses in the cat's superior colliculus. *Acta Neurobiol Exp*, 53, 409–414.

154. Wallace SF, Rosenquist AC & Sprague JM (1989). Recovery from cortical blindness mediated by destruction of nontectotectal fibers in the commissure of the superior colliculus in the cat. J Comp Neurol, 284, 429–50.

155. Wallace SF, Rosenquist AC & Sprague JM (1990). Ibotenic acid lesions of the lateral substantia nigra restore visual orientation behavior in the hemianopic cat. J Comp Neurol, 296, 222–52.

156. Watson RT, Valenstein E, Day A & Heilman KM (1994). Posterior neocortical systems subserving awareness and neglect: neglect associated with superior temporal sulcus but not area 7 lesions. Archives of Neurology. 51, 1014–21.

157. Wässle H & Boycott BB (1991). Functional architecture of the mammalian retina. Physiol. Rev, 71, 447–480.

158. Wässle H & Illing RB (1980). The retinal projection to the superior colliculus in the cat: a quantitative study with HRP. *J. Comp Neurol*. 190, 333-356.

159. Whitlock JR, Sutherland RJ, Witter MP, Moser MB & Moser EI (2008). Navigating from hippocampus to parietal cortex. Proceedings of the National Academy of Science. 105, 14755-14762.

160. Wilke M, Kagan I & Andersen RA (2012). Functional imaging reveals rapid reorganization of cortical activity after parietal inactivation in monkeys. Proceedings of the National Academy of Sciences of the United States of America, 109(21), 8274–8279.

Ehrenwörtliche Erklärung

Ich erkläre hiermit ehrenwörtlich, dass ich die vorliegende Arbeit selbständig angefertigt habe. Sämtliche aus fremden Quellen direkt oder indirekt übernommene Gedanken sind als solche kenntlich gemacht. Die Arbeit wurde bisher keiner anderen Prüfungsbehörde vorgelegt und noch nicht veröffentlicht.

Ffm., 12.01.2015

Curriculum Vitae

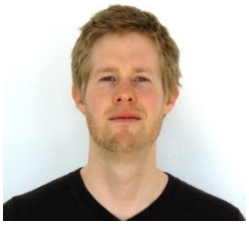

Personal Data

Name: William Halley Barnes

Date of Birth: Feburary 2, 1979 (Dallas, USA)

Nationality: American

Address: Schuetzenhuettenweg 34

60598 Frankfurt am Main

Germany

E-mail Address: willhbarnes@gmail.com

Education

1984-1992 Elementary and Middle School Dallas, USA

1992-1997 High School – Plano, USA

1997-2003 Bachelors of Neuroscience, cum laude

2004-2005 Masters in Cognition and Neuroscience, summa cum laude

2005-2013 Doctorate in Natural Sciences, magna cum laude

Information Technology Knowledge

Office: Word, Excel, Powerpoint

Adobe: Illistrator, Photoshop, InDesign

Programming: Matlab

Research Skills

-Optical imaging of intrinsic signals and voltage sensitive dye optical imaging – acquiring data in both anesthetized and awake preperation, analysis of data

-Electrophysiology – acquiring of data in the chronically-implanted awake-behaving preparation and in the acute preparation, analysis of spike and LFP signals

-Competance in histological preparation if brain tissue

Scientific Abstracts

2002 –

Society for Neuroscience, Orlando, Florida,POSTER: Extrastriate Cortical Areas Mediating Neglect: Eximination of 15 Loci in the Cat. WH Barnes, EW Lakes, S Malhotra, BR Payne

2003 –

Society for Neuroscience, New Orleans, Louisiana, POSTER: Be Prepared: What High School Students Really Want to Know About the Brain. AJ Hall, S Malhotra, WH Barnes, EM Woller, JG Mellott, G Hawksworth, M Bolinger, SG Lomber

2003 –

Society for Neuroscience, New Orleans, Louisana, POSTER: Cerebral Areas Mediating Pattern Discrimination in Auditory Cortex of the Behaving Cat. WH Barnes, SG Lomber.

2004 –

Society for Neuroscience, San Diego, California, POSTER: Visual neglect during unilateral deactivation of cat posterior parietal cortex: Egocentric or Allocentric?

2005 –

Society for Neuroscience, Washington DC, POSTER: Superior colliculus strongly influences sensory processing in primary visual cortex. B Ebisch, WH Barnes, Y Egenolf, SG Lomber, RAW Galuske

Society for Neuroscience POSTER: Functional topography od parietal feedback systems in the cat visual cortex. RAW Galuske, SG Lomber, WH Barnes, Y Egenolf, B Ebisch.

2008 –

Society for Neuroscience, Washing DC, POSTER: Interhemispheric imbalances of oscilliatory activity and visual neglect. WH Barnes, B Ebisch, MK Rieder, K Geider, RAW Galuske

2010 –

Society for Neuroscience, San Diego, California, POSTER: Neural mechanisms underlying visual neglect. WE Barnes, M Mueller, RAW Galuske

Additional Training

2014 ESI SYNC Workshop, Frankfurt am Main, Germany

2013 ESI Fieldtrip Workshop, Frankfurt am Main, Germany

2013 ESI Alpha Workshop, Frankfurt am Main, Germany

2012 ESI Interareal Workshop, Frankfurt am Main, Germany

2009 Matlab Introduction Course, Frankfurt am Main, Germany